Structural dynamic response
of the
Glass Truss Bridge

E.M. de Vries Robbé

TUDelft

Witteveen+Bos

Structural dynamic response of the Glass Truss Bridge

by

Eva Maria de Vries Robbé

to obtain the degree of Master of Science
at the Delft University of Technology,
to be defended publicly on Friday October 16th 2020, at 10:00 AM

Student number: 4218361
Project duration: December 10, 2019 – Oktober 16, 2020
Thesis committee: Prof. ir. R. Nijsse,   Delft University of Technology, chair
                     Dr. F. Messali,   Delft University of Technology
                     Ir. Dr. A. Cabboi ,   Delft University of Technology
                     Ir. P. Schoutens,   Witteveen+Bos

An electronic version of this thesis is available at `http://repository.tudelft.nl/`.

TUDelft

Witteveen+Bos

Acknowledgements

Abstract

Bridges are exposed to dynamic forces – such as pedestrians crossing a bridge or the wind force acting on a bridge – which cause vibration of the structure. When a structure is forced at one of its eigenfrequencies it deforms into a corresponding shape leading to major deformations, which, in the worst-case scenario, can lead to collapse of the structure, as happened to the Tacoma Narrows bridge in 1940. It is thus very important to know the dynamic characteristics of a structure. For glass structures no specific limit values are defined, this is why it is interesting to investigate the dynamic behaviour of a glass bridge This thesis aims to predict the structural response of TU Delft's Glass Truss Bridge when subjected to static and dynamic loads. The studied bridge is a footbridge, connecting the TU Delft campus to the Green Village, and is unique in the aspect that glass diagonals have been used in its construction.

Through an iterative procedure of modeling, virtual testing and updating the model of the bridge, the dynamic response of the bridge is predicted. The study shows that the response of the bridge is between the European Guidelines' limits for (steel) footbridges. Maximum acceleration of the bridge is found at 500mm/s and the lowest eigenfrequency is out of range of that of joggers. The sensitivity analysis shows that the parameters having the most influence on the bridge's response are the diameter of the glass diagonals and the soil density. Using the outcome of the sensitivity analysis a dynamic testing protocol is recommended that outlines the optimal test setup for modal testing of the bridge. Through the simulated dynamic tests ten of the twenty eigenfrequencies of the bridge are found. For each of these frequencies, the damping is approach and modeshapes are reconstructed based on the imaginary plots of the Frequency Response Functions. The latter show a good correlation with the modeshapes obtained from the model.

Contents

List of Figures

List of Tables

The first phase gives an introduction to the Glass Truss Bridge, a pedestrian bridge built at the University of Technology in Delft, where glass is used as a structural material. It also defines the aim and methodology of this graduation thesis and gives examples from literature.

1

Introduction

Figure 1.1: Plots of different Glass structures [pictures retrieved from Octatube, Iculture and Inspiration Detail on 21-3-2020] [27]

Structures which consist of a large amount of glass are generally considered aesthetically attractive because of their transparency and brightness. The more glass, the more open and light a structure appears to be. The glass used in most buildings does not have any structural function, it merely gives resistance to a wind load when it is used in a window. The glass research group of Delft University of Technology has investigated the design of structural glass elements, among which transparent glass columns which can take axial forces. These columns could be used in buildings, bridges or other structures. A first application of such glass columns is realized by implementing these elements as diagonals in a truss bridge, see the lower left picture of figure 1.1.

Some examples of structures where glass is used in a structural sense are depicted in figure 1.1. The first picture is the Markthal in Rotterdam where the façade consists of a great glass panel connected to several horizontal and vertical steel strings making use of the principle of a tennis racket. The interesting thing of this concept is that the facade can deform horizontally to a maximum of 70cm during high wind loads. The second photo shows a glass structure that is the entrance of the Applestore in Shanghai providing light for the underground store. Here the glass is formed in a cylindrical shape and the structure makes use of glass fins which ensures the stabilization of the whole. Then the Chanel

store in Amsterdam is depicted, which façade is made of structural glass bricks glued together with a transparent high-strength glue. The upper rightmost picture is the Zhangjiajie bridge in China where the walking deck is made out of 120 glass panels providing a great view over the 300m wide valley between two cliffs in the Zhangjiajie park. The lower two pictures are the glass truss bridge built at the University of Technology Delft (left) and the glass bridge in the Basilica of Aquileia, Italia (right) where laminated glass beams are used.

Glass has been increasingly used as load-bearing material in past decades. Although it is a new solution for constructions, glass is increasingly used for roofs, façades and footbridges as observed in the examples given before. However, challenges when constructing with glass still exist and special care should be given at the design stage to ensure fail-safe requirements, as well as also in the service life of glass structures [8]. The prediction of the response of glass systems under dynamic loads (seismic events, human-induced vibrations, impacts, etc.) is still a great challenge. More knowledge is needed about some key input parameters like stiffness- and damping properties, restraint conditions and contact details to predict the dynamic behavior and serviceability of glass structures. With this information it will be possible to design optimally, avoiding over-engineering.

In this thesis the focus is on predicting the dynamic behaviour of hybrid glass-steel structures. The glass truss bridge built at the TU Delft mentioned previously (figure 1.1) will be used as a case study. Section 1.1 gives a short introduction to this bridge as it is built on the "Green Village" at the campus in Delft after which the problem description and research objective are listed. Chapter 2 gives an overview of the relevant literature. In chapter 3 an example of previously made sensitivity analyses for existing footbridges is given. In chapter 4 the case study is treated, here the relevant information of the glass truss bridge is listed. Chapter 5 is a description of the simplified finite element model. Chapter 6 gives the protocol for the Hammer test which is performed on the Finite Element model of the glass truss bridge.

1.1. Glass structures

In general most bridges are constructed of steel and concrete. However there is a growing importance of sustainability and a scarcity of natural resources. This has led to innovative developments in the construction sector as is using glass as a load bearing material. The use of glass in structures is not new, the first large-scale glass construction was the Crystal Palace dating from 1850. This building, being more than 92.000 square meter, was designed by Joseph Paxton, a gardener. It was constructed with 300.000 pieces of glass. The glass used in the Crystal Palace could be seen as an example of glass used in a structure, it needed to withstand wind load and other influences of outside climate. However this is called a secondary structure. What we are interested now is the use of glass in primary structures. Therefore, glass structures have to be robust (Eurocode). In previous section several examples are given of buildings and bridges where glass is used in a load bearing sense (1.1). Another example of a bridge where glass is used as a primary structure is the bridge in Rotterdam designed in 1994 by architect Dirk Jan Postel. The bridge spans the 3.5 meter wide space between two buildings in the city of Rotterdam 1.2.

The Glass & Transparency Research Group at TU Delft focuses on new and sustainable glass solutions for buildings, bridges and other structures investigating their structural performance. Next to the static structural performance, it is also important to look at the dynamic performance of the structure. Due to the slenderness of the structural elements when using glass as a structural material in bridges, 1.2 the structure might be susceptible to vibration problems. Currently, a lack of experimental data on the dynamic characteristics of glass structures is hindering their application and development of the design guidelines.

Figure 1.2: Glass bridge, Rotterdam, the Netherlands

1.2. Technical challenges

Glass has different physical causes of failure. Although the strength of glass depends heavily on material properties such as ductility and impurities, research shows that the failure behaviour of glass is mainly contributed by geometrical imperfections rather than its material properties [30]. Compared to steel, when loaded in tension, steel tends to yield at a particular stress (the yield strength, a known material property depending on the steel type) while glass has a theoretically very high ultimate strength, due to the chemical bonds within the glass, but fails at a very low tensile stress. This is mainly attributable to geometrical imperfections within the glass (scratches, bubbles or microscopic flaws) causing stress concentrations and significantly decreases in tensile strength at those imperfect points. Therefore, knowing the theoretical material properties, like the ultimate strength of glass, is not enough to predict the failure behaviour of a piece of glass [31]. More important is the production process giving information about possible imperfections and their direction.

In the construction industry brittleness - a materials'property of showing little deformation or ductility before fracturing rapidly [27] - is not a desirable property, it is preferable that a material gives a warning by showing deformation prior to failure. When using concrete, this problem is solved by adding reinforcement steel, in that way, when the concrete is loaded in tension the steel is activated allowing the concrete to crack without the structure failing. In other words, robustness is needed when designing glass structures. In that way failure of one component does not endanger the stability of the whole structure leading to collapse.

Three levels of ensuring redundancy can be distinguished [15]. The first is at component level, here sacrificial layers which are not considered in the calculations provide extra capacity. Beside giving a warning, these layers are also facilitate maintenance as they are easy to replace. The second is at structural level. In case of failure of an individual element alternative load paths may provide redundancy to the structural system. The third level is at material level and is divided into thermal and chemical treatment. The main principle used during thermal treatment is the differences in temperature drop between the inside and outside of the material. The outer edge is cooled down, while the inside is still hot. When the inside cools down it tries to shrink and thus pulls on the already cold outer surface causing a compression in the outer surface. Chemical treated glass is put in a potassium-salt bath. The principle is ionic exchange, large sodium ions in the molten salt bath replace the smaller ions in the glass surface. This also results in compression in the outer surface.

In the design of the Glass Truss Bridge the second redundancy level consists of the different glass rods: in case of failure of one or more glass rods the load can still be beared by the other rods.

1.3. Introduction to the glass truss bridge

The bridge is designed by the Glass and Transparency Research group and located in Delft. It forms the entrance to the 'Green Village', a quiet environment which makes it a perfect place to carry out measurements. The main goal of this Glass Truss Bridge is to gain knowledge of the different aspects of glass in the structure. Tests can be carried out and measurements can be taken to compare life results with numerical predictions. The bridge is designed as a temporary footbridge with a span (L) of 13.5 m and a width (b) of 2 m 1.4. The structural part of the bridge consists of two trusses in a lenticular form. The depth (c) in the middle is 1.5 meter to have a 1 to 10-15 ratio with the span of the bridge 1.3. The upper chord has a HEA120 steel profile to account for the secondary bending between the nodes of the truss. The lower chord is made of a steel strip to be able to resist large tension forces [27].

The structural safety of the glass components is guaranteed using a bundle of small massive glass rods. This is a common and safe way of designing with glass as failure of one or two glass elements does not immediately lead to collapse, but replacement of the broken element needs to be done in the short future [19]. In the center of the glass bundle a steel rod is placed. Glass can resist high compressive stresses (even higher than concrete) and steel can resist high tensile stresses. Combining these two materials and prestressing the bundle, leads to a capacity for high compressive and tensile forces [27].
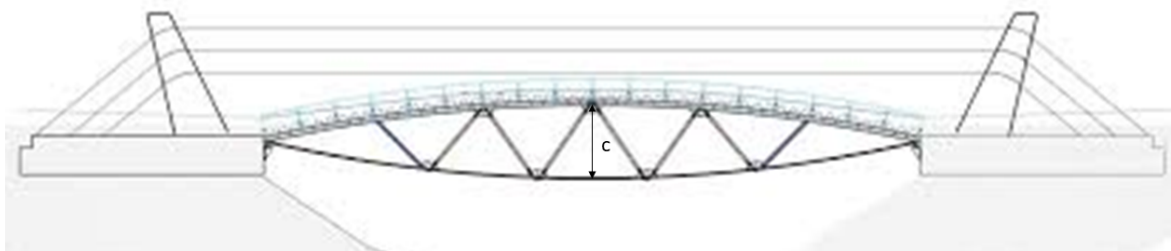
Figure 1.3: Side view bridge [27]
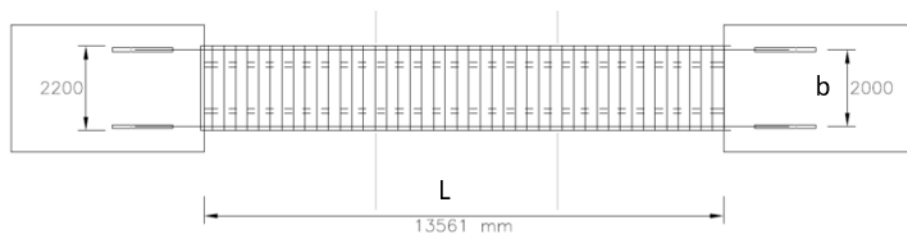
Figure 1.4: Plan view of the Glass Truss Bridge [27]

1.4. Structural properties of the Glass Truss Bridge

In 2018 a structural analysis is performed on the glass truss bridge [27]. The consequence class of the bridge was CC1 (low consequences of failure) and the reliability class RC1 (high level of reliability) [3]. In this analysis four load cases have been examined as can be seen in figure 1.5. The load cases were chosen according to NEN-EN 1991-2. A horizontal load of ten percent of the live load has been taken into account. The four load cases are stated hereafter:

  • LC1: Two point loads of 80kN and 40kN representing an emergency vehicle

  • LC2: Live load of crowd of 67 students on entire bridge

- LC3: An asymmetric live load on one half of the bridge

- LC4: The point loads from the vehicle and one diagonal collapsed

The first load case (LC1) resulted in a mid span deflection of 21mm, the second load case gave a deflection of 25.5mm, the third 25.6mm and the fourth case 38.1mm. The results are also stated in the subscript of each subfigure in figure 1.5.
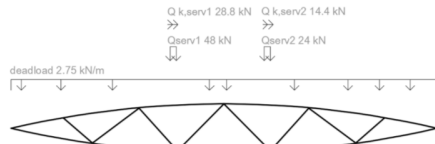
(a) 1a: Emergency vehicle. Deflection: 21.0 mm
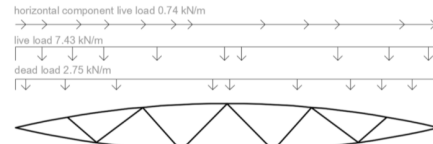
(b) 1b: Crowd load. Deflection: 25.5 mm
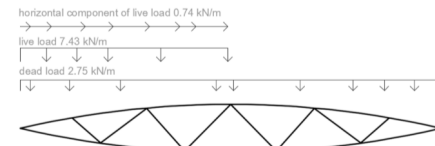
(c) 1c: Asymmetric crowd load. Deflection: 25.6 mm
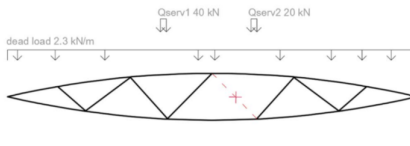
(d) 1d: Emergency vehicle and one diagonal collapsed. Deflection: 38.1 mm

Figure 1.5: Plots of different load cases [27]

The maximum axial forces were calculated in Ultimate Limit State[1] (ULS), from left to right each glass-diagonal is given a letter A to F. The results are listed in table 1.1.

Glass diagonal	Load case 1	Load case 2	Load case 3	Load case 4
A	-10.4	-2.23	-31.3	-26.3
B	-5.29	-16.9	-11.2	-17.0
C	-7.51	7.69	-2.88	3.56
D	-8.49	-18.2	-26.0	X
E	-4.19	11.1	13.4	-9.82
F	-11.2	-11.5	-27.8	-31.6

Table 1.1: Results of static calculation of the Glass Truss Bridge. Forces are shown in kN [27]

From table 1.1 it can be seen that maximum tensile stress is found in diagonal E during load case 3 (asymmetric live load on one half of the bridge) whereas maximum compression is found in diagonal F during load case 4 (emergency vehicle passing and one diagonal collapsed). As mentioned before each diagonal consists of 6 glass rods, providing robustness to the whole structure. The connection of the diagonals with the steel beam are addressed in this report as nodes. More detailed information on the diagonals, the nodes and how the structure is connected to the shore (i.e. the supports) is elaborated in next section.

1.4.1. Nodes and supports

The top of the rods are held together with an aluminium head to account for the differences in length of the individual glass rods. The surface area of the truncated end of the cone is as small as the stresses allow. This means the diagonal can still freely rotate around the node, ensuring the critical buckling length to be equal to the length of the diagonal, without accounting for bending moments that results from a fixed connection. The connections can thus be seen as hinged connections [27]. Figure 1.6

---

[1]ULS is the computational condition that must be fulfilled in order to comply with the engineering demands for strength and stability under design loads

shows the design of the nodes. Glass blocks, which were left-over from the Crystal House project in Amsterdam 1.1 (retrieved from MVDR projects) are used for the nodes, the steel rods are passing through these glass blocks. The connection is made in a non eccentric way, which means no moments are generated in the nodes connecting the glass rods with the bridge span. This is taken into account when modelling the bridge.
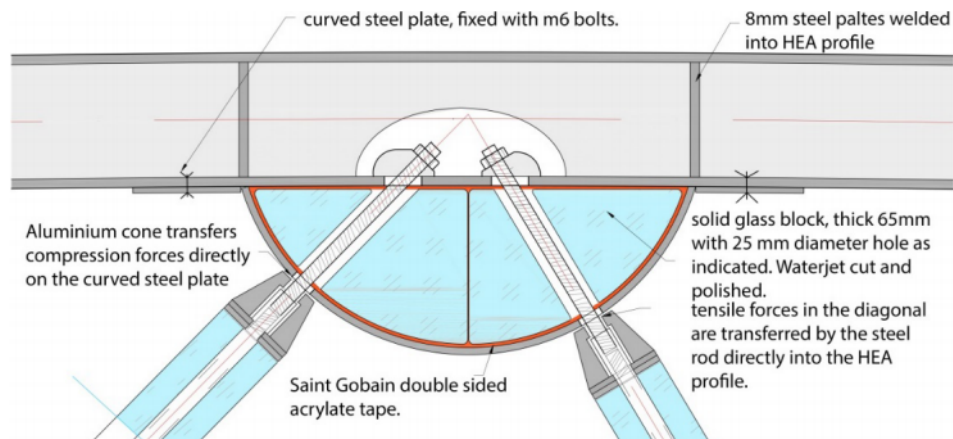
Figure 1.6: Node detail [27]

1.4.2. Glass diagonals
The cross section of the diagonals used in the Glass Truss Bridge are shown in figure 1.9. The glass diagonals are composed of six single rods bundled as one column as mentioned before. The single rods have a diameter of 22mm and lengths vary between 728-1392mm depending on the location along the bridge, (figure 1.3). The elements are glued to a hollow star shaped PLA ring where the steel rod is placed inside (figure 1.9), the star-shape helps to avoid peak stresses in the PLA ring. A steel ring is placed on top of this aluminium ring to spread the load. The bundle is post-tensioned in order to ensure a compression force in the glass at all times, as tension is an unfavourable load condition for glass. This is done using a nut on top of the steel ring. By turning the nut, the steel rod in the middle of the diagonal is tensioned, causing compression stress in the glass rods. Pre-tensioning is necessary to allow for variation in compression and tension in the diagonals, which is needed for a truss structure. For a closeup of the construction phase, see figure 1.8.
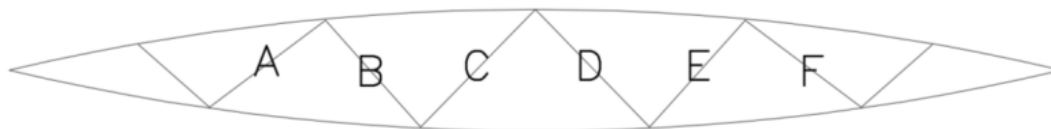
Figure 1.7: Column numbers [27]

Figure 1.8: Closeup of the diagonals [19]
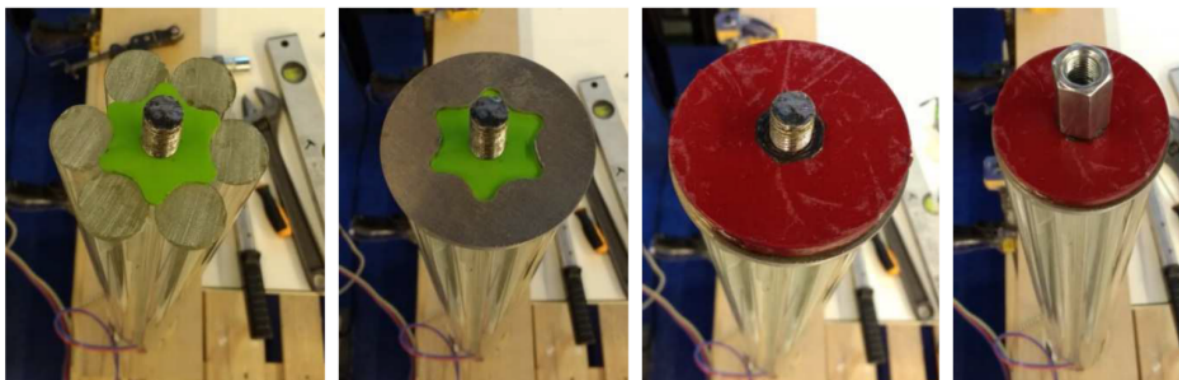
Figure 1.9: Cross section diagonals from left to right: Pretension steel rod and PLA centering ring. Aluminium ring to avoid peek stresses in PLA. Steel ring to distribute load. Extension nut to enable prestressing [31]

1.5. Problem description

In the engineering world, allowable serviceability limits (SLS [2]) are barely defined for any type of hybrid glass structures. The main problem is the lack of knowledge regarding the dynamic properties of glass as a construction material. More knowledge is needed about some key input parameters like the damping properties, restraint conditions and contact details between different elements. To gain insight into this, the Glass Truss Bridge is used as a case study.

A structure like the Glass Truss Bridge has several vibration modes which can be determined through a modal analysis. Each vibration mode has its own natural frequency. When the structure is forced at one of its eigenfrequencies it will move in a certain pattern. Some examples of vibration modes are shown in figure 1.10

---

[2]SLS is a criteria involving various stress-, deformation-, flexibility- and dynamic behaviour-limits all concerning the durability of the structure, its everyday service level and the human comfort level to be achieved.
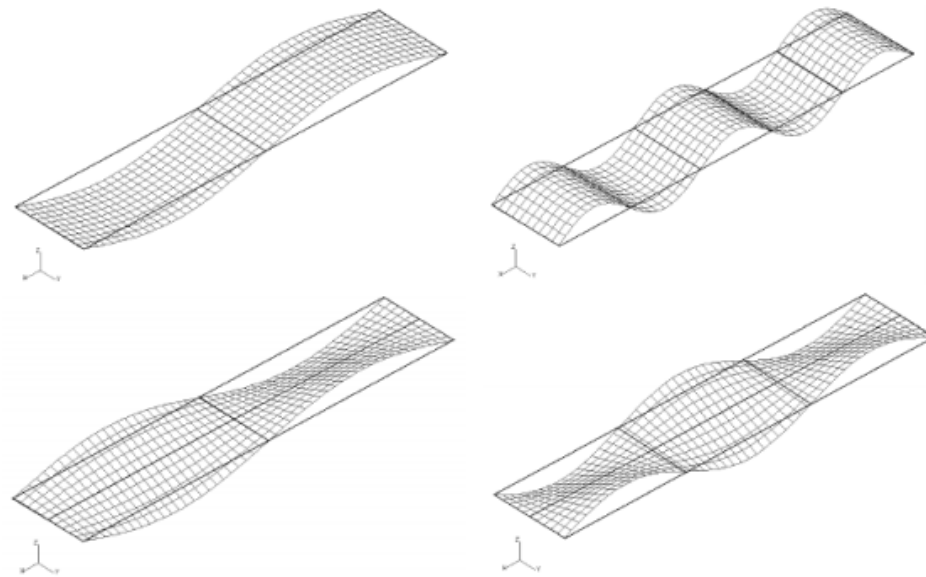
Figure 1.10: Examples of mode shapes. Top figures: bending modes. Bottom figures: torsional modes [25].

Knowing the vibration mode shapes is essential to understand the dynamic behavior of a bridge. A few cases from history show the importance of knowing the dynamic characteristics of bridges. The Tacoma Narrows bridge for example collapsed because of its extreme flexibility. The response of the bridge was a so called flutter mechanism, which is a combination of torsional and bending vibrations.

Ideally, an experimental campaign is to be carried out to test the bridge and measure static and dynamic responses. The measurements can then be used to provide an updated and calibrated version of a numerical model of the structure, tuning the uncertain input parameters. In this way increased knowledge is retrieved from the updating of finite element (FE) model, based upon prototype or full scale testing.

1.6. Research objective and starting points

The objective of this study is to predict the dynamic behavior, carry out a sensitivity study concerning the more uncertain parameters and plan a dynamic testing campaign of a glass-steel pedestrian bridge. Therefore the Glass Truss Bridge built at the TU Delft is used as a case study.

This bridge is one of the first civil structures where glass trusses are implemented as structural elements. Many aspects are uncertain and the exact response of the bridge depends on factors which are difficult to predict. The starting points are given hereafter.

- **Design** - The available information about the design of the bridge is assumed to be correct and reliable.

- **Construction** - During the construction phase of the bridge possible imperfections might have been overseen.

- **Loads** - Next to the self-weight of the entire bridge and the permanent load, being the stepping stones on top of the deck, only human induced loads are considered to be present. These loads are analysed and realistic assumptions are made based on prescriptions from European codes. Wind induced and temperature loads are neglected.

- **Model** - The connections between the glass diagonals and the steel profile are assumed as hinged connections. The properties of the glass diagonals are retrieved from earlier studies on the same diagonals.

The following research question is used to guide the study.

> **'What is the structural static and dynamic response of the Glass Truss Bridge in its current design when it is subjected to static and dynamic loading for footbridges?'**

To answer this questions it is helpful to loop through modelling, testing and updating the model by tuning the unknown parameters. Figure 1.11 shows an overview of the procedure.
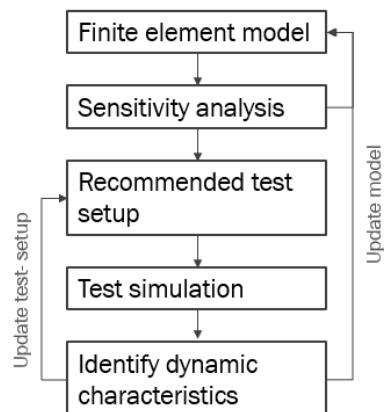
Figure 1.11: Overview of modelling, testing and updating the model

Three different phases are identified, the first phase has already been treated. Phase 2 is the modelling part where the model is built and the sensitivity analysis is carried out. In the third phase a setup for the test campaign is given and simulated. At the end conclusions and recommendations for future research are given. An overview is presented below, under each phase the sub-questions to be answered are stated.

Phase II: Numerical study of the Glass Truss Bridge

- What are static and dynamic loads where the bridge can be subjected to?

- What are the dynamic properties of the glass diagonals and how can this be implemented in a finite element model?

- What are the eigenfrequencies of the bridge in its current design?

- What are the mode shapes of the bridge?

- Which parameters do influence the dynamic behavior of the bridge?

Phase III: Recommended experimental setup for modal testing

- What are optimal locations for placing the accelerometers to measure the accelerations of the bridge to identify most of the eigenmodes?

- What are the steps that need to be taken in order to process all measurements and retrieve the dynamic properties of the bridge?

Discussion and conclusions

- Discussion

- Conclusions and recommendations

2

Example of a dynamic analysis on existing footbridges

In this chapter an example is given of a dynamic analysis done on existing steel footbridges to give an impression of possibilities about how a construction is tested dynamically. In 2013 a study is performed by van Nimmen et al. on the performance of a prediction model by comparing the numerical simulations with the measurements of the human-induced vibrations of eight footbridges 2.1. The main purpose was to evaluate existing guidelines for the serviceability of pedestrian bridges.
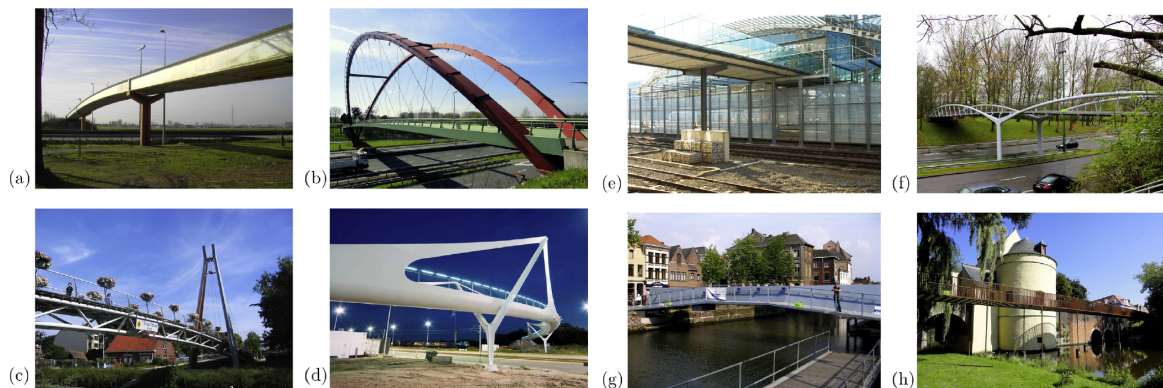
Figure 2.1: The eight case studies considered in the study of Van Nimmen [29]

2.1. Modelling framework

2.1.1. Human induced loads

Van Nimmen et al.2014 describes the walking force exerted on their analyzed bridges as a sum of Fourier harmonic components:

$$F(t) = G + \sum (G * \alpha * sin(2\pi * f_s - \theta)) \tag{2.1}$$

Where:

- G is static weight of the pedestrian
- i is the order number of the harmonic
- n is the total number of contributing harmonics
- α_i is the Fourrier coeficient of the ith harmonic normalised to the weight of the pedestrian (dynamic loading factor)
- f_s is the step frequency
- θ_i is the phase shift of the ith harmonic where the pedestrian is moving at constant speed v

The force can be represented as the product of the time component F(t) and a Dirac delta function which describes its time-dependent position $\delta(x - vt)$.

In practice, footbridges are subjected to the simultaneous actions of groups of pedestrians or crowds. This example follows prescriptions of both Setra and HiVoSS to account for a stream of pedestrians crossing the bridge. The simplified load model consists of an equivalent number (N_{eq}) of perfectly synchronised pedestrians.

$$N_{eq} = 10.8 \sqrt{\eta_j * N} \tag{2.2}$$

$$N_{eq} = 1.85 * \sqrt{N} \tag{2.3}$$

Where:

- Equation 2.2 applies for d < 1 p/m2
- Equation 2.3 applies for d > 1 p/m2
- d is the pedestrian density
- η_j is the modal damping ratio
- N is the number of people standing on the bridge

The corresponding amplitude in direction e (vertical, lateral or longitudinal) can then be defined as:

$$q_{eq,e} = N_{eq}/S * \alpha_{eh} * G * \gamma_{eh}(f_j) \tag{2.4}$$

Where:

- f_j is the natural frequency of mode j under consideration
- S is the bridge deck surface area
- a_{eh} is the dynamic load factor of the hth harmonic of the load in direction e generated by a single pedestrian
- $\gamma_{eh}(f_j)$ is the reduction coefficient that accounts for the probability that the step frequency equals the natural frequency of mode j under consideration

The mass of the pedestrians (70 kg/person) on the bridge deck modifies the natural frequencies and the corresponding modal displacements. The HiVoSS guideline states that the influence of the added modal mass (being equal to the mass of all pedestrians) is only to be considered when it exceeds 5% of the modal mass of the unoccupied bridge deck of the considered mode. According to Setra, the assessment should consider the range of natural frequencies for which the upper limit is determined by the empty footbridge and the lower limit is found by adding a uniformly distributed mass corresponding to the highest pedestrian density.

2.1.2. Acceleration levels

The maximum acceleration levels are calculated considering resonant conditions for mode j of the structure.

$$\ddot{u}_{j,emax} = q_{eq,e} * \sum (S_i |phi_{j,pe}|)/(2\eta_j) * max_p * [\phi_{j,pe}] \qquad (2.5)$$

With:

- $\ddot{u}_{j,emax}$ [m/s^2] is the maximum acceleration in direction e

- $q_{eq,e}$ [N/m^2] is the amplitude of the equivalent load in direction e

- S_i [m^2] is the discretisation of the bridge deck surface area

- p(i) is the position on the bridge deck according to the discretisation

- $\phi_{j,pe}$ [m] is the mass normalised modal displacement of mode j

- η_j [-] is the corresponding damping ratio

2.2. Results

As mentioned before, eight footbridges have been studied in Van Nimmen et al.2014. For each case, a finite element model has been built to simulate the behavior of the structure and to predict the response under human induced loading. The side views and cross sections of the bridges are shown in figure 2.1.

For all cases, an operational modal analysis (OMA[1]) is carried out. More information about OMA and other possible modal analyses can be found in Appendix B.

Van Nimmen et al. compares the FE model and the in-situ measurements. The comparison clearly illustrates that predicting the dynamic behaviour of structures is difficult, even with refined FE models. This is due to the poor prior knowledge regarding certain parameters as the stiffnesses of the supports and connections. A deviation of about 10% in natural frequency of the in-situ measurements with respect to those predicted by the initial finite element model is found.

A comparison is then made for the vibration serviceability of two bridges according to the guidelines. First, an evaluation is performed in design stage based on the FE model, second, the assessment is performed at completion. The results are presented below.

2.2.1. In design stage

In design stage, the natural frequencies and mode shapes are retrieved from the FE models. In the analysis, the modification of the natural frequencies due to the mass of the pedestrians on the bridge deck is taken into account as well. The added mass results in a lower value of the natural frequencies and also reduces the predicted acceleration levels.

Damping ratios have an important influence on the predictions but are difficult to estimate accurately in design stage. Generally, damping coefficients ranging between 0.1% and 2.0% are used.

In case of steel structures, a minimum value of 0.2% and a mean value of 0.4% are suggested. It is observed here that modal damping ratios of bending modes are between 0.15 and 0.9% whereas for torsional modes they may increase to 2% (figure 2.2). It is acknowledged that the in-situ defined damping ratios also have a degree of uncertainty.

It is also found that once dense crowd conditions are considered, an increase in the acceleration levels occurs (figure 2.3). This is interesting to take into account when studying the Glass Truss Bridge, as the maximum comfort level must not be exceeded.

---

[1]Modal analysis is the process of determining the inherent dynamic characteristics of a system in forms of natural frequencies, damping factors and mode shapes, and using them to formulate a mathematical model for its dynamic behaviour.
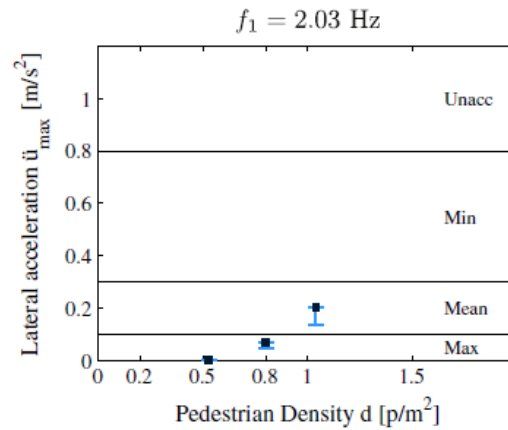
Figure 2.3: Predicted maximum lateral acceleration levels for the Eeklo footbridge in design stage according to Sétra (light) and HiVoSS (dark) for the first mode. The error bar represents the range of 10% on the predicted natural frequencies [29].
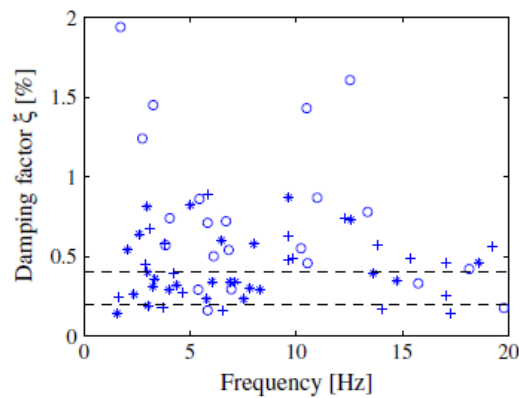
Figure 2.2: Identified modal damping ratios of the investigated footbridges as a function of the corresponding natural frequency, for (*) vertical bending, (+) lateral bending and (o) torsional modes. The upper and lower dashed line represent the mean and minimum damping value, respectively [29].

2.2.2. At completion

Once the footbridge is constructed, the modal parameters of the structure can be identified. A more reliable prediction of the expected vibration comfort of the pedestrians can now be obtained by using the experimentally identified natural frequencies and damping ratios.

Some relevant modes identified from in-situ tests are not accurately predicted by the numerical model, the finite element model should be revised. A possible solution is to tune or calibrate the FE model in order to obtain a better agreement between the calculated and identified natural frequencies and mode shapes.
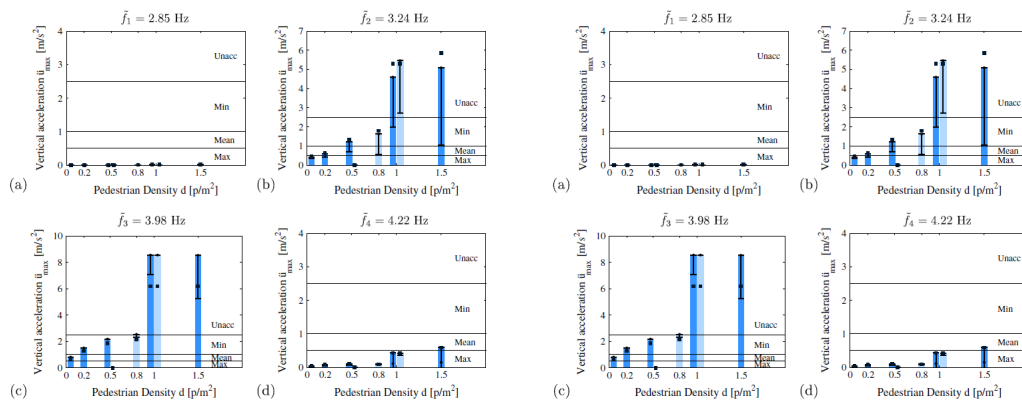
Figure 2.4: Predicted maximum vertical acceleration levels for the Anderlecht (left) and the Eeklo footbridge (right) at completion according to Sétra (light) and HiVoSS (dark) for mode 1 (a), 2 (b), 3 (c) and 4 (d) and the influence of the added mass of the considered pedestrian density (error bar). [29].

For both the Eeklo and the Anderlecht footbridge, all relevant modes were identified by the initial finite element model. The results of the reassessment of the vibration serviceability based on the in-situ identified natural frequencies and modal damping ratios, are presented in figures 2.4. The error bars present the range of predicted acceleration levels when considering the influence of the additional mass on the natural frequencies and mode shapes of the FE model. The range of the predicted acceleration levels is significantly smaller than in design stage, since the uncertainty with respect to the natural frequencies can now be excluded.

At least a comparison is made between the measured frequencies and modal damping ratios. Both Eeklo and Anderlecht performed good and the prediction was close to the measured values.

2.3. Discussion

The example shown above is one possibility of assessing existing footbridges on its dynamic performance. More examples are given in appendix G. In the example shown in section 2.2 the methodology of the codes of practice is discussed and reviewed with respect to the in-design-stage application and after construction. It is shown that dynamic properties of a footbridge are very difficult to predict and uncertainties are inevitable. Even with very detailed finite element models, deviations of 10% in terms of natural frequencies are likely to be expected. These evaluations are very sensitive to small variations in predicted natural frequencies.

A known method of matching the predictions with the measurements is using an updating model. Here some selected input parameters are updated until the eigenfrequencies and modeshapes match with the measured ones. One of the pitfalls here is that some input parameters are changed to values that lay far from their actual values, for instance the density of concrete is known to be around 2400 kg/m^3, when updating this parameter to a value of 1900, this is becoming very unlikely and also not useful for application of different models, as those in Appendix G.

The selection of the updating parameters is thus very important as well as the range of uncertainty of each selected parameter. Another important issue is to know what effect the parameter of interest has on the overall performance of the bridge. For instance if a certain parameter has a broad uncertainty range but has a negligible influence on the dynamic performance of the bridge updating this parameter is unnecessary as it will not change the outcome of the model.

To perform an estimation of the dynamic behavior of the bridge it is better to do a sensitivity analysis on selected parameters within their range of uncertainty. Once the parameters' sensitivity is known the 'best fit' can be determined using the updating method.

II
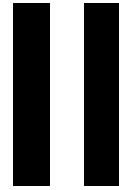
The second phase of this thesis presents and explains the numerical model of the Glass Truss Bridge together with the assumptions made. Furthermore the parameters' sensitivity on the dynamic behavior of the bridge is discussed.

<div style="text-align: right; font-size: 3em;">3</div>

Case study: The Glass Truss Bridge

Figure 3.1: The Glass Truss Bridge [1]

3.1. Load assessment

The Glass Truss Bridge is mainly subjected to pedestrian loading. Pedestrian loading is unsteady and transient and usually in a small range of frequencies. In this chapter several significant design situations will be specified (physical conditions representing the real conditions occurring at a certain time interval). Each design situation is defined by an expected traffic class and a chosen comfort level. This is done in line with Joint Research Centre (JRC) design prescriptions [14]. The procedure of how to determine the pedestrian loading given in JRC is explained briefly in this chapter.

In figure E.1 from appendix E the structure of the system of the different Eurocodes is shown. It can be seen that the guidelines for designing with structural glass are not defined. There are however guidelines for designing steel footbridges and pedestrian loads so these are elaborated and used as a guideline in this study.

The JRC report, 'Design of Lightweight Footbridges for Human Induced Vibrations', publicated in 2009 is prepared in a field where so far no unified design rules existed in the Eurocodes. Recommendations from JRC are used during this thesis to estimate the limits for the vibrations of the Glass Truss Bridge. Therefor first the traffic and comfort classification are defined after which the loads acting on the bridge are defined and a way to model these loads is given, in the end of this chapter the limit values for the lateral accelerations is given..

3.1.1. Traffic and comfort classification

Figure 3.2 depicts different load scenarios where a footbridge can be subjected to.

<div style="text-align: center;">21</div>

Figure 3.2: Traffic situations [14]

Criteria for pedestrian comfort are most commonly represented as a limiting acceleration for the footbridge. Four comfort classes are recommended and are presented in Appendix E.

Generally, the perception and assessment of motion and vibration are different for each pedestrian. Users of pedestrian bridges located near hospitals and nursing homes may be more sensitive to vibrations than for example hikers crossing a pedestrian bridge along a hiking trail.

For the current situation being a temporary pedestrian glass bridge with a life span of 5 years and situated at the campus of the University of Technology Delft, comfort class CL1 (maximum comfort) is considered. The bridge is built as an experimental bridge where students can perform lively tests. All traffic situations are possible, even jumping or marching people. This means that a traffic situation must be chosen that is expected to be critical. In this case two load cases are considered:

1. Joggers: TC2 0.1 P/m^2

2. Dense crowd walking synchronized: TC4 1.5P/m^2

3.1.2. Pedestrian load model

After assessing the design situation, i.e. traffic and comfort class, load models can be generated. Harmonic load models are given for each traffic class TC1 to TC5. Two different load models are considered for this case study.

1. Load model for TC1 to TC3 (density d < 1 P/m2)

2. Load model for TC4 and TC5 (density d > 1.0 P/m2)

Both models can be described by a uniformly distributed harmonic load representing the equivalent pedestrian stream:

$$p(t) = P * cos(2\pi * f_s t)n'\gamma \tag{3.1}$$

Where:

- $P * cos(2\pi * f_s t)$ is the harmonic load due to a single pedestrian
- P is the component of the force due to a single pedestrian with a walking frequency f_s
- f_s is the step frequency
- n' is the equivalent number of pedestrians on the loaded surface S
- S is the area of the loaded surface
- γ is the reduction coefficient taking into account the probability that the footfall frequency approaches the critical range of natural frequencies under consideration

The equivalent number of pedestrians is defined as:

$$n' = 10.8\sqrt{\epsilon * n}/S for TC1 to TC3 n' = 1.85\sqrt{n}/S for TC4 and TC5 \tag{3.2}$$

The harmonic models described above are a rough simplifications of the real load caused by pedestrians. As mentioned before walking pedestrians do not always move in one harmonic frequency, most likely the load caused by walking is unsteady and waddling. Research points out that a human body acts like a damping device itself. This is because humans tent to react on other movements causing a counter movement (for vertical displacements). This causes the vibration of the bridge to damp. The effect of damping behavior of the human body on the vibration of pedestrian bridges is currently being studied at Witteveen+Bos, no results are yet available.

Table E.2 shows the load decomposition for a single pedestrian walking over the bridge with a velocity of 1.7m/s and for a jogger running with a velocity of 3m/s. For joggers the load which needs to be taken into account is only in vertical direction. The equivalent number of pedestrians is also defined in table E.2. Figure 3.3 shows the reduction coefficient to be taken into account for both load cases. The second harmonic is also shown.

	Vertical	Longitudinal	Lateral
LC2	280	140	35
LC4	1250 N	-	-

Table 3.1: Components of force P caused by a single walker or a single runner
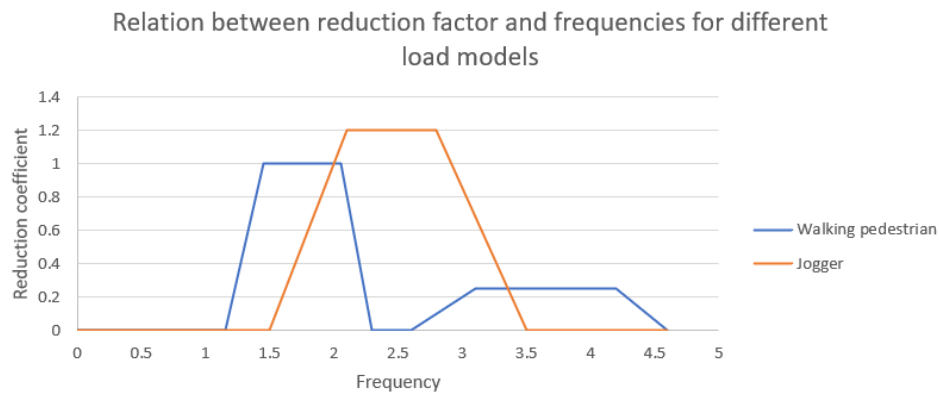
Figure 3.3: Reduction coefficient for load models TC2 (walking pedestrians) and TC4 (joggers) according to [14]

According to European guidelines the maximum allowed acceleration of a part of the deck are the following:

- 0.7 m/s^2 in case of vertical vibrations

- 0.2 m/s^2 in case of horizontal vibrations

- 0.4 m/s^2 in case of exceptional circumstances of a crowd

Furthermore verification of the requirements of the comfort criteria should be made if the natural frequency is smaller than 5Hz for vertical vibrations and 2.5Hz for horizontal and torsional vibrations.

The following notes can be made for the different traffic classes: the load model for TC1 to TC3 (individuals or small groups) takes into account free movement of the pedestrians, synchronization among individual pedestrians is not likely. In the case of dense streams (TC4 and TC5), free walking is obstructed, people tend to walk slower and synchronization between individuals increases. This can lead to a lateral lock-in effect.

3.1.3. Lateral lock-in
According to literature pedestrians react much more sensibly to lateral vibrations compared to vertical ones. A pedestrian walking on a laterally vibrating bridge tries to compensate this additional movement by swaying with the bridge displacement. This behaviour is intuitive and even small vibrations cause an adjustment of the centre of gravity of the pedestrian. Research points out that people tend to walk with twice the vibration frequency to move in time with the vibration [7]. The swaying of the body causes the lateral ground reaction forces to be applied in such a way that it causes lateral resonance. Furthermore, the widening of the steps - which is a common reaction of the human body to counteract lateral vibrations - causes an increase in the lateral ground reaction forces producing positive energy in the sway direction of the bridge (figure 3.4).
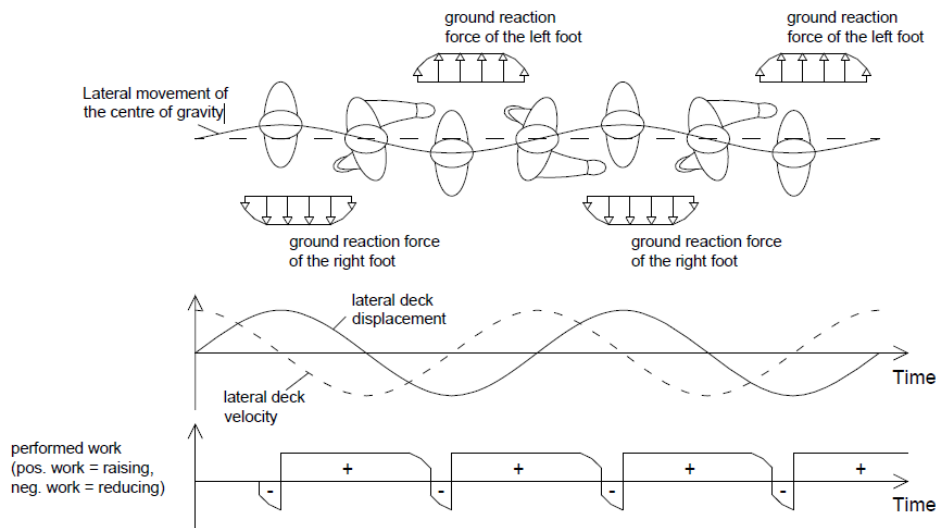
Figure 3.4: Schematic description of synchronous walking [14]

Thus, if a footbridge vibrates slightly in lateral direction causing pedestrians to adjust their walking pattern, or the phase steps of people in a crowd walking with random frequency gradually synchronizes with the deck lateral motion, a low damped bridge can be excited to large vibrations. This is called the lock-in effect and can have disastrous consequences as happened to the Millennium bridge in London at its opening ceremony [18]. This phenomena is triggered under certain conditions:

- Critical number of pedestrians
- Critical acceleration
- Self-excited lateral response of footbridges due synchronised pedestrian loading

The critical number of pedestrians can be approached by:

$$N_L = (8\pi * \eta * m^* * f)/k[-]$$
(3.3)

Where:

- η is the structural damping ratio
- m* is the modal mass
- f is the natural frequency
- k is a constant (300 Ns/m approximately over the range 0,5-1,0 Hz)

The critical lateral acceleration is:

$$a_L = 0.1 - 0.15[m/s^2]$$
(3.4)

3.2. Conclusion

The following subquestion has been answered in this chapter: *What are static and dynamic loads where the bridge can be subjected to?* The loads where this bridge can be subjected to are mainly pedestrian loads, a selection is made for the most critical loads which are joggers and a crowd load walking in sync.

3.3. Discussion

Based on recommendations of codes the critical loading was defined. It is difficult to predict what loading is most critical in terms of dynamics. When considering a fully loaded bridge (TC4: dense crowd walking synchronized) the load must be taken into account for determining the eigenfrequencies of the bridge. Due time-limitations not all possible loads were taken into account as ambient loads might be interesting to investigate as well, the focus in this thesis was on pedestrian loading.

Although it is important to take into consideration the lateral load on a bridge, in this case study only vertical bending and torsional modes are considered. The critical lateral acceleration is thus neglected. The guidelines used for defining the load for this case study are mainly focused on steel structures.

<div align="right">

4

</div>

Finite element model

In order to simulate the behavior of the bridge and numerically estimate its static and modal responses, a finite element model is created. The effects of some key input parameters on the overall performance of the bridge (such as boundary conditions, structural detailing, material properties) are investigated by doing a sensitivity analysis on selected parameters. These parameters are carefully selected based on the predicted level of inaccuracy of that particular parameter together with the influence it has on the performance of the bridge. For example the properties of the boundary restraints are not known with high accuracy although it is expected that they do have a relatively large influence on the static and dynamic performance of the bridge.

In this chapter first the finite element model is discussed, after which the selected parameters on which the sensitivity analysis is done are presented.
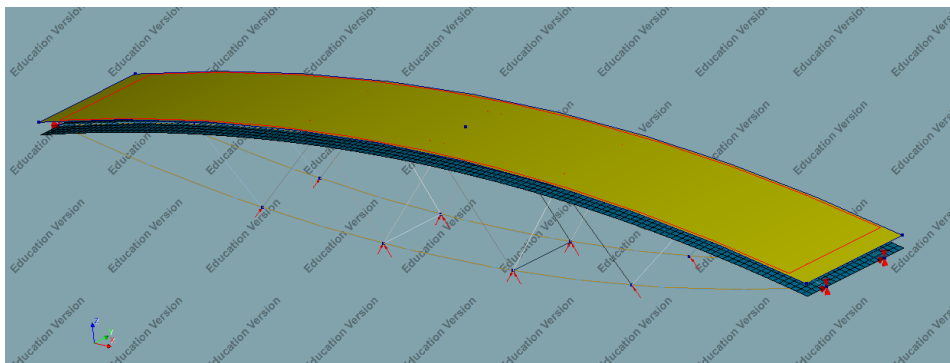
Figure 4.1: Geometry of FE model, including boundary conditions and mesh. The offset can be seen and also the prestress at the diagonals are modelled

The finite element model made in DIANA is depicted in figure 4.1, the boundary conditions and the mesh are also visible. The model consists of two beams with a lenticular form and a layered deck on top of it. The deck is modelled in such a way to account for the presence of a node at the locations of the junctions between the diagonals and the spans. To avoid overlapping of the deck and the beams, a virtual offset is applied to the deck, this is illustrated in figure 4.2.

(a) Offset explained, total offset: 182mm

(b) Closeup of FE model in DIANA
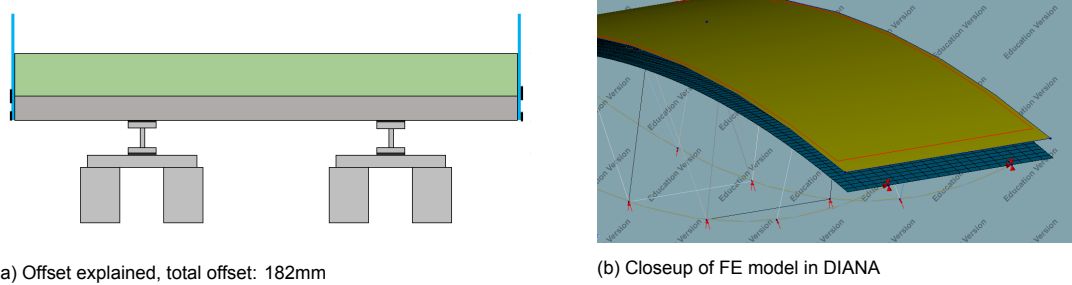
Figure 4.2: Boundary conditions of the Glass Truss Bridge, offset of the soil layer

4.1. Cross sections, element- and material properties

4.1.1. Cross sections

Figure 4.3 shows the locations of the cross section details of the FE model enumerated from 1 to 4. The dimensions of each cross section are also stated.

Steel diagonals

H = 70mm
B = 70mm
t = 4mm

Steel strips

H = 30mm
B = 120mm

Steel beams

H = 114mm
B = 120mm
t_{fl} = 5mm
t_{wb} = 8mm

Glass diagonals

d = 47mm

Eccentricity in y-direction: 6.5mm
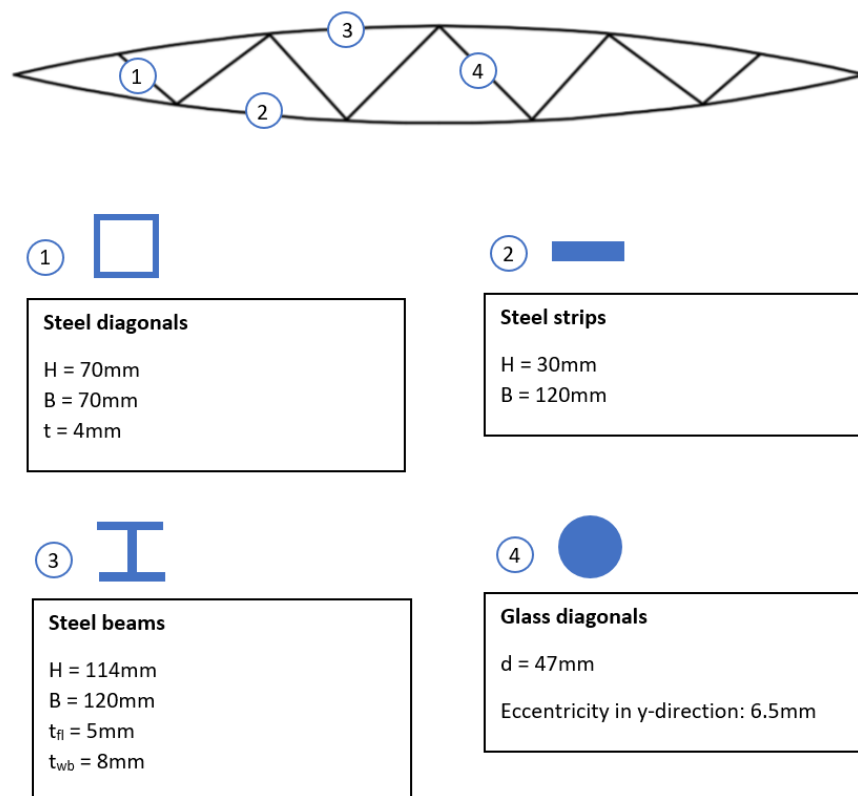
Figure 4.3: Location of cross section details and dimensions

4.1.2. Element properties

Truss, beam and shell elements are used to model the bridge. An overview of the element properties is given in figures 4.4a, 4.4b and 4.4c.

(a) CL9BEA Class III beam elements

(b) L6TRU truss elements

(c) CQ40S layered curved shell elements
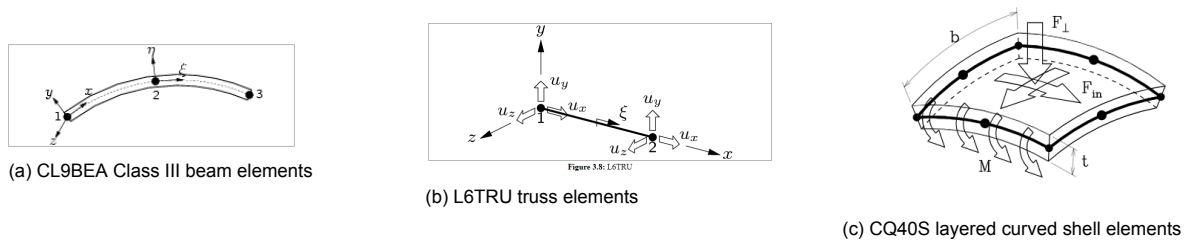
Figure 4.4: Different elements used in the finite element model

The beam elements have three nodes and nine degrees of freedom (three per node: u_x, u_y and ϕ_x). The truss elements have two nodes and 4 degrees of freedom (two per node: u_x and u_y). In the curved layered elements the thickness is subdivided in two layers. Each layer has its own material properties and is numerically integrated separately. The number of degrees of freedom of curved layered shell elements are the same as for the regular curved shell elements, namely 45 (9 nodes, 5 degrees of freedom per node: u_x, u_y, u_z, ϕ_x and ϕ_y).

4.1.3. Material properties
Glass rods

The glass rods are modelled as one rod with diameter of 47 mm and an eccentricity of 6.5 mm. This diameter is derived from the study done by Verleg, 2019. In her study the glass diagonals are tested in compression until failure. An extruded view of the physical elements used at the ends of the diagonals (the nodes) is depicted in figure 4.5.
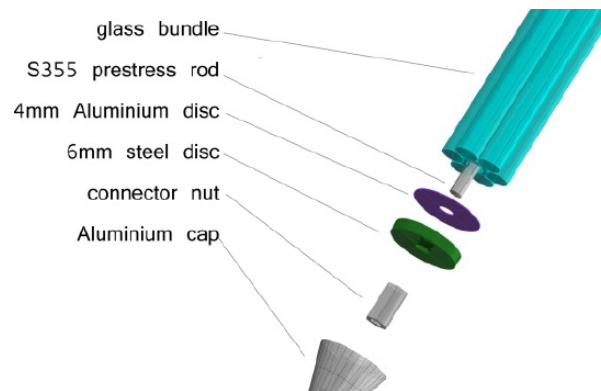
Figure 4.5: Composition of one of the ends of the diagonals [31]

One of the main findings of this research is that not all rods are activated during loading. This is due to small deviations in the length of the rods which is hard to overcome due to the production error and the error generated when placing the rods in one bundle. Aluminum is used at top of the rods, but even though aluminum is a soft material, it does not fully ensure the equal distribution of the stress over all rods [31]. The different rod configurations used in Verleg et al.2019 are shown in figure 4.6 in which a blue rod indicates it is activated. Configurations 5, 4-3 and 4-2 have highest probability of occurrence, indicating that only 4 or 5 of the 6 rods are activated when the diagonal is subjected to a compression load.
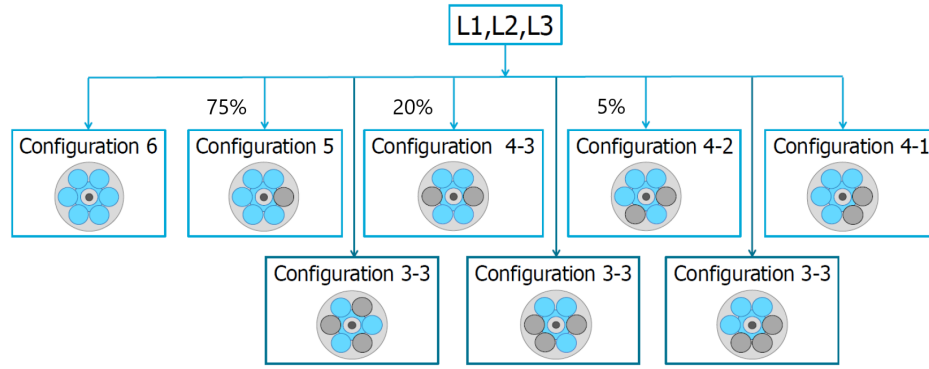
Figure 4.6: Different rod configurations and their probability of occurrence. Blue indicates activated, grey means not activated during loading. In the middle of the bundle a steel rod is depicted [31].

The equivalent area of the activated rods can be determined based on these conclusions. For comparison a different method of deriving the equivalent cross sectional area is presented hereafter. This second method makes use of the principle of in-homogeneous cross sections, mainly used for concrete sections [33]. This method takes into account the properties of the steel bar, which is present in the middle of the glass bundle. Equation 4.1 shows the formula for calculating the equivalent area for the diagonal.

$$A_{eq,d} = (E_{gl}A_{gl} + E_{st}A_{st})/E_{gl} \qquad (4.1)$$

Applying this formula and comparing the equivalent area using both methods gives the following results:

- Configuration 5 : 1900mm^2

- Configurations 4-2 and 4-3 : 1520mm^2

- In-homogeneous cross-section : 2658mm^2

The exact area of the glass diagonals activated during loading of the bridge lays somewhere in between 1520 and 2658 mm^2. The study of the different configurations is more reliable for this case. Calculating the mean value for the equivalent cross section with following relation:

$$A_{eq} = P_5 * A_5 + P_{4-3} * A_{4-3} \qquad (4.2)$$

Where:

- P_5 is the probability of occurrence of configuration 5

- P_{4-3} is the probability of occurence of configuration 4-3 and 4-2 together

- A_5 is the total area of 5 glass rods (the activated rods)

- A_4 is the total area of 4 glass rods (the activated rods)

This gives an equivalent area of 1805mm^2 which is used as a base value for the area of the glass rods in the FE model. The sensitivity of this parameter on the dynamic behavior of the bridge is checked in section 5.3.

The steel bar also accounts for a prestress in the glass rods. This is done to prevent the diagonals of being in tension, which, as mentioned in chapter 1 of this report, is not a preferred situation when constructing with glass. The applied prestress is equal to the highest stress acting in one of the diagonals modelled as a force acting in the axial direction of the diagonals (figure 4.7).
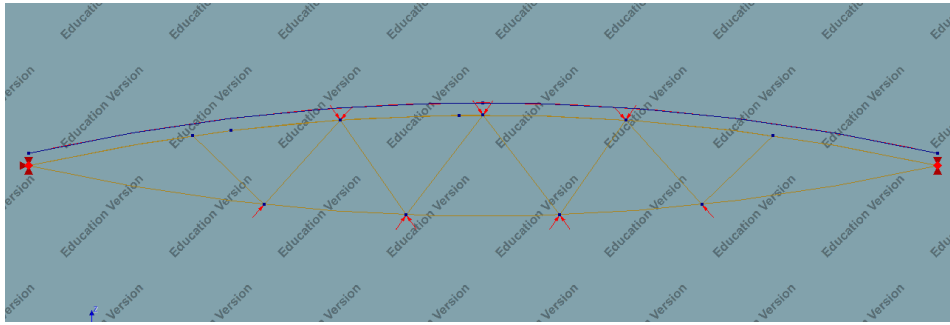
Figure 4.7: Prestress acting on all glass diagonals

Soil deck

The deck of the bridge is modelled with layered curved shell elements. It consists of a corrugated curved steel sheet with a layer of soil, partly covered by pavement and grass on top, also shown in the technical drawings in appendix A. It's geometry gives the steel sheet different material properties in each direction. To account for this phenomenon, orthotropic material properties are assigned to the steel sheet.

Figure 4.8: Paper folded up and down [retrieved from DeKleineLadder on 1-07-2020]

The steel sheet's orthotropy can be visualised with a paper sheet folded alternately up and down (figure 4.8). The two different in-plane directions are: 1. The direction perpendicular to the corrugation (x) and 2. The direction parallel to the corrugation (y). The sheet can barely take any tension in the x-direction and it will immediately start to extend when a force is applied, flattening out the paper sheet. In this direction, large deformations are generated with a relatively small force. In the y-direction the material behaves much stiffer. It can take much more tension leaving the geometry undeformed.

When looking at the deformations out of plane, boundary conditions play an important role. When the sheet is spanned in the direction perpendicular to the corrugations, the sheet acts very flexible and starts to bend almost immediately (due to only self-weight). When the spanning direction is parallel to the corrugations, the sheet behaves much stiffer 4.8.

The dimensions of the corrugated steel sheet used in the Glass Truss Bridge 106R/750 are as follows (figure 4.9).
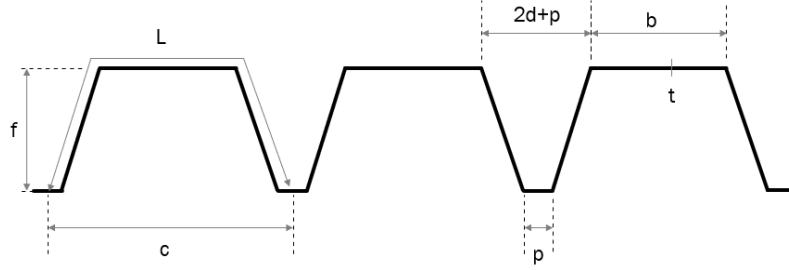
Figure 4.9: Cross section of corrugated steel sheet 106R-750

Parameter	Value	Unit
f	108	[mm]
L	402	[mm]
c	172	[mm]
d	38	[mm]
b	134	[mm]
p	40	[mm]
t	1.5	[mm]
θ	1.23	rad
I_y	3.92E6	[mm^4/m]
E	2.10E5	[MPa]
v	3.00	[-]
ρ	7.85E-9	[T/mm^3]

Table 4.1: Dimensions of corrugated steel sheet

Assuming the sheet used in the bridge is a large corrugated sheet, i.e. the corrugation size is small in comparison to the overall size of the sheet. In that case the sheet can be modelled as a thin orthotropic plate with the stress-strain relationship as presented in equation 4.3.

$$\begin{bmatrix} \sigma_x \\ \sigma_y \\ \tau_{xy} \end{bmatrix} = 1/(1 - v_{xy}v_{yx}) * \begin{bmatrix} E_x & v_{xy}E_x & 0 \\ v_{xy}E_x & E_y & 0 \\ 0 & 0 & (1 - v_{xy}v_{yx})G_{xy} \end{bmatrix} \begin{bmatrix} \epsilon_x \\ \epsilon_y \\ \gamma_{xy} \end{bmatrix} \tag{4.3}$$

For an orthotropic, thin plate, the flexural rigidity's are expressed by the following relations. In these expressions the Moduli are different for each direction (E_x, E_y and G_{xy}) and the thickness is the equivalent thickness of the orthotropic sheet calculated with $t_o = A_c/L_o$ where L_o is the length of the orthotropic sheet which is taken as 1m (i.e length of 5 corrugations).

$$D_x = E_x t^3/12(1 - v_{xy}v_{yx}) \tag{4.4}$$

$$D_y = E_y t^3/12(1 - v_{xy}v_{yx}) \tag{4.5}$$

$$D_{xy} = G_{xy} t^3/6 \tag{4.6}$$

Flexural rigidity's are calculated using the relations from equations 4.7 4.8 4.9 based on models from Samantha and Mukhopadhyay [32].

$$D_x = c/l * E t^3/12 \tag{4.7}$$

$$D_y = E I_y/c \tag{4.8}$$

$$D_{xy} = l/c * E t^3/6(1 + v) \tag{4.9}$$

Where:

- E is the Young's Modulus of the material

- v is the Poisson's ratio

Using 4.7 to 4.9 in the relations 4.4 to 4.6 and the parameters presented in figure 4.9 the Young's Moduli for the different directions (x, y) are determined.

To determine the extensional rigidity's a set of different relations is used (equations 4.10 to 4.12). The symbols D_e and E_e are used to distinguish from the flexural expressions.

$$D_{e,x} = E_{e,x}t \tag{4.10}$$

$$D_{e,y} = E_{e,y}t \tag{4.11}$$

$$D_{e,xy} = G_{e,xy}t \tag{4.12}$$

With relations

$$D_{e,x} = E(t/f)^2 t/6[(2/c)((c - lcos(\theta)/(1 - cos\theta)) + (4f/3sin\theta)] \tag{4.13}$$

$$D_{e,y} = Etl/c \tag{4.14}$$

$$D_{e,xy} = cEt/2l(1 + v) \tag{4.15}$$

Four finite element models have been built in DIANA (figure 4.10 to determine the orthotropic properties of the corrugated steel sheet used in the Glass Truss Bridge. Four different load cases are tested: a unit distributed load in the two in-plane directions, x and y, and a distributed load in the out of plane direction, z. The latter is applied to the sheet spanned in two different directions, one is spanned in the x-direction perpendicular to the corrugation, and the other is spanned in y-direction parallel to the corrugations (the stiffer direction). Unit loads are applied in all load cases (see table 4.2) except for the third load case, sheet spanned in x-direction, in this case the sheet was already bending due to only self weight. An overview of the extensional and bending material properties and the loading scenarios is shown in table 4.2.

	Extensional	Bending
E_x	25.8 [N/mm^2]	1.31e5 [N/mm^2]
E_y	1.8e6 [N/mm^2]	1.17e10 [N/mm^2]
v_{xy}	4.3e-6 [-]	3.35e-6 [-]
G_{xy}	1.34e5 [N/mm^2]	2.6e5 [N/mm^2]

Load-cases	Magnitude [N/mm]	Direction
LC1	1	x
LC2	1	y
LC3	0.001	z_1
LC4	1	z_2

Table 4.2: Orthotropic extensional and bending properties derived from [32] and four different loading scenarios

(a) Model, boundary conditions and mesh: extension

(b) Model, boundary conditions and mesh: bending

(c) Validation of extensional steel properties (x)

(d) Validation of bending steel properties (x)

(e) Validation of extensional steel properties (y)

(f) Validation of bending steel properties (y)
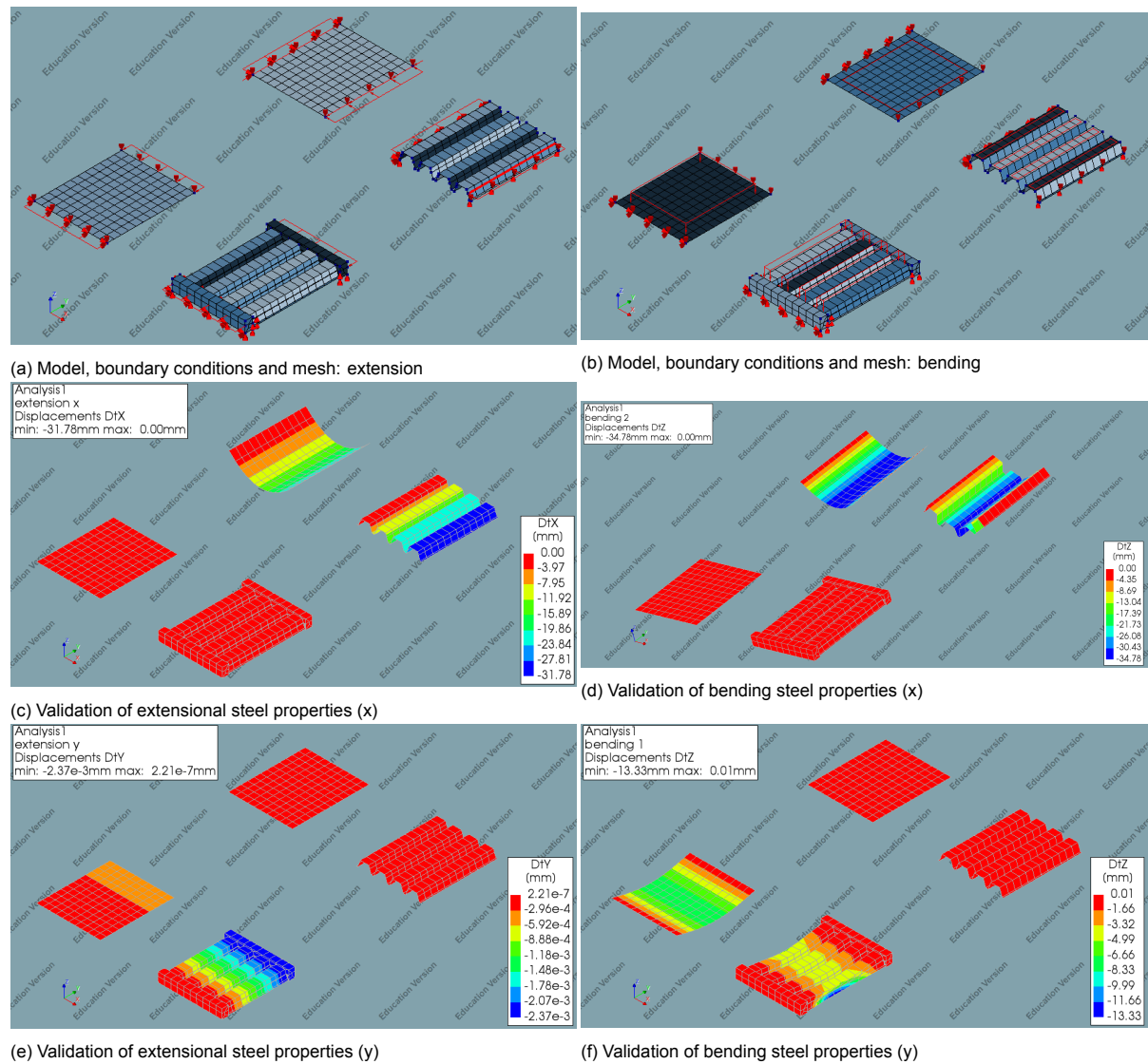
Figure 4.10: Model validation in DIANA

Results of applying the different load cases to the corrugated steel plate in extension and bending direction are presented in figures 4.10. Both bending load cases (figure d and f from 4.10) almost perfectly match the corrugated model. In the first case the model shows a deformation of 34.8mm and in the second case the deformation is 8.33mm. Figures c and e show results from the two extensional load cases. The extensional load in the x-direction (c) shows a deformation of 16mm whether in the y-direction (e) a deformation of 0.0005mm is experienced, meaning that the y-direction is the stiffer direction. The properties of the orthotropic model are inserted in the simplified model of the Glass Truss Bridge, which models the entire plate as one single element, significantly reducing the computational and modelling time.

The resulting flexural properties of the corrugated steel sheet are taken into account in the FE model of the Glass Truss Bridge. These properties are the more relevant ones for this case study, the bridge is mainly loaded in bending.

On top of the steel sheet a layer of soil is present, which has its own material property. Soils can be classified in several ways, one commonly used classification is presented in table 4.3 together with the corresponding values for the density, porosity and shear modulus [22].

Soil Type	Dry Density [kg/m3]	Porosity	Shear Modulus [MPa]
Dense sands and gravels	1442 - 2483	10^{-3} - 10^{-1}	69 - 345
Silty Sands	1410 - 2275	10^{-6} - 10^{-3}	27.6 - 138
Medium Stiff Clay	1506 - 2130	10^{-8}-10^{-6}	6.9 - 34.5
Soft Clays	1297 - 2002	10^{-10}-10^{-8}	2.75 - 13.75

Table 4.3: Typical ranges of characteristics for different types of soils [22]

Sandy soil has been used on top of the Glass Truss Bridge and results of the samples taken from the Glass Truss Bridge can be found in Appendix F.4. Based on varying density values (shown in table 4.3 the sandy top layer can be classified into dense sands and gravels. The main function of the sandy soil is to simulate the mass of the glass blocks which will be placed in the future [26].

Boundary conditions

The beams of the bridge are supported at both ends. The left supports are restrained in all directions and the right supports are restrained in y and z direction allowing the bridge to extend in longitudinal (x) direction. The choice for right boundary conditions is based on the technical drawings showing a layer of neopreen between the support and the steel beam, this means the friction between the two is low, allowing for relative displacement of the bridge (Appendix A.8). The rotational stiffness of the boundaries (k_r) are designed to be simply supported, i.e. free to rotate and no moment resistance. In practice this is not the case, the continuity of the soil might partially constrain the rotations, it can be said that the k_r of the boundaries for the case of the Glass Truss Bridge lay somewhere in between simply supported and fixed restraints. To estimate the threshold where the stiffness of these boundary conditions starts playing a relevant role in the deflection affecting the modeshapes of the bridge, an iterative analysis is performed in DIANA changing the stiffness of the rotational springs at the four support positions. Structural Linear Static analyses are performed with a specified load case: selfweight + weight of 1 person (700N). The results are depicted in table 4.4.

BC	w_{mid} [mm]
fixed	1.35
k_r = 20E6 Nm/rad	1.47
simply supported	1.6

Table 4.4: Rotational spring stiffness at both boundaries of the Glass Truss Bridge

The applied load case gives a deflection between 1.35mm (fixed) and 1.6mm (simply supported), values calculated with DIANA. A threshold of 20E6 Nmm/rad is found after an iterative analysis performed in DIANA where the rotational stiffness was updated with an increasing value starting from 500Nmm/rad, after each step the deflection of the bridge was compared with the deflection for the two limit cases (simply supported and fixed). The value of k_r is chosen so that the deflection was in between the two limit cases. This estimate of 20E6 Nm/rad is used as a starting value of the rotational springs at the boundaries to investigate the sensitivity of the aforementioned parameter (k_r) on the eigenfrequencies of the bridge.

4.2. Mesh

The mesh is generated choosing an equal element size for the entire structure. First the mesh uses an element size of h=200mm, which is equal to 1/6th of the distance between two supports (1.2m). Changing the mesh size, alters the eigenfrequencies, as observed in table 4.5, where the eigenfrequencies for the first ten eigenmodes are shown. Table 4.5 also presents the differences in percentages from the values generated with the smallest mesh size. For the 100mm mesh size the eigenfrequencies are around 0.2% larger, while some of the eigenfrequencies calculated with the 200mm mesh differ more than 1% from the smallest mesh eigenfrequencies. Since the tolerance for this study is set to 1%, the 100mm mesh will be used for further calculations.The advantage in terms of accuracy when using a 50mm mesh is rather small and the computational time is much higher.

Modeshape	$EF_{h=50}$ [Hz]	$EF_{h=100}$ [Hz]	$EF_{h=200}$ [Hz]	EF_{100}-EF_{50}[%]	EF_{200}-EF_{50}[%]
T1	5.1424	5.1498	5.1775	0.1439	0.6816
T2	7.682	7.7019	7.7406	0.259	0.7609
T3	8.05	8.0637	8.1139	0.1702	0.7924
B1	8.6503	8.6616	8.6792	0.1306	0.3337
L1	10.132	10.152	10.223	0.1974	0.8964
T4	10.213	10.236	10.324	0.2448	1.0842
L2	10.423	10.444	10.52	0.2015	1.0842
T5	10.83	10.855	10.946	0.2308	1.0686
T6	13.304	13.334	13.447	0.2255	1.0724
T7	13.849	13.884	14.017	0.2527	1.2100

Table 4.5: Eigenfrequencies for the first ten modes with different mesh size, h=200, h=100 and h=50mm (values in Hz). Computation time is 3, 4 and 14 seconds respectively

4.3. Loads

The dynamic load on the bridge is determined following European JRC prescriptions which are mainly based on the HiVoSS guidelines (Human induced Vibrations of Steel Structures).

A reference is made to chapter 3, where the assessment of the applied load for this case study is elaborated more in detail.Two different loadcases are considered, one dynamic (joggers) and one static (dense crowd). In this section it is explained how these loadcases are modelled in DIANA. The dynamic loadcase considered in the finite element model is a stream of people jogging at a constant frequency of 3 Hz. This is modelled as one point-load representing 5 pedestrians. The load is concentrated at the center of the bridge and pointing in negative z-direction with a time dependency of 3 Hz, this is according to the JRC guidelines. For an impression of the modelled load and its time-dependency see figure 4.11 and 4.12.

The static loadcase is modelled as a distributed load representing a dense crowd. A load of 1.8 kN/m is taken into account representing 67 students with an average weight of 70kg. These values are taken to match the performed live tests which were carried out on the bridge after construction [27].
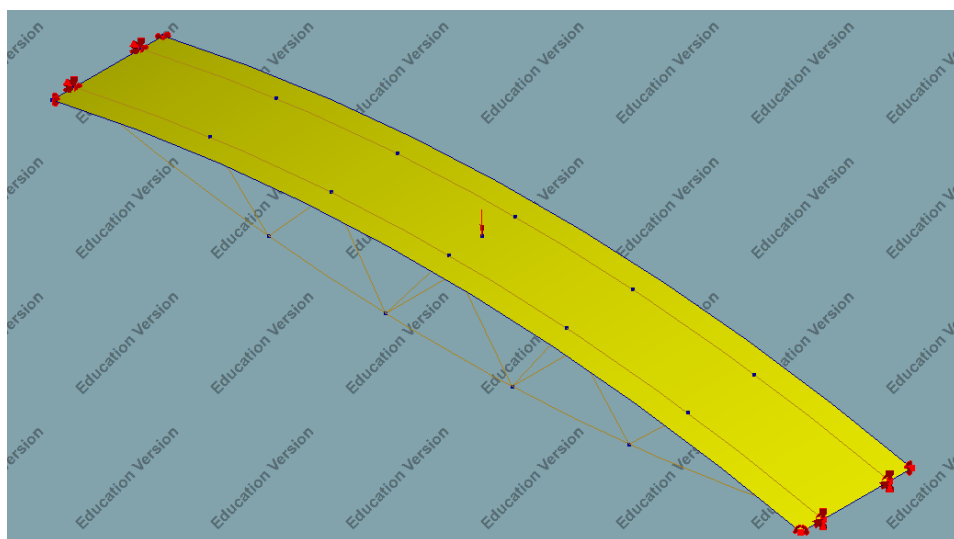
Figure 4.11: Load: Joggers running with a frequency of 3Hz (11km/h)
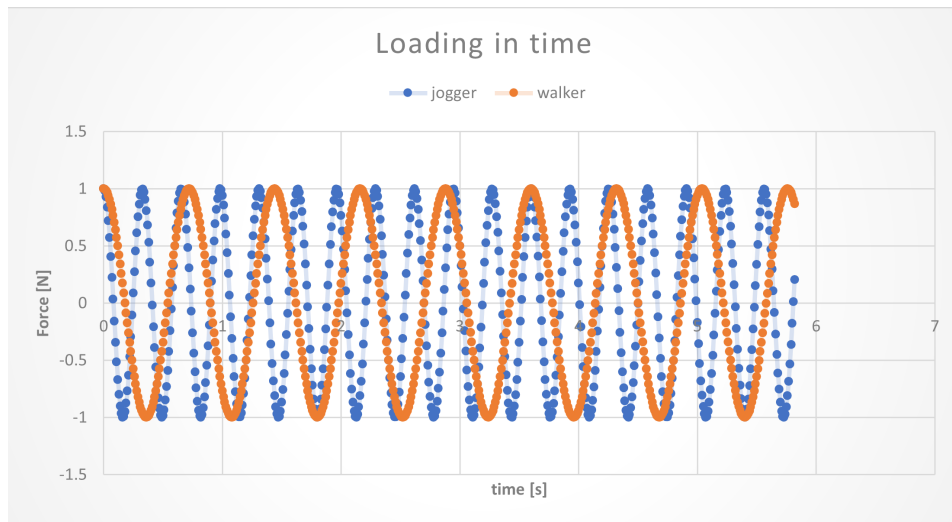
Figure 4.12: Time-dependency of jogging and walking person (3 an 2 Hz resp)

Following the prescriptions of HiVoSS an added mass must be considered when the mass of the pedestrians exceeds 5% of the modal mass of the unoccupied bridge deck of the considered mode. When considering the stream of joggers this percentage is not exceeded. Whereas when considering the second loadcase, the limit-value of 5% is indeed exceeded, meaning that in this case the added mass must be taken into account being equal to the total mass of the crowd, see table 4.6 for the calculated percentages of the load on the bridge deck.

Load-case	Amount	Total live weight	Modal weight bridge	Percentage
Joggers	5	375 [kg]	15167 [kg]	2.3 [%]
Extremely dense	42	2940	15167	19.4

Table 4.6: Percentage of live load (pedestrians) from total weight of the bridge (values in kg and %)

4.4. Model validation (static)

The model built in DIANA is tested for its accuracy by doing a static model validation. First a static analysis is performed in DIANA for two different load cases: fully loaded and half loaded. The results of this analysis is shown in figure 4.13
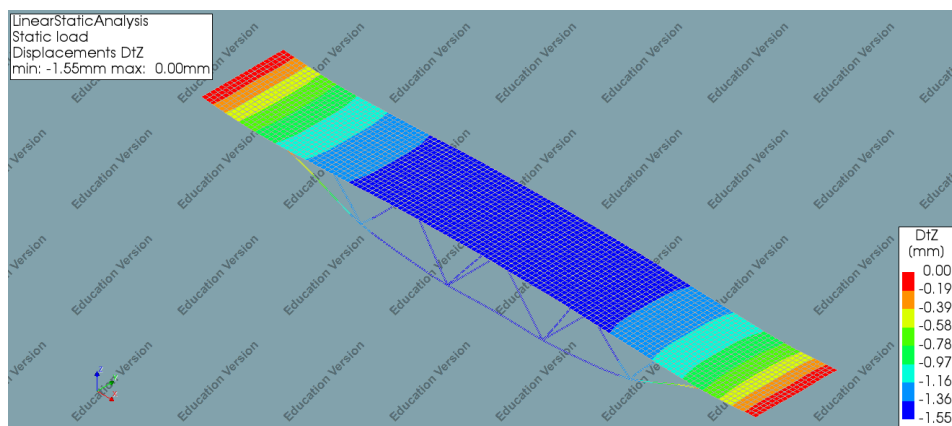
Figure 4.13: Contour plot DtZ Linear static analysis

As can be seen in figure 4.13, the maximum displacement at mid-span is 1.55mm, which is far

below the limit value of 21mm [27]. The summation of the reaction forces is equal to the applied load (this is done to check if DIANA correctly processes the introduced loads).

The results of the static analysis performed in DIANA are compared with the measurements from the tests carried out in 2018 [27]. This is done by comparing the compressive forces in the diagonals, since those were the only results available from the live tests. The comparison is shown in table 4.7. The letters assigned to the diagonals are depicted in figure 4.14
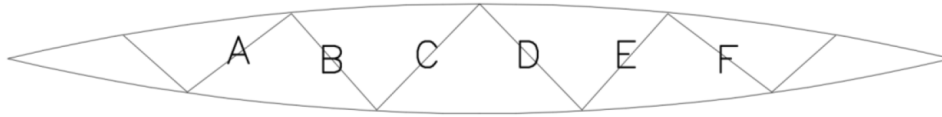
Figure 4.14: Letters assigned to diagonals

	A	B	C	D	E	F
Test fully loaded [kN]	-2.36	-0.94	-1.39	-0.99	-1.23	-2.21
FEM results [kN]	-1.94	-2.16	-1.48	-1.5	-2.12	-1.93
Difference[%]	22	56	6	34	44	145
Test half loaded [kN]	1.59	1.92	-0.21	2.52	-0.92	2.34
FEM results [kN]	-2.58	2.13	-4.20	2.32	-4.72	0.18
Difference [%]	162	10	95	9	80	1200

Table 4.7: Model validation: comparison of test results with results from FE model for the fully loaded case (top) and the half loaded case (bottom). The differences are given in absolute percentages of the test values.

Table 4.7 shows that the results obtained from the FE model show the same order of magnitude with the measured forces. The first case, when the bridge is fully loaded with students, a load of 0.026N/mm^2 is applied to the model, all diagonals are in compression. The difference between the tests and the numerical calculation are presented in absolute percentages and are in a range of 6-56%. The second case, where only the right half of the bridge is loaded with a load of 0.026N/mm^2, show higher differences, a range of 9-1200% relative to the test value is obtained.

4.5. Damping

For the design of structural damping linear viscous dampers (sometimes referred to as dashpot dampers) are generally used, which implies that the generation of damping forces is proportional to the velocity. This model has the advantage that it can be expressed in linear dynamic equilibrium equations whose analytical solution can be obtained for trivial and specific loading conditions [24]. A side note is that it only approximates the real damping of a structure for low levels of oscillation [14].

Figure 4.15 schematically presents the effect that different damping ratios have on the resonance curves. It can be seen that with a higher damping ratio the curves do flatten, meaning physically that the amplitude of the oscillation is getting smaller in time.

Most civil engineering structures are lightly damped, this is also the case for the Glass Truss Bridge, and develop low levels of stress under service loads, linear behaviour can be considered. For this case the structure is assumed to be linear and the displacements are small. Both assumptions enables the use of Rayleigh damping which allows a decoupling of the dynamic equilibrium equations. Next to that the use of the modal superposition analysis in the evaluation of dynamic effects induced by pedestrians is allowed [28].
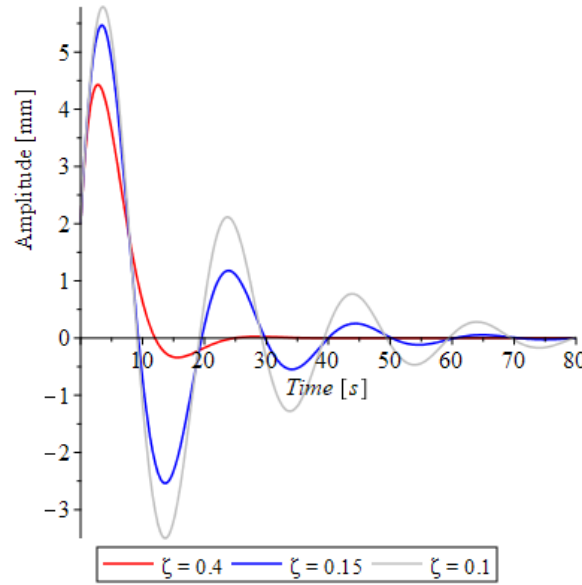
Figure 4.15: Amplitude curve for different damping coefficients, (deflections calculated with maple)

In DIANA a distinction is made between different types of damping (viscous, continuous and structural- damping). Appendix C gives a short explanation of these different types of damping. For the model of the Glass Truss Bridge viscous damping is made use of. To simulate viscous damping, Rayleigh damping coefficients are approximated.

The following relation is used to approach the damping coefficients α and β:

$$C = \alpha M + \beta K \tag{4.16}$$

Where C is the damping matrix, M is the mass matrix and K is the stiffness matrix related to the Glass Truss Bridge, α is the mass-proportional damping coefficient and β is the stiffness-proportional damping coefficient. These constants are determined based on typical damping ratios for steel pedestrian bridges, for the case of the Glass Truss Bridge the damping ratio is assumed to be 0.4 % [14].

In equation 4.16, damping matrix C satisfies the orthogonality condition, which is assumed when modal analysis is considered, this is expressed with following notation [2].

$$C_n = \Phi^T C \Phi \tag{4.17}$$

Where Φ is containing all modeshape vectors.

Figure 4.16 shows the graphical relation for the Rayleigh damping. In this graph β is the stiffness proportional damping coefficient and α is the mass proportional damping coefficient.
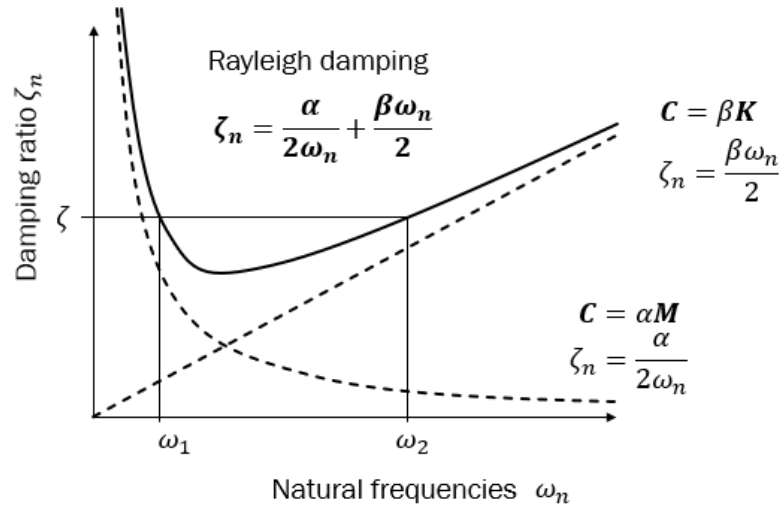
Figure 4.16: Total Rayleigh damping for modes i and j

The coefficients α and β are determined from specified damping ratios ζ_i and ζ_j using two dominating modes (i and j) [5]. The relation for ζ_n shown in figure 4.16 can be expressed in matrix-notation 4.18

$$1/2 \begin{bmatrix} 1/\omega_i & \omega_i \\ 1/\omega_j & \omega_j \end{bmatrix} \begin{bmatrix} \alpha \\ \beta \end{bmatrix} = \begin{bmatrix} \zeta_i \\ \zeta_j \end{bmatrix} \tag{4.18}$$

Two dominating modes are selected and inserted in 4.18. Mode 3, denoted as B1, and mode 9, denoted as T6 are selected. The corresponding eigenfrequencies are ω_3 = 7.6Hz and ω_9 = 12.969 respectively. Using ζ=0.004 this results in α = 0.04 s^{-1} and β = 0.0004 s. These values for α and β are are inserted in DIANA under material properties of the soil deck.

4.6. Conclusion

A numerical FE model is built for the Glass Truss Bridge using DIANA. The properties of the deck, the glass diagonals and the steel beams are discussed in this chapter. The deck consists of a corrugated steel sheet and a soil layer on top of it and is therefore modelled with layered elements, the lower layer having orthotropic steel properties assigned and the upper layer having soil properties assigned. The corrugated steel sheet has different properties for each in-plane direction, this resulted in an orthotropic layer with the following properties:

- E_x = 131000 [N/mm^2]
- E_y = 1.17e10 [N/mm^2]
- G_{xy} = 260000 [N/mm^2]
- v_{xy} = 3.35e-6 [-]

The glass diagonals were modelled as a single glass rod with an equivalent area of 1805mm^2 and a prestress of 13.5kN, modelled as a compressive force acting in the axial direction of each diagonal.

The model validation is done comparing the axial stresses in the diagonals from the FE model with the real life experiments done in 2018.

4.7. Discussion

It was not possible to validate the FE model with the available information. One possible explanation of the differences obtained by comparing the tests with the FE model is the uncertainty of some input

parameters, the soil density, the mass of the stepping stones, the glass properties and the properties of the boundary restraints are values that are assumed in the model. The prestress is modelled in DIANA as an axial force acting in the middle of the glass diagonals. A better way to model the prestress is to add a prescribed strain to the diagonals, this will prevent the (axial) force to be acting in a non-axial way when the bridge deformations are present. Furthermore the density of the stepping stones is approximated. From the photos of the bridge it can clearly be seen that the thickness of the deck is higher at the boundaries, in the model it is assumed to be equal over the length of the bridge. These assumptions and choices might influence the results of the axial forces measured in the diagonals. Another interesting remark is that from [31] it was concluded previously that not all glass rods are activated during loading, this changes the magnitude of the compressive stress which might be higher for some of the diagonals (the force is distributed over less area). Moreover this might also differ per diagonal.

A different explanation for the differences found in the axial forces of the diagonals might be that the measured values were not correctly written down in 2018, it is recommended to measure the deflection of the bridge to a specific loadcase to statically validate the FE model.

The model built in DIANA is a rough representation of the actual bridge, next to the selected parameters there are much more influences that might change the results. Assumptions are made regarding the rotational stiffness of the boundary restraints, the way of modelling the glass rods as one single rod, the vertical connections at the sides are neglected, the prestress in the glass rods is attached to the diagonals as an axial force neglecting any discontinuities in the connections. All these factors may influence the outcome of the eigenfrequency analysis and also the sensitivity analysis. This is why it is hard to predict the dynamic behavior of the Glass Truss Bridge with high accuracy.

At last the damping of a structure is a property that is difficult to predict because it depends on a lot of variables. The damping assumed in the model of the Glass Truss Bridge is the recommended damping for steel pedestrian bridges [14]. In this study a hybrid steel-glass bridge is considered, no prescriptions about the damping for this kind of bridge is given. This should be investigated more in depth to have a more reliable model of the Glass Truss Bridge it is important to take the damping into account accordingly.

5

Sensitivity analysis

A sensitivity analysis comparing the eigenfrequencies of the Glass Truss Bridge by tuning the parameters of the model is performed in this chapter.

5.1. Introduction to eigenfrequencies

To explain the principle of eigenfrequencies of a structure, an example is given of a two Degrees of Freedom (2DoF) system where a dynamic load is applied, see figure 5.1. A dynamic load is a time-dependent load, some examples are windloads, pedestrian loading or an impact load. To derive the Equation of Motion (EoM) two different formulations are commonly used. The first is based on the Lagrangian formalism, the second is based on Newton's second law, also known as the displacement method. For this example the displacement method is used to derive the governing EoM's. In appendix I the derivation of the EoM is elaborated more in detail resulting in equation 5.1.
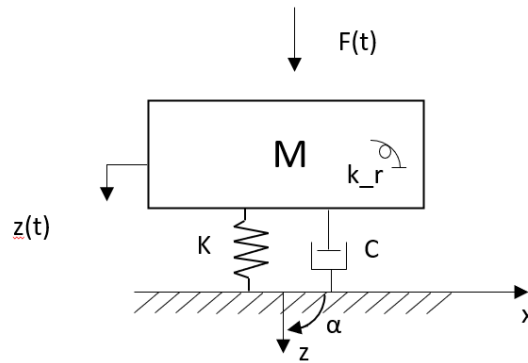
Figure 5.1: Example of a 2DoF system

$$M\ddot{x} + C\dot{x} + Kx = F(t) \tag{5.1}$$

Here, the right hand side describes the forcing side which can be a dynamic load in the form of a harmonic load, a pulse or a random excitation. The left hand side describes the structural response. The mass (M), damping (C) and stiffness (K) matrices represent all degrees of freedom possible for the structure under consideration. In this case, two degrees of freedom are considered (bending (z) and torsion (α)). The eigenfrequencies, also known as natural frequencies, can be found using an unknown amplitude vector x and an auxiliary function $e^{(i\omega t)}$. Equation 5.2 is obtained.

$$(-\omega_0{}^2 * M + K)e^{(i\omega t)} = 0 \tag{5.2}$$

Since an exponent can not be zero at every moment in time and the unknown amplitude vector being equal to zero would be a trivial solution, equation 5.3 is retrieved [28].

$$det(-{\omega_0}^2 * M + K) = 0 \qquad (5.3)$$

Solving this system of equations the natural frequencies (ω_0) are determined.

Resonance is defined as the response of a model when it is periodically forced at or close to its natural frequencies. When a structure is forced at one of its natural frequencies, physically it means that per unit of input force the response will be very large [25]. In structures, the response has to be compared with the comfort limits. As mentioned earlier not only the frequency is of importance but also the acceleration limit needs to be checked. If, when designing a structure, these limits are not complied, measures that improve the dynamic behaviour should be taken. This can be modification of the mass, loading frequency or structural damping [14]. The effect of adding dampers to the system is explained theoretically in Appendix C.

5.2. Eigenvalue analysis of the Glass Truss Bridge

A structural eigenvalue analysis is performed on the Glass Truss Bridge with DIANA to obtain the first 20 modes. The modeshapes are named after whether they are bending (B), torsional (T) or local (L) modes.

(a) Mode T1 (4.46 Hz)

(b) Mode T2 (7.2044 Hz)

(c) Mode B1 (7.8018 Hz)

(d) Mode T3 (7.8723 Hz)

(e) Mode T4 (10.313 Hz)

(f) Mode L1 (10.337 Hz)

(g) Mode L2 (10.675 Hz)

(h) Mode T5 (11.197 Hz)

(i) Mode T6 (12.969 Hz)

(j) Mode T7 (13.747 Hz)

(k) Mode T8 (14.405 Hz)

(l) Mode L3 (14.703 Hz)

(m) Mode B2 (16.539 Hz)

(n) Mode T9 (17.462 Hz)

(o) Mode T10 (18.255 Hz)

(p) Mode T11 (22.458 Hz)

(q) Mode B3 (23.108 Hz)

(r) Mode B4 (23.827 Hz)
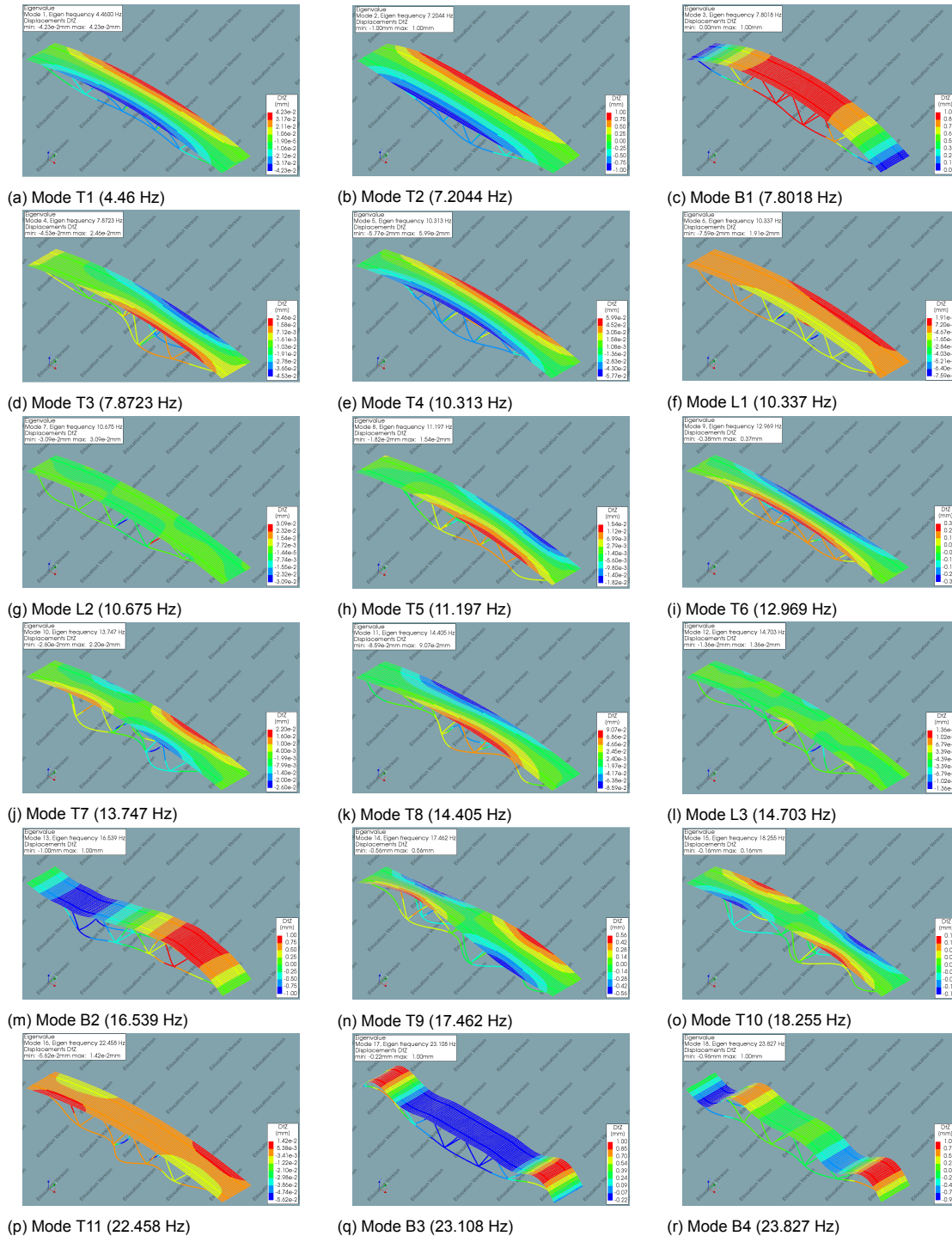
Figure 5.2: Mode shapes of the preliminary FE model of the Glass Truss Bridge, considering the base values for the aforementioned parameters

5.3. Sensitivity of different parameters on the eigenfrequencies

First the variation of the parameters to its extreme values is analysed. The effect of this change is checked for the frequencies of the first 20 modes. The mean value of each parameter is determined together with its range of uncertainty based on literature and measurements (section 4.1), from this range the extremes are taken to perform the eigenvalue analysis on the bridge. After this the sensitivity is checked by changing the magnitude of the parameter with +/-10%. The input parameters are stated in table 5.1 and in figure 5.3 the level of uncertainty of each parameter is illustrated, results of the sensitivity analysis are shown thereafter.

Parameter	min	midvalue	max	Unit
Boundary flexibility	pinned	20E6	fixed	[Nmm/rad]
Diameter glass diagonals	44	47	50	[mm]
Density soil	1250	1530	1800	[kg/m^3]
Young's modulus soil	300	350	400	[MPa]

Table 5.1: Parameters of sensitivity study, ranges according to literature [10], [31] and measurements Appendix F
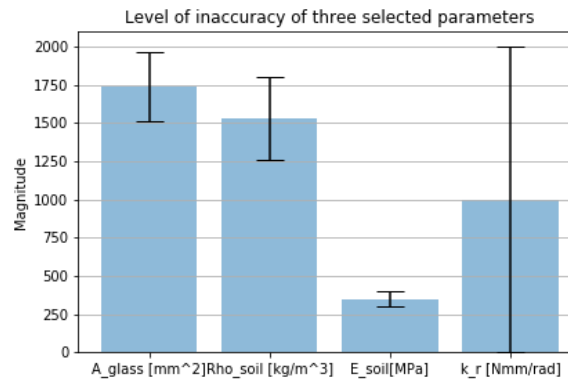
Figure 5.3: Bar plot with level of uncertainty of three selected parameter values: area of the glass diagonals (A_{glass}), soil density (Rho_{soil}), Young's Modulus of soil (E_{soil}) and boundary flexibility (k_r). The error of the boundary flexibility is between pinned (minimum) and fixed (maximum) mid-value is 20E6Nmm/rad

Mode shape	T1	T2	T3	B1	L1	T4	L2	T5	T6
rho_1	4.4685	7.8567	8.2343	8.8617	10.336	10.396	10.675	11.200	13.3749
rho_2	4.4573	6.985	7.87	7.5681	10.336	10.281	10.674	11.196	12.641
d_1	4.0729	7.4730	7.6158	8.1271	10.278	10.290	10.656	11.155	13.375
d_2	4.845	7.5304	8.1256	8.1758	10.394	10.419	10.696	11.255	13.452
E_1	4.4568	7.4019	7.8727	8.0842	10.328	10.337	10.672	11.194	13.304
E_2	4.4688	7.6081	7.8848	8.1690	10.337	10.364	10.677	11.203	13.511
k_1	4.4631	7.5081	7.8780	8.1274	10.334	10.350	10.675	11.199	13.411
k_2	4.460	7.8247	8.3058	8.3461	10.293	10.570	10.633	11.214	13.638

Table 5.2: Sensitivity study results of first nine modes, extreme values for selected parameters (all values in Hz)

Mode shape	T7	T8	L3	B2	T9	T10	T11	B3	B4
rho_1	14.070	14.981	14.703	18.837	18.038	20.154	22.482	26.277	27.191
rho_2	13.745	14.376	14.703	16.038	16.994	18.179	22.455	22.404	23.094
d_1	13.594	14.318	14.578	16.838	17.649	18.320	22.341	23.901	24.738
d_2	13.928	14.642	14.848	17.593	18.054	18.911	22.605	24.224	24.926
E_1	13.747	14.449	14.701	17.163	17.769	18.436	22.46	23.789	24.492
E_2	13.750	14.491	14.743	17.314	17.940	18.794	22.465	24.364	25.169
k_1	13.748	14.468	14.703	17.241	17.876	18.599	22.463	24.085	24.841
k_2	14.146	14.608	16.391	17.660	17.911	18.900	22.360	25.839	27.245

Table 5.3: Sensitivity study results modes 10-18, extreme values for selected parameters (all values in Hz)

The modeshapes for all parameter changes are depicted in figure appendix H. The sensitivity range is retrieved by dividing the total parameter value by the corresponding frequency and multiplying that value by the change in frequency divided by the change in parameter value. In this way the magnitude of each parameter value is taken into account when calculating its sensitivity. Following formula is used [11]:

$$S_i = 100 * (X_i/f_i) * (df_i/dX_i) \tag{5.4}$$

In figure 5.4 a diagram is depicted where the sensitivity to the extremes of each parameter is illustrated (all values are in %).
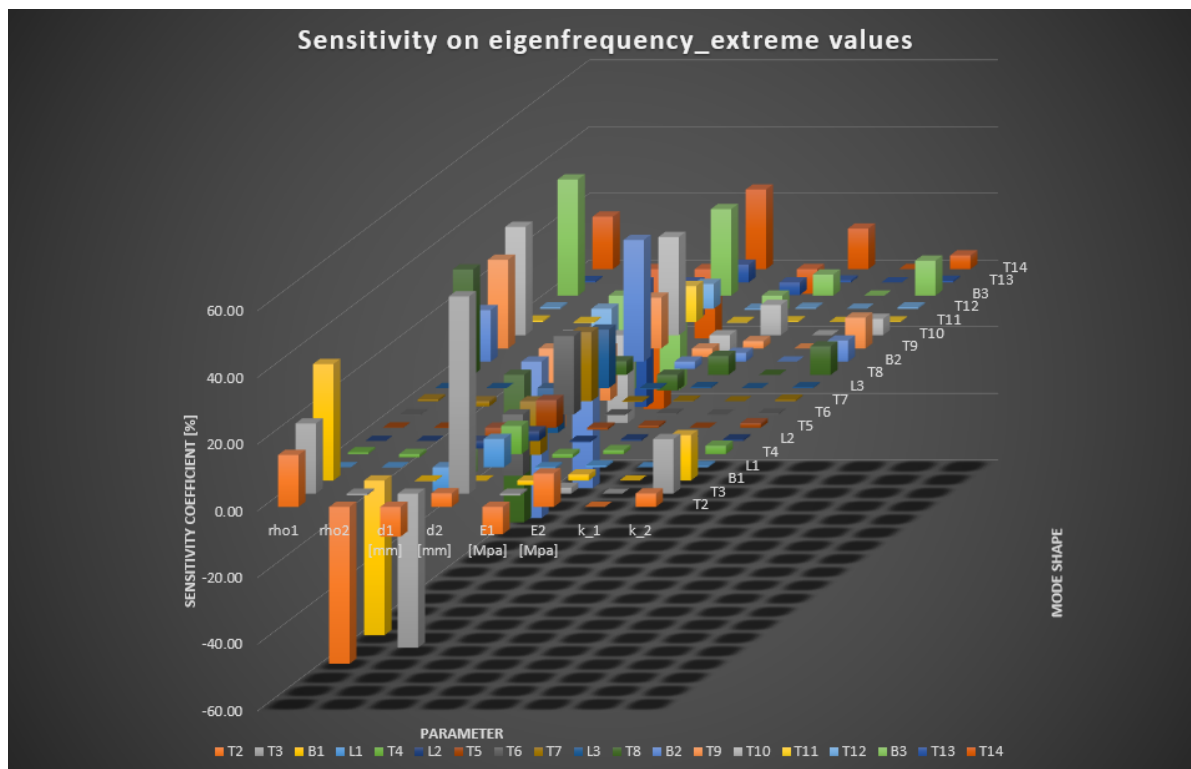
Figure 5.4: Graphical visualization of the sensitivity on the eigenfrequencies to the extreme values of the parameters. The different parameters are displayed in the lower axis, where the lower and upper value of the parameters are denoted with 1 and 2 respectively, the modeshapes are depicted on the right axis, the sensitivity is measured in terms of percentage (height of the block diagram). A positive value denotes a higher eigenfrequency.

A sensitivity study changing the parameter with a certain percentage is then performed. These results give an impression on the sensitivity of each parameter on its variation. Therefor each value is changed with 10% and the effect on the natural frequencies is checked in the same way as is done previously with the extreme case.

Results of the performed sensitivity analysis changing the parameter values with 10% up and down are presented in figure 5.5.
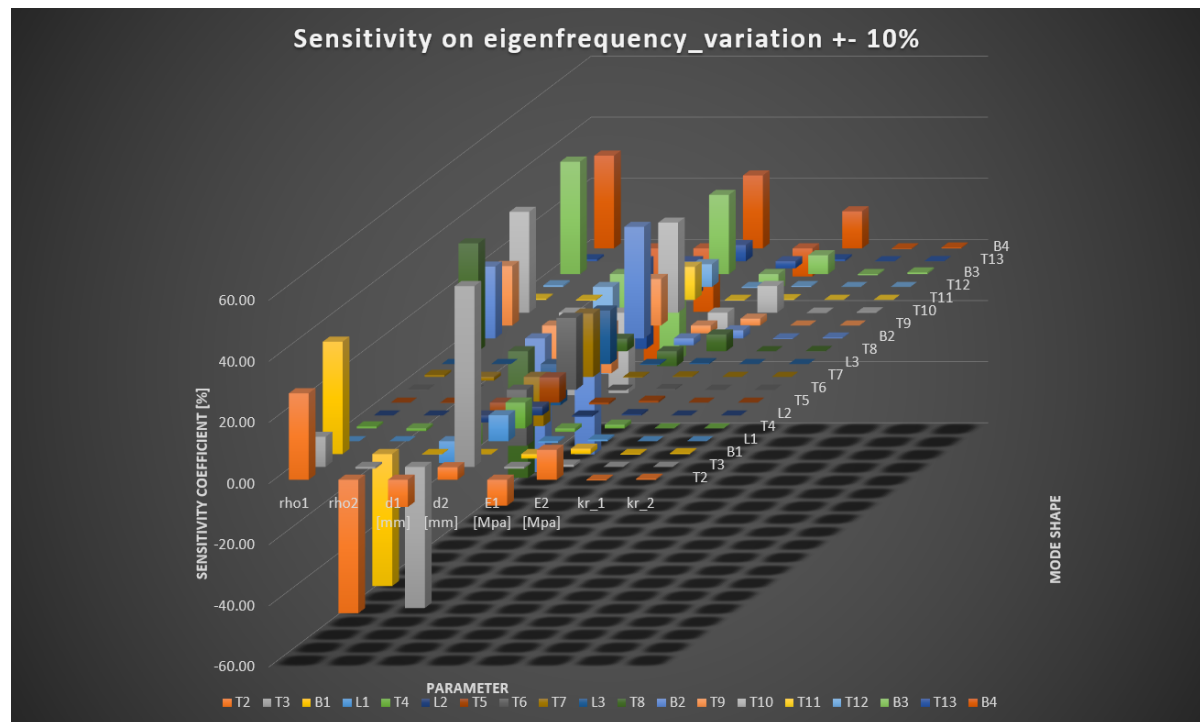
Figure 5.5: Graphical visualization of the sensitivity of the parameters on the eigenfrequencies, the parameters are displayed in lower axis, the - and + 10% are denoted with subscript 1 and 2 respectively, the modeshapes are depicted on the right axis, the sensitivity is measured in terms of percentage (height of the block diagram). A positive value denotes a higher eigenfrequency.

5.4. Analysis of the modeshapes

In H.1 the contourplots of the generated modeshapes are illustrated. The used parameter values are stated in table 5.1. In figures 5.7 and 5.6 two contourplots are given showing the minimum amount of accelerometers needed to reconstruct the selected modeshape.
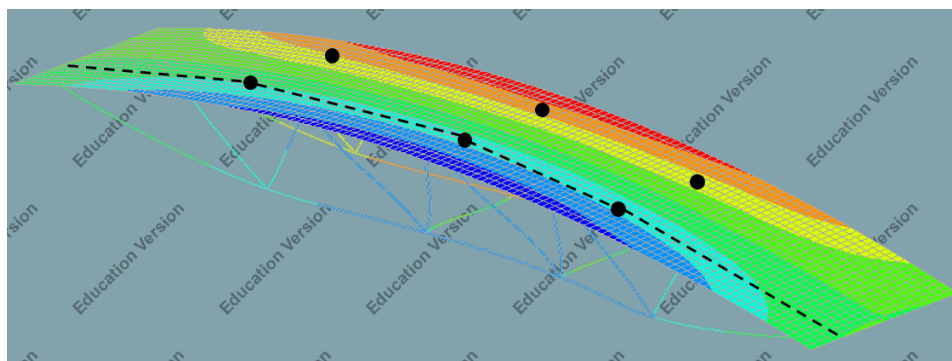
Figure 5.6: Reconstruction of T1 with 6 accelerometers
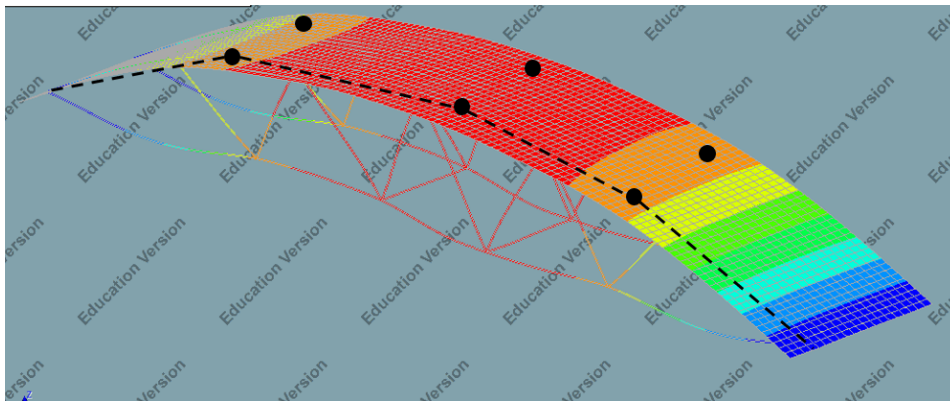
Figure 5.7: Reconstruction of B1 with 6 accelerometers

From the animated view in DIANA the countourplots are analysed more in detail and valuable information is obtained regarding the modeshapes. The diameter of the glass diagonals and the density of the soil deck are the parameters with highest sensitivity for the eigenmodes of the Glass Truss Bridge as can be seen from 5.5. Looking at the animation plots from the first 4 modes, T2 and B1 are mainly contributed by the soil deck (upper part of the bridge) whereas T1 and T3 are modes which movements are mainly contributed by the glass diagonals (lower part). In torsional mode T1 for example it is observed that the glass diagonals are moving horizontally and the deck is following this movement. An overview of all modes and their main contribution, based on the animations retrieved from DIANA, is given in table 5.4. A distinction is made between upper and lower part of the bridge, these refer to the deck-properties and the glass diagonal properties respectively. Some modes are contributed by both the soil deck and the glass diagonals.

Modeshape	Contribution	Modeshape	Contribution
T1	Lower part	T9	Lower part
T2	Upper part	L2	-
B1	Upper and lower part	B2	Upper and lower part
T3	Lower part	T10	Upper and lower part
T4	Lower part	T11	Upper part
T5	Lower part	T12	Upper and lower part
L1	-	B3	Upper and lower part
T6	Lower part	B4	Upper and lower part
T7	Upper and lower part	T13	Upper and lower part
T8	Lower part	B5	Upper and lower part

Table 5.4: Modeshapes contribution (modes 1-20). Upper part refers to the soil deck properties whereas lower part refers to the properties of the glass diagonals

From the diagram presented in figure 5.5 the parameters having most influence on the eigenfrequencies of the GTB are the diameter of the glass diagonals and the soil properties. This is in line with expectations because changing the diameter of the diagonals, the stiffness is changed giving direct influence on the eigenfrequencies and mode shapes. When changing the soil density the mass of the structure is changed, which is also directly influencing the eigenfrequencies of the bridge, see Appendix I for the derivation of the equation of motion and the relation of the eigenfrequencies with the mass and stiffness of the structure.

From here preliminary conclusions are drawn about which measurements are needed in order to fully validate the model. It was already advised by Verleg et al. to perform a hammer test in order to get clear measured data. There are however other possibilities to do a vibration test in order to update the model. In the next chapter (ch.6) a comparison is made between a hammer test and a shaker test. Based on results of the eigenvalue and sensitivity analysis two scenarios are chosen to perform the hammer test. To excite a high range of eigenfrequencies with a minimum amount of hits, the bridge should not be excited at a point where a node is present. This means no hit should be at midspan,

1/4th, 1/8th, etc. It is expected that each hammer-hit will generate both torsional and bending modes. An overview of hit points and measurement locations is presented in figure 5.8. This is simulated on the finite element model in order to validate the chosen measurement locations.

(a) Location of hammer excitation for torsional and bending modes 1   (b) Location of hammer excitation for torsional and bending modes 2
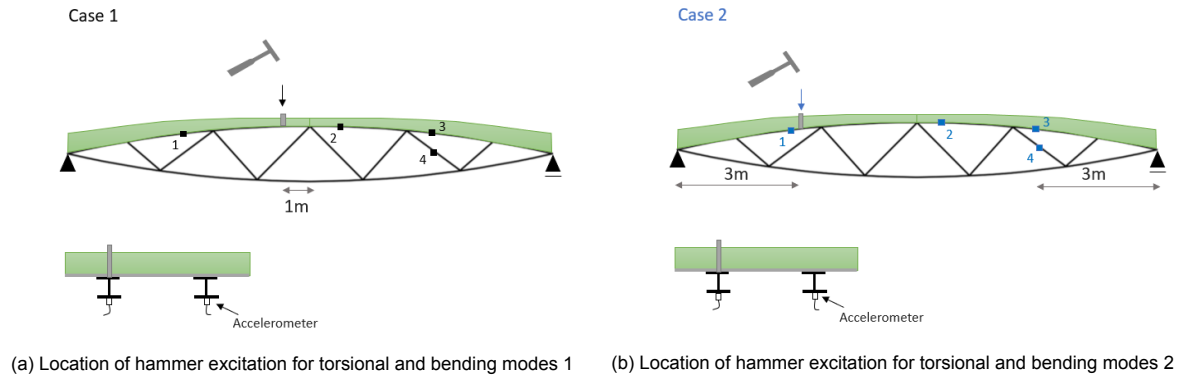
Figure 5.8: Locations of hammer excitation

It is important to place the accelerometers on the steel beams since deformations of these beams are of interest for present study. The best place to put the accelerometers is at the bottomside of the beams, in this way the cable connecting the device to the computer does not show a kink, minimizing the noise coming from the cable. Another advantage is that the measured data is certainly coming from the movement of the steel beams giving information about the structural modeshapes in stead of the local modes of the beam flanges. It is also important to place the accelerometers at both beams, in this way it is possible to identify if a mode is a torsional- or a bending mode. Furthermore it is advised to place accelerometers on all six glass rods of one of the diagonals in order to have more information about the behavior of the glass rods when the structure is excited dynamically. Information retrieved from these measurements can be used to verify the assumption regarding the cross sectional area of the glass rods.

The procedure of performing a hammer test on the Glass Truss Bridge is explained in chapter 6.

5.5. Conclusion

The first twenty eigenfrequencies of the model are calculated, in figure H.2 the first six modeshapes are presented.

(a) Mode T1 (4.46 Hz)   (b) Mode T2 (7.2044 Hz)   (c) Mode B1 (7.8018 Hz)

(d) Mode T3 (7.8723 Hz)   (e) Mode T4 (10.313 Hz)   (f) Mode L1 (10.337 Hz)
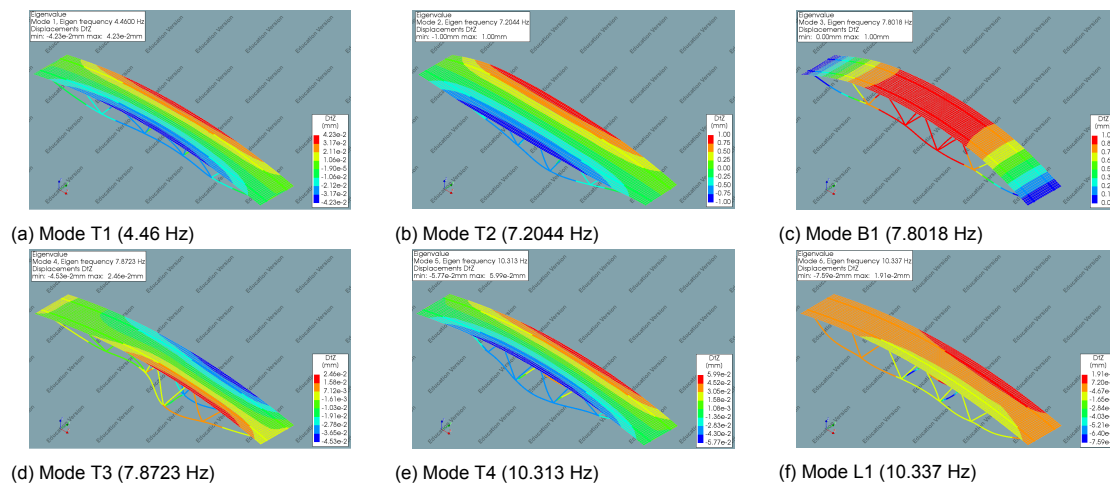
Figure 5.9: First six mode shapes of the Glass Truss Bridge

Based on the sensitivity analysis done in this chapter, it can be concluded that the parameters having most influence on the different eigenfrequencies and modes are the area of the glass diagonals

and the soil density. From the twenty modeshapes a selection is made for the optimal locations for placing the accelerometers in order to identify most of the eigenmodes. At least six accelerometers are needed, three per beam. Figure 5.8 shows an overview of the optimal test setup for this case study.

5.6. Discussion

The considered parameters are not the only ones influencing the modal properties of the Glass Truss Bridge. There are many others but due to time limitations a selection was made. In this study the effect of variation of the selected parameters on the eigenfrequencies of the structure is investigated. From this analysis two parameters turn out to have most influence. We are not only interested in the eigenfrequencies but also the damping parameters and the modeshapes of the bridge, it is possible that other parameters influence the latter properties.

III
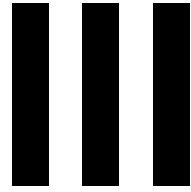
The third phase gives the test setup and simulates the hammer test. Results are elaborated and the protocol for performing the hammer tests on the Glass Truss Bridge is presented. In the end of this phase recommendations and conclusions to the research question are given.

$$6$$

Test setup

6.1. Requirements

To be able to assess the dynamic characteristics of the Glass Truss Bridge i.e. natural frequencies, modal damping ratio and mode shapes, vibration measurements are carried out. The obtained results are then compared to values retrieved from numerical estimation. In practice different techniques are known to obtain the needed information, some examples are a hammer excitation or a shaker excitation. The advantages and disadvantages between these two methods are stated below:

Hammer excitation	
Advantages	**Disadvantages**
+ Fast	- Might drive structure into nonlinear behaviour
+ No fixturing	- High peakforce might lead to damage
+ Excitation force is known	
+ Portable	
+ Inexpensive	
Shaker excitation	
Advantages	**Disadvantages**
+ Broad range of excitation signals	- Fixturing of structure and shakers
+ Posibility of doin MIMO	- Potential mechanical coupling between shakers
	- More expensive

Table 6.1: Advantages(+) and disadvantages(-) of Hammer excitation (top) and Shaker excitation (bottom)

For the case of the Glass Truss Bridge a hammer test is best to carry out. As the size of the bridge increases, the mass of the hammer must increase accordingly [12]. Increasing the mass compromises the portability of the same. The optimal span for performing a hammer-test is <30m. The span of the Glass Truss Bridge is 14m, which makes this testing method very suitable. The impact will be at one of the steel beams, damaging of the structure will be minor. The test can be carried out with a minimum group of 3 persons and all instruments are available at the University of Technology Delft. The procedure is explained in next section, basically the hammer test involves the following steps: the structure is hit by a hammer, the accelerations are measured at certain selected locations along the bridge and the obtained results are post-processed in order to get the Frequency Response Functions (FRF's). Several techniques are available to obtain the modal parameters of the structure from the FRF's. An overview of the procedure is given in 6.1.
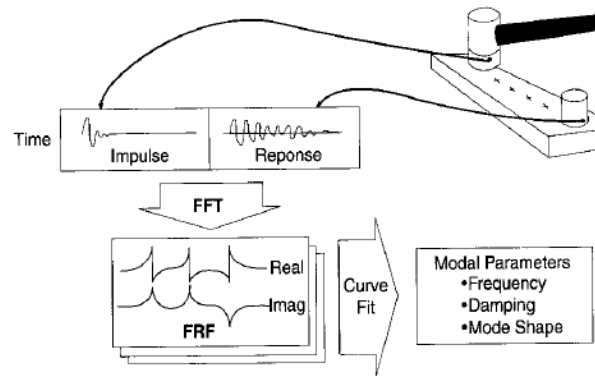
Figure 6.1: Set up Modal testing [25]. Curve fitting is one of the available techniques to extract modal parameters of the structure.

The devices and items needed for performing the hammer test are the following:

- Multiple accelerometers, these devices must be able to measure frequencies higher than the frequencies of interest and the sampling rate should be double the maximum frequency (according to the Nyquist theorem)

- A PC or laptop with post-processing modal software

- An Analogue to Digital Converter

- A micro SD memory card to store the recorded data

- A real time clock to keep the synchronization between the devices consistent

- An impact hammer with enough weight to be able to reach numerous frequencies (the one available at TU Delft is a hammer weighing 55N with a piezoelectric force sensor at its tip having a dynamic range of 22kN)

Prior to testing the devices should be synchronized and a check wave should be sent to check the reliability of the accelerometers.

6.2. Test setup: hitting- and measuring locations

From the preliminary analysis the locations where accelerometers should be placed were determined. Figure 6.2 and 6.3 show the two cases based on the generated modeshapes and the conclusions from chapter 4.
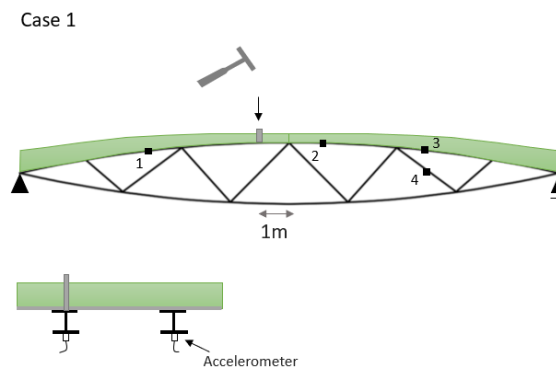
Figure 6.2: Case 1: Testing setup, hit-point is 1m from midspan and measuring locations are at 1m from midspan and 3m from boundaries, accelerometers are installed at both beams, scale=1:200
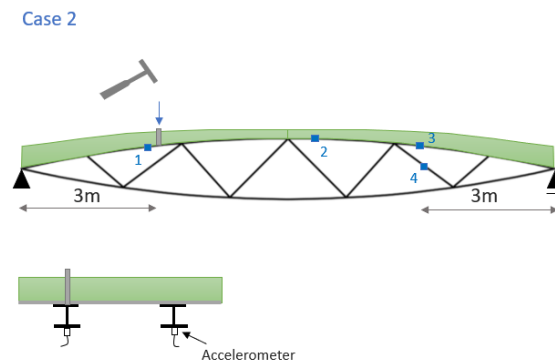
Figure 6.3: Case 2: Testing setup, hit-point is at 3.5m from left boundary, measuring locations are at 1m from midspan and 3m from both boundaries, accelerometers are installed at both beams,scale=1:200

From the sensitivity analysis it is known for the investigated parameter its sensitivity to each natural frequency, (chapter 4). This relation is important to know because when updating the finite element model it is difficult to decide which parameter should be updated and to what extend (up or down). In the next table 6.4 all modes are listed and the parameters that can be updated to fit each mode to the test results are given. The rotational stiffness is not included in this table because this parameter showed no difference in eigenfrequencies for the current case.

#	Modeshape	parameter 1	sensitivity	par ameter 2	sensitivity	parameter 3	sensitivity
1	T1	d_glass	-107				
2	T2	rho_soil	28	d_glass	-9	E_soil	-8
3	B1	d_glass	-46	rho_soil	10		
4	T3	rho_soil	37	E_soil	-1		
5	T4	d_glass	-7				
6	T5	d_glass	-7				
7	L1	d_glass	-2				
8	T6	d_glass	-6				
9	T7	d_glass	-18				
10	T8	d_glass	-16				
11	T9	d_glass	-13				
12	L2	rho_soil	35				
13	B2	d_glass	-38	rho_soil	23		
14	T10	d_glass	19	rho_soil	-16	E_soil	-3
15	T11	rho_soil	33	d_glass	-26	E_soil	-7
16	T12	rho_soil	-8				
17	B3	rho_soil	-28	d_glass	-6		
18	B4	rho_soil	37	d_glass	-28		
19	T13	rho_soil	-29	d_glass	-11		
20	B5	rho_soil	30	d_glass	-21	E_soil	-9

Figure 6.4: Updating parameter per mode of the Glass Truss Bridge. The sensitivity is calculated in percentages. A negative sensitivity means the given parameter should be lowered when the eigenfrequency must be updated to a higher value

6.3. Hammer test procedure

This section gives a protocol of how to perform such an impact hammer test on the current case study: The Glass Truss Bridge, based on HiVoSS guidelines. First the procedure is explained in detail after which a simulation of the Hammer test is done on the DIANA-model of the Glass Truss Bridge.

Hammer excitation produces a pulse of typically 10 ms on a hard surface. Soft tips produce a slightly longer pulse. The frequency content is of a wide range, meaning a lot of frequencies are being

excited [14]. The pulse can be represented by a half sinusoid, therefor three points should be minimally used to describe the curve of the hammer excitement, a starting point at the left-base, ona at the peak-value and the end point at the right-base forming a triangular shape.

The frequency content of interest lies between 0 and 30Hz. According to the Nyquist theorem a sampling ratio of double the maximum frequency of interest is minimally needed to describe all frequencies. The samples of two sine waves can be identical when at least one of them is at a frequency above half the sample rate. In DIANA a sampling ratio of 100Hz is taken into account. The impulse duration considered in the model is 40ms, this is done in order to reduce the computational time. Furthermore a spacing of 10ms is considered, which is below the maximum spacing of 20ms needed to be able to describe the load pattern. A spacing of 10ms equals a sampling ratio of 100Hz.

When performing the real live tests, it must be taken into account that some differences in quality of the signal is in-avoidable. Noise from external factors might be present but also some noise from the measurement equipment. For the Glass Truss Bridge it is also important to hit the steel beams, not the soil deck, in order to do so two holes need to be dug and a steel pipe or column should be placed which allows to hit the steel beam from the top (see figure 6.2). The transfer of the force through the steel pipe might also affect the impulse signal received by the bridge.

In Appendix K a protocol for performing the Hammer Test on the Glass Truss Bridge is given.

In next section the hammer test is validated via a simulation on a simply supported beam. This is done by applying an impulse load at two predetermined locations. Then a transient analysis is performed and accelerations are retrieved at selected locations (where the accelerometers would be physically placed).

6.4. Simulation of Hammer Test: simply supported beam

The procedure is validated through a simulation on a simply supported beam. After the procedure is validated, the simulation is performed on the model of the Glass Truss Bridge (section 7). For the simply supported beam a standard I-profile is used, HEA120, the same as is used in the Glass Truss Bridge.

6.4.1. Validation of proposed procedure

In figure 6.5 an overview is given of all steps included when simulating the hammer test on a simple supported beam. Two cases are considered: in case 1 the load is applied at 0.1*L left from midspan, in case 2 the load is applied at 0.2*L from the left support (see figure 6.6). The modes of interest are the first three eigenmodes, the two scenarios are good to identify the three expected eigenmodes (other modes are excited as well). The model is built in DIANA, damping is not considered. Data of the response of the system is retrieved from DIANA by performing a transient analysis, which implies a non linear analysis with transient effects activated. The input signal is shown in figure 6.8. The transient analysis basically calculates the response of the system to a load in a specified time domain. In this case an impulse load of 1N is applied for a duration of 0.04 seconds.
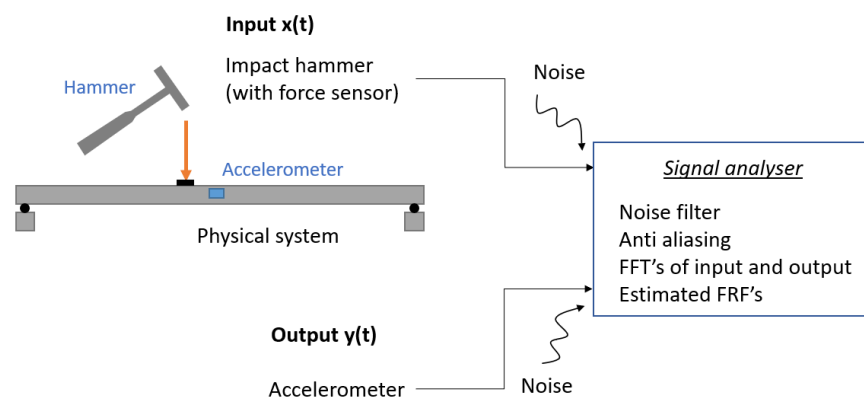
Figure 6.5: Hammer test: Case 1
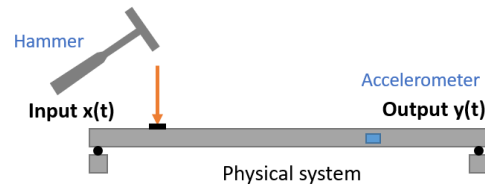
Figure 6.6: Hammer test: Case 2

To avoid aliasing the sampling rate is more than twice the highest frequency contained in the signal (following Nyquist theorem). With a sampling rate[1] of 100 Hz frequencies up to 50Hz can be recorded. This is within the range of interest (30Hz). Another important aspect is to see if the input load can be described with time steps of 0.01s. The hammer impact load is applied in 0.04s, a minimum of three points are needed to describe this graph, a sampling rate of 100Hz is good to prevent aliasing. In DIANA a transient analysis is performed, the load is applied in time steps of 0.01s (100Hz), in each step the response is calculated for all nodes. The interesting quantities are the displacement, velocities and accelerations of the bridge, these quantities are selected as output in DIANA.

6.4.2. Case 1
The modeshapes of interest are the first three modes, see figure 6.7
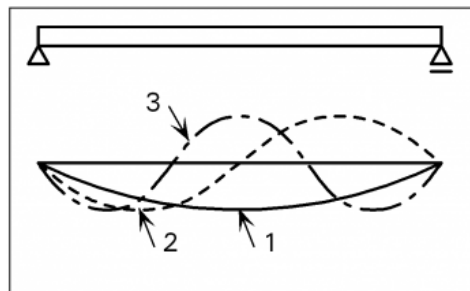
Figure 6.7: First three modeshapes of simply supported beam

After performing the transient analysis in DIANA the data set of input (hammer excitation) and output (accelerometers) is extracted. The two previously presented cases are investigated, figure 6.9 shows the response in terms of displacement of the beam in time-domain. The excitation of the force gauge instrumented hammer is also shown in figure 6.8 as a time history. When performing the test a set of 5-10 measurements should be taken, for this simulation input- and output- data sets are monitored digitally, one set is thus enough to obtain the desired results.

---

[1]The sampling rate is the average number of samples in one second. Accelerometers of the University of Technology Delft have a sampling rate up to 200Hz.
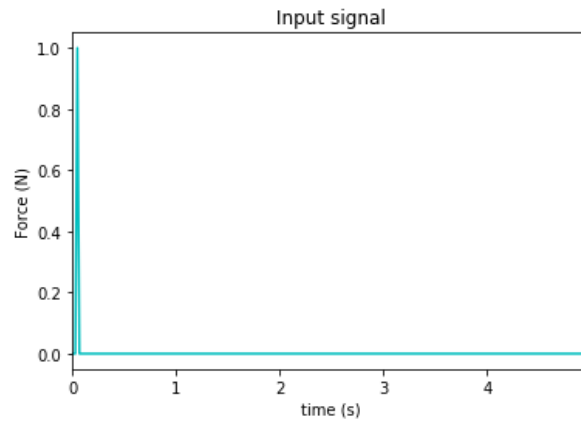
Figure 6.8: Time-history of hammer excitation
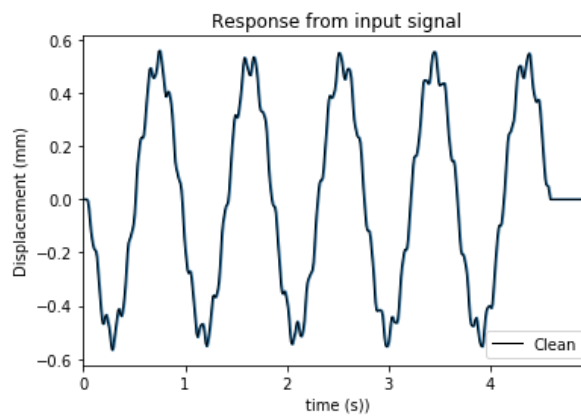
Figure 6.9: Case 1: Response in terms of displacement of middle node to a unit impulse load

When performing the hammer tests in the open air, it is not possible to obtain a clean signal. The input and output signal will always be contaminated with noise, this can be due to for example passengers walking on the sides, a bus passing by, etc. This is why noise is also added to the data set obtained from DIANA. Noise is defined as a random signal that does not have meaningful data or information. A random signal is added to the 'clean' data using the python command *np.random.randn*. The random signal is a significant noisy signal, it blurs away the actual signal as can be seen in figure 6.10.
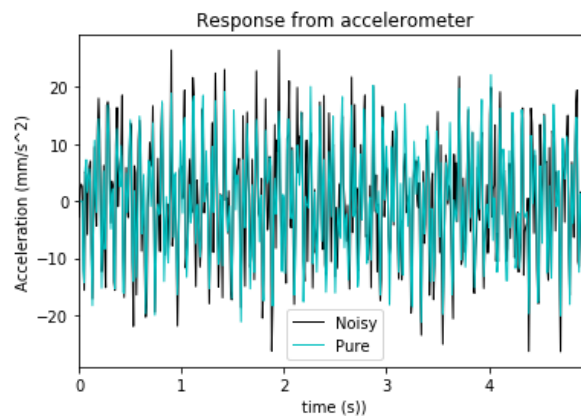
Figure 6.10: Case 1: Response in terms of acceleration of middle node, black is the signal with added noise

Following the procedure explained in section 6.3 a Fast Fourier Transform is performed on the first data set (input- and output signal of case 1), this changes the data from time- into frequency domain. Spectral descriptions of the input and output-signals are now retrieved. The cross spectrum relating the input signal with the output signal is depicted in figure 6.11a. This is the cross spectrum of the pure input signal, when considering the noisy data set a noise filter needs to be implemented. After applying the filter a similar cross spectrum is obtained, only the positive part is needed (figure 6.11b).

(a) Cross spectrum of input and output

(b) Cross spectrum of input and output, filtered data
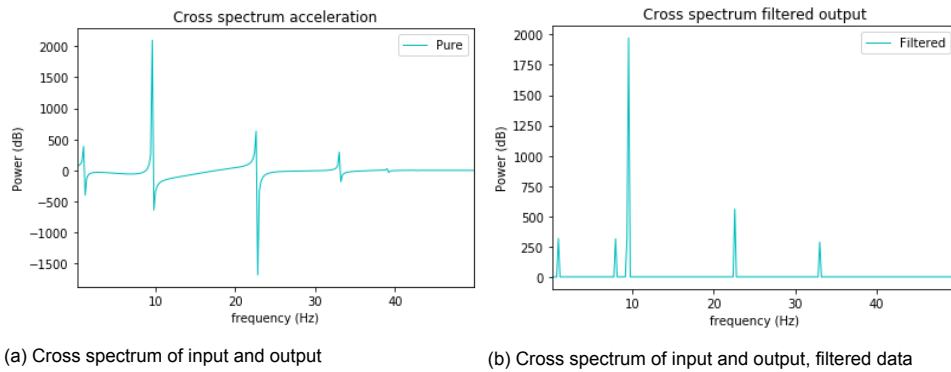
Figure 6.11: Case 1: Cross spectra of pure data (a) and filtered data (b)

When dividing the cross spectrum of the output by the input spectrum, the FRF is obtained (H2). Figure 6.12 gives the FRF of the simply supported beam.
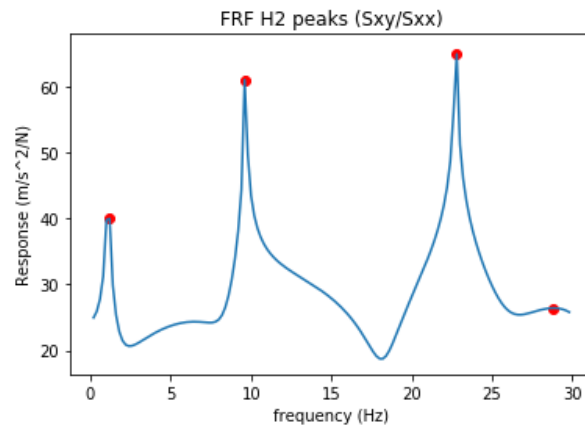
Figure 6.12: Case 1: FRF of simply supported beam, peaks at 1.1, 9.9, 22.8Hz

From this FRF the modal frequencies and damping are retrieved using the ERA method described previously. The peaks are found at the following frequencies: 1.1Hz, 9.9Hz and 22.8Hz.

6.4.3. Case 2

The same procedure is performed for case 2, the input load is of the same magnitude but at a different location and the output is extracted from a different location as well. The first figure gives the response of the beam in time domain, the blue line is the pure response, the black line is the response with noise added to the output. The obtained signals are transformed into frequency domain (figure 6.14a). From here the FRF is generated (figure 6.15).
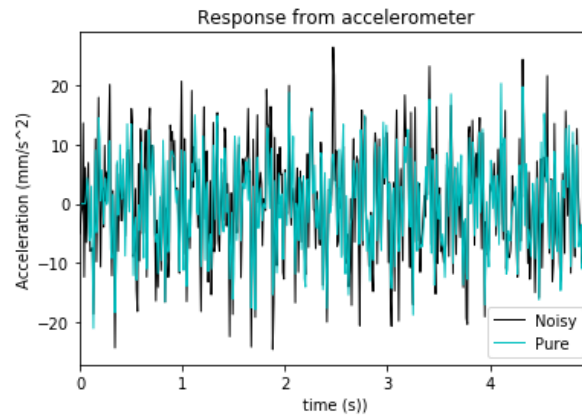
Figure 6.13: Case 2: Response of the beam in time domain, black is with added noise

(a) Case 2: Cross spectrum of input and output

(b) Case 2: Cross spectrum of input and output, filtered data
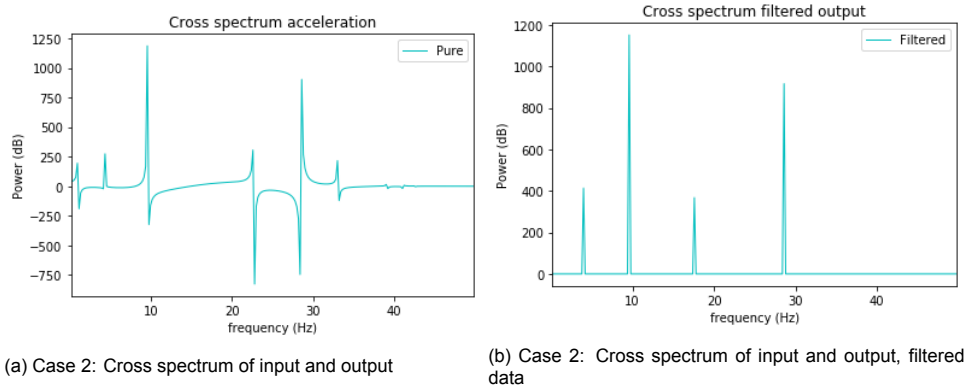
Figure 6.14: Cross spectra of pure data (a) and filtered data (b)
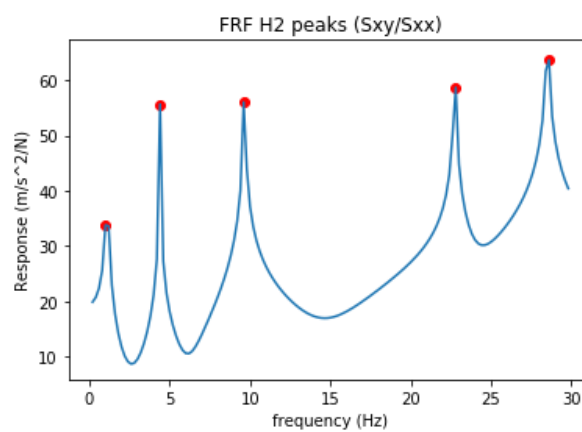
Figure 6.15: Case 2: FRF, peaks at 1.1, 4.4, 9.9, 22.8, 28.6 Hz

Using the peak picking method the peaks are found to be at 1.1, 4.4, 9.9, 22.8 and 28.6 Hz. These values represent the eigenfrequencies of the beam.
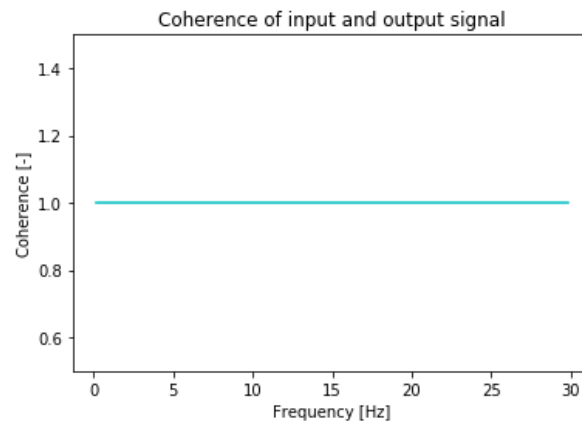
Figure 6.16: Coherence of input and output

6.4.4. Comparison of results with eigenvalue analysis simply supported beam

When the amplitude of the FRF shows a peak it usually indicates a resonance, figure 6.15. Other parameters should be checked as well to be sure no erroneous conclusions are drawn. As stated in the procedure of the hammer test, the coherence needs to be checked between the input and the output. This indicates the degree of correlation between the input and the output as a function of frequency. Low values of coherence represent a weak relation, in that case the measurement must be repeated. Figure 6.16 shows the coherence for the case of the simply supported beam.

(a) Mode B1, eigenfrequency: 1.1Hz

(b) Mode B2, eigenfrequency: 4.4Hz

(c) Mode B3, eigenfrequency: 9.9Hz

(d) Mode B4, eigenfrequency: 23.9

(e) Mode B5, eigenfrequency: 27.6
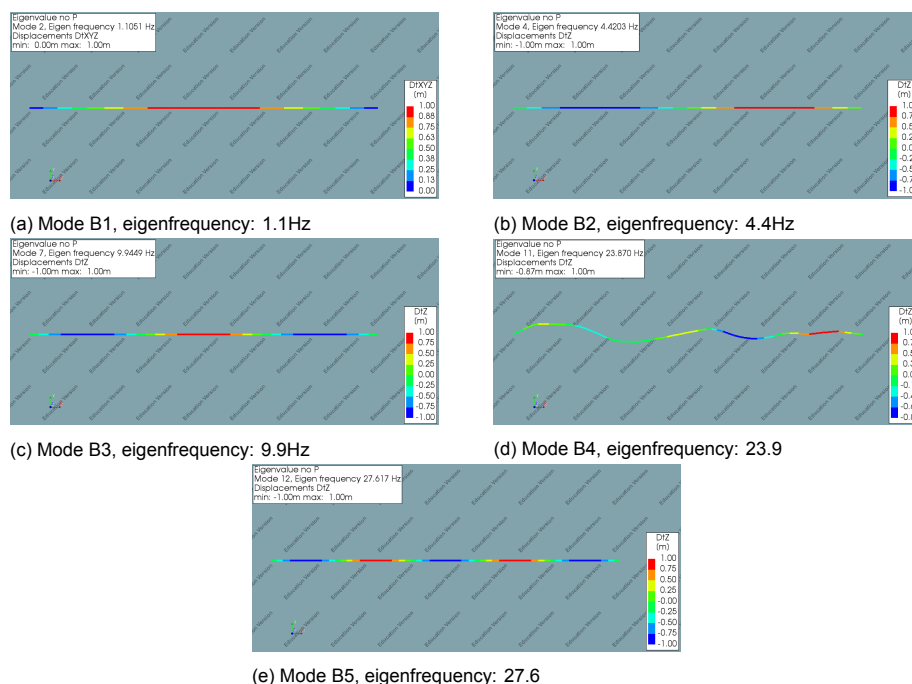
Figure 6.17: Five first bending modeshapes of interest, simple beam from DIANA

To validate the procedure the results presented in previous sections are compared to the eigen-frequencies found in DIANA for the simply supported beam. When looking at the results from case 2 (figure 6.15) the peaks are at 1.1 Hz, 4.4Hz, 9.9Hz 23.9Hz and 27.6Hz. The comparison is depicted in table 6.2.

Mode	DIANA [Hz]	Case 1 [Hz]	Case 2 [Hz]
B1	1.1	1.1	1.1
B2	4.4	4.4	4.4
B3	9.9	9.9	9.9
B4	23.9	-	23.9
B5	27.6	-	27.6

Table 6.2: Comparison of Eigenfrequencies found with DIANA with the ones found via the simulation of the hammer test

Case 1 shows the first three eigenmodes, which also are identified in case 2. One explanation is that in case 1 the modeshapes have a node at the location of the accelerometer (see figure 6.2), no acceleration is recorded if a node is present. The eigenfrequencies of case 2 perfectly match. The procedure presented in this section can be used to test the model of the Glass Truss Bridge. In order to prevent hitting at a nodal point, but at the same time be able to generate most of the modeshapes, two test setups proposed at the end of chapter 5 are simulated in next section.

6.5. Conclusion

The hammer test procedure is validated by performing the test on a simply supported beam. First a 2D FE model is made, element, geometry and material properties are assigned and the boundary are chosen such that the beam is simply supported at both ends. The eigenfrequencies are then calculated and the first three (bending) eigenmodes are identified. The results show a perfect match in eigenfrequencies and also the modeshapes are the ones that were expected for a simply supported beam. It could thus be concluded that the method is working.

7

Simulation of hammer test: the Glass Truss Bridge
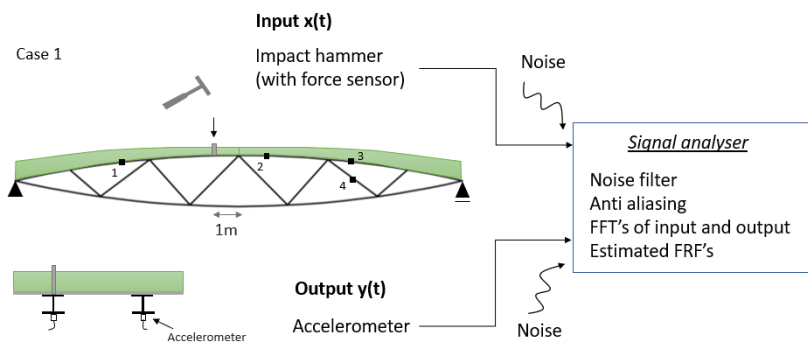
Figure 7.1: Hammer test setup: Case 1
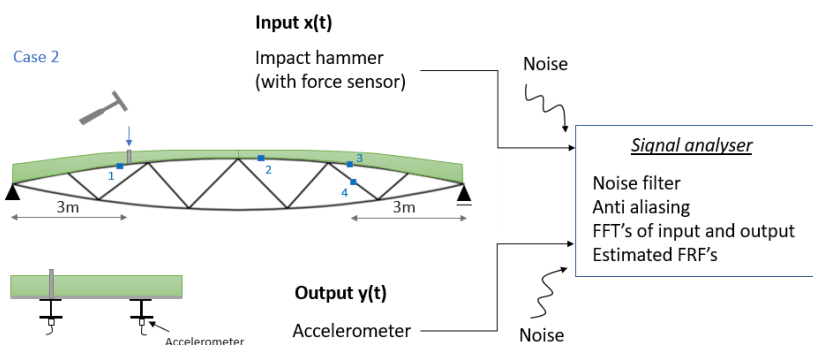
Figure 7.2: Hammer test setup: Case 2

7.1. Results simulation hammer test Glass Truss Bridge: Case 1

In case 1 the hammer impact load is applied at 1m right from mid-span, information is acquired at location 1, 2 and 3 from both beams (figure 7.1). This is done in order to prevent hitting the bridge at a nodal point and to be able to reconstruct the modeshapes. With 6 measurement locations it is possible to roughly reconstruct most of the modeshapes. In appendix J the python script used to acquire the FRFs of the Glass Truss Bridge model is added. This script can also be used when data of the live hammer tests are being processed.

The input load is depicted in figure 7.3. This load represents the hammer impact on the bridge and is the same for case 1 and case 2. The magnitude of the load is 1N and the duration 0.04s as recommended in HiVoSS guideline [14].
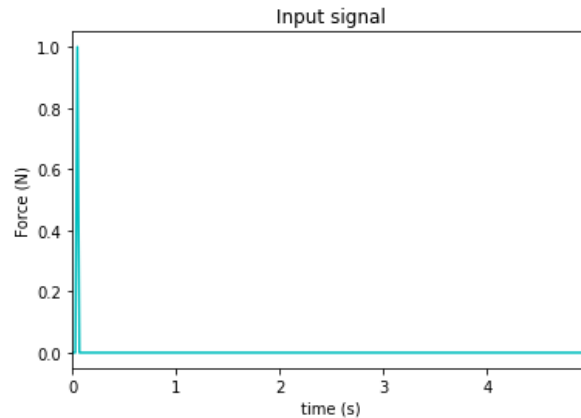
Figure 7.3: Input load: Case 1 and 2

Figure 7.4 shows the response of the bridge measured at 1m from midspan (location 2 from 7.1). From the 'accelerometers' four time-history's are retrieved as depicted in figure 7.4. The amplitude of the signal represents the acceleration of that point.

(a) Response of input signal GTB, location 1

(b) Response of input signal GTB, location 2, first beam

(c) Response of input signal GTB, location 2, second beam

(d) Response of input signal GTB, location 3
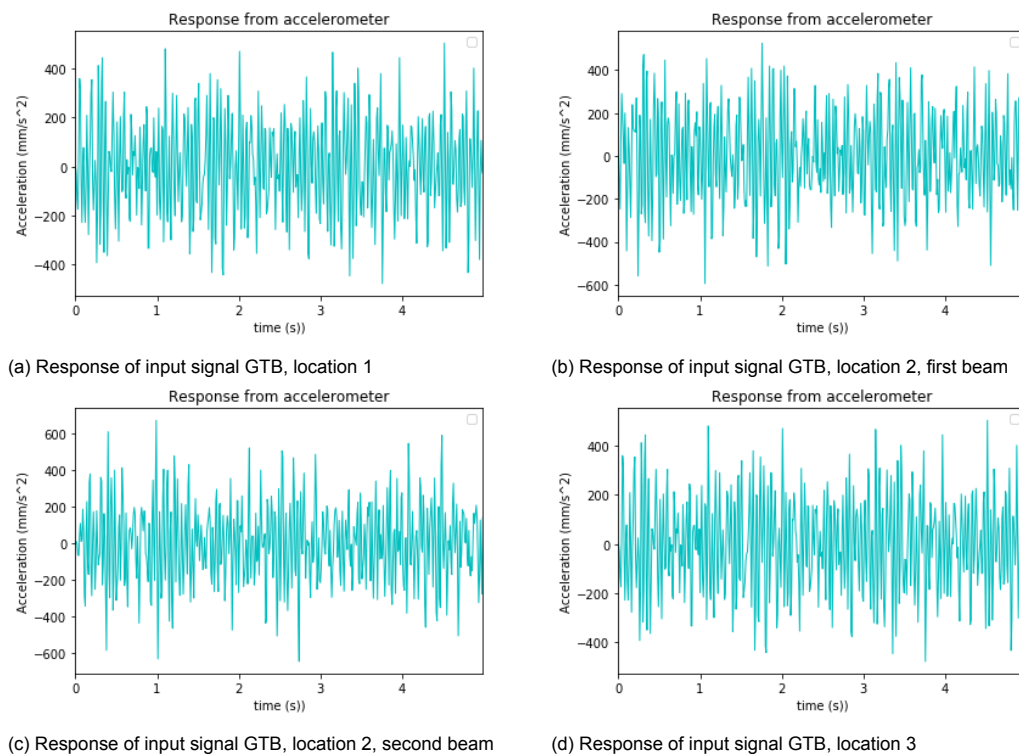
Figure 7.4: Case 1: Response of input signal measured from locations 1, 2 (both beams) and 3

A Fast Fourier Transorm is applied to the input- and output- data transforming the signals from time- into frequency-domain. Figure 7.5 shows the cross spectrum of the acceleration, this graph gives a relation between the input and the output signal. A high peak is found at a frequency between 7 and 8 HZ. This already gives some information about the resonance frequencies. One dominating is around that value.

(a) Response of input signal, location 2, first beam   (b) Response of input signal, location 2, second beam
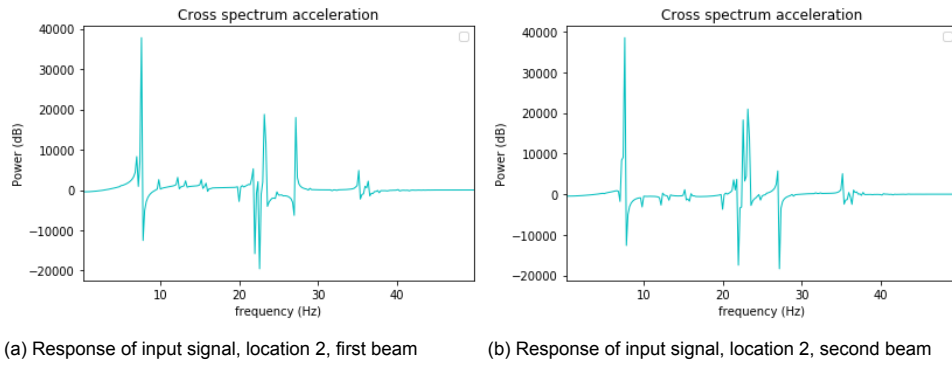
Figure 7.5: Case 1: Cross spectrum location 2, first beam (a) and second beam (b)

The FRF's of the signals give more insight in the dynamic properties of the bridge. The procedure of how to generate an FRF is already elaborated in section 6.3. Next to an FRF a phase spectrum is also generated. The phase spectrum is usually plotted together with the FRF to identify resonance peaks. If the phase plot shows a 90 degree angle this means there is a resonance peak. Figure 7.6 shows the phase spectrum of the FRF's for case 1 at location 2 for both beams. The peaks are found and indicated with a red dot in the graphs shown in figure 7.7.

(a) Amplitude and phase spectrum location 2, first beam   (b) Amplitude and phase spectrum location 2, second beam
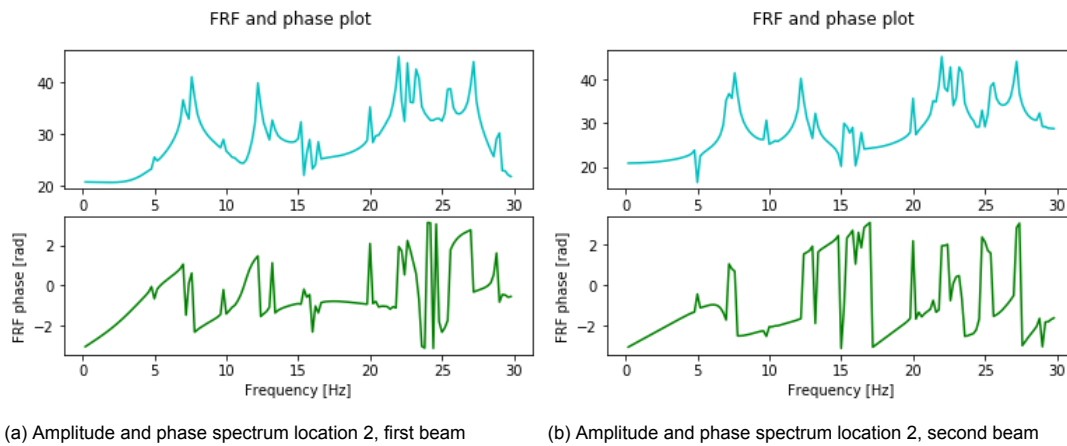
Figure 7.6: Case 1: FRF's, amplitude and phaseplot for measurements from location 2 of first beam (a) and second beam (b)

(a) FRF and peakvalues location 2   (b) FRF and peakvalues location 2, second beam
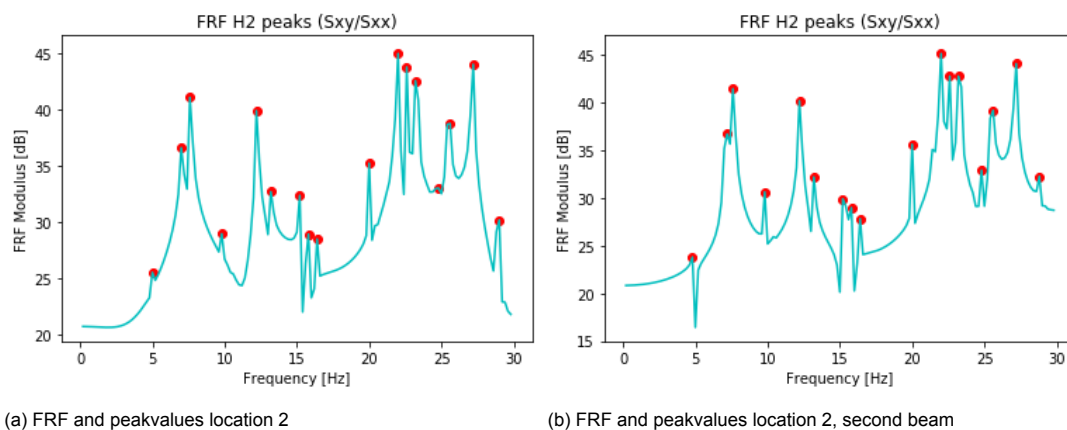
Figure 7.7: Case 1: FRF and peakvalues (red dots) of location 2 of first beam (a) and second beam (b)

The coherence is calculated with the formula addressed in Appendix K. Figure 7.8 shows that the the coherence calculated for case 1 has a constant value of 1 meaning that the input and output signal

are perfectly correlated. This was as expected because results are treated numerically and no noise is added to the input nor the output signal.
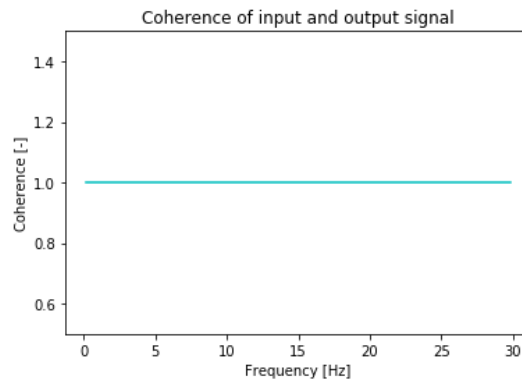
Figure 7.8: Case 1: coherence of input and output signals

The maxima are selected manually based on weather the peak is actually a peak. For example the two first red dots are small peaks. The found frequencies for case 1 are 7.6, 12.2, 15.2, 15.8, 20, 22, 25.6 and 27.2 (all values in Hz). An overview of the selected peaks is given in figure 7.9.
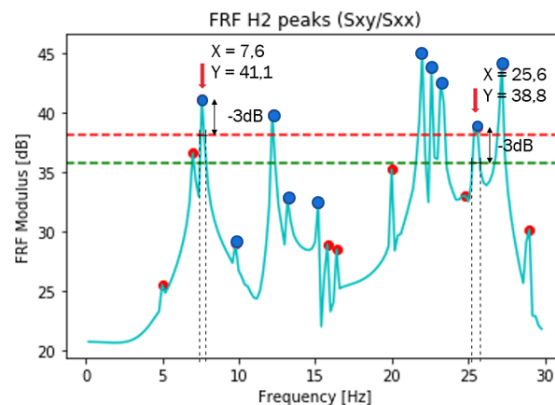
Figure 7.9: Picked peaks and derivation of damping for two resonance peaks

According to [13] the width of the peak is related to the damping. The wider the peak, the more damping is experienced for that specific eigenfrequency. When comparing the width of the peak at 7.6Hz and the width of the peak at 25.6Hz (figure 7.9), it is observed that the latter resonance peak has more damping. When looking at the modeshapes, the eigenmode with a frequency of 7.6Hz is a bending mode mainly contributed by the soil deck while the second is a torsional mode mainly contributed by the glass diagonals.

7.2. Results hammer test Glass Truss Bridge: Case 2
In case 2 the hammer impact load is applied at 3m from the left boundary. Accelerations are recorded at 3m from the right boundary (location 3), one at each steel beam (figure 7.1). The results are presented hereafter in the same manner as for case 1.
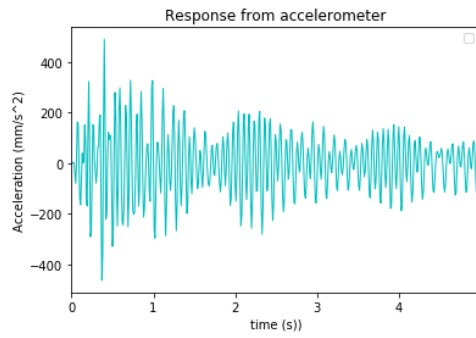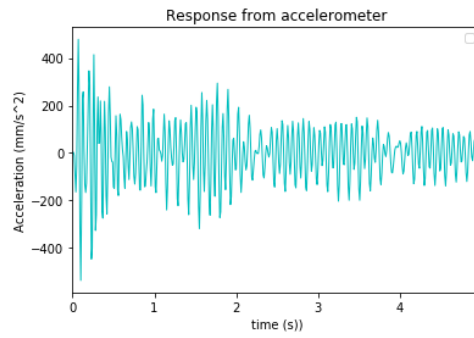
(a) Response of input signal GTB, location 3   (b) Response of input signal GTB, location 3, second beam

Figure 7.10: Case 1: Response of input signal measured from location 3 (both beams)
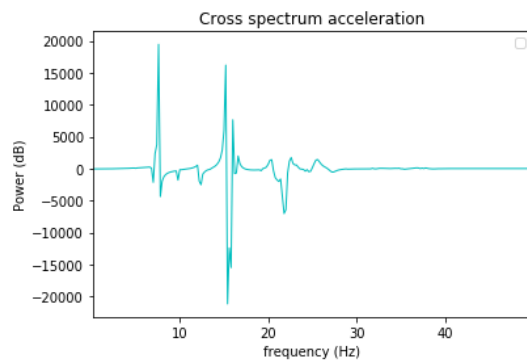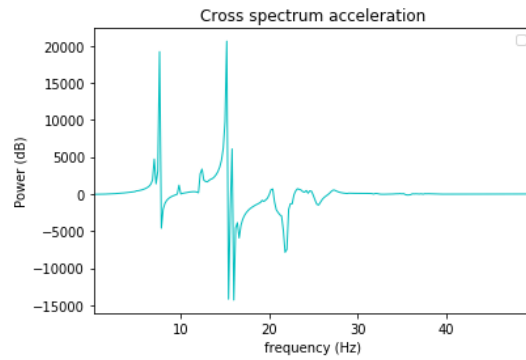
(a) Cross spectrum of input and output signal, location 3   (b) Cross spectrum of input and output signal, location 3 second beam

Figure 7.11: Case 2: Cross spectrum location 3, beam 1 (a) and 2 (b)
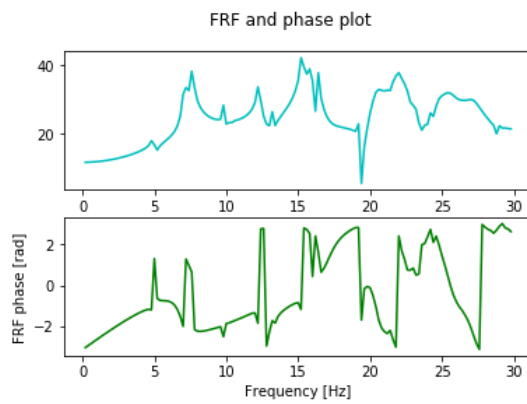
(a) FRF and phase angle location 3, first beam   (b) FRF and phase angle location 3, second beam
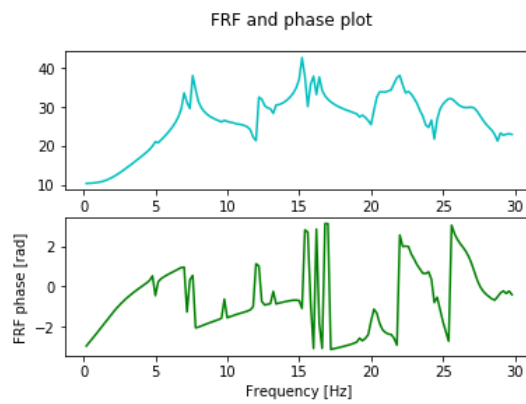
Figure 7.12: Case 2: FRF and phase angle plots of location 3 of first beam (a) and second beam (b)

(a) FRF and peakvalues location 3

(b) FRF and peakvalues location 3 second beam
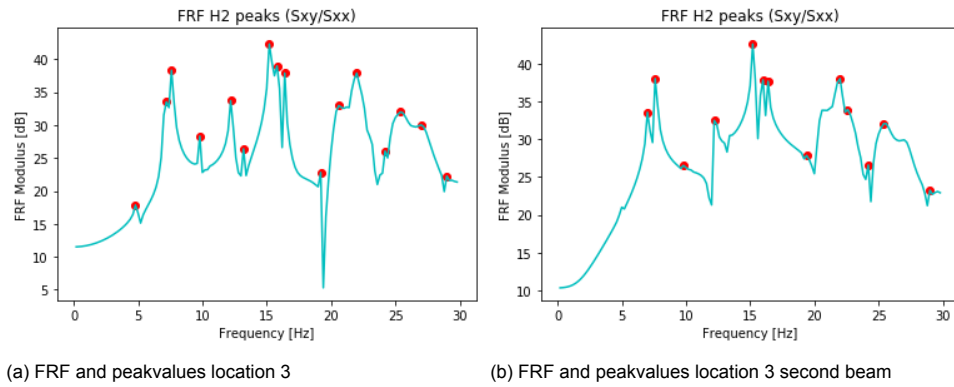
Figure 7.13: Case 2: FRF and peakvalues (red dots) of location 3 of first beam (a) and second beam (b)
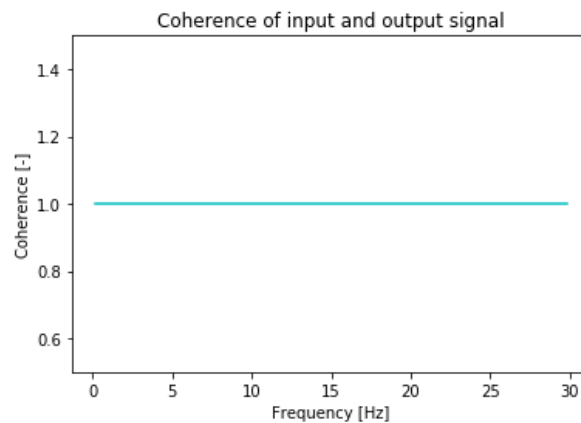
Figure 7.14: Case 2: coherence of input and output signals

The maxima are again selected manually based on weather the peak is actually a peak. The found frequencies for case 2 are 7.6, 12.2, 13.2, 15.2, 16.4, 20.6, 22, 25.4 and 27 (all values in Hz). An overview of the selected peaks is given in figure 7.15a. Interesting here is that some of the peaks are merged because they appear close to each other. This results is a very wide bandwidth, this is treated as two different peaks, figure 7.15a.
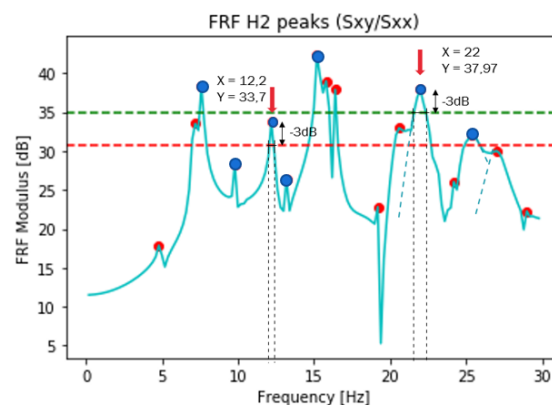
(a) Picked peaks and derivation of damping for two resonance peaks

The location of the peaks is compared to the obtained eigenfrequencies from DIANA. Not all maxima are resonance peaks. The first red dot denotes an extremely small peak and the second dot is a

small peak right before another peak, these small peaks are neglected. An overview of the eigenfrequencies and a comparison between case 1 and case 2 can be found in table 7.1

Nr	Mode	DIANA	Case 1	Case 2		Mode	DIANA	Case 1	Case 2
1	T1	4.46	-	-	11	T8	14.405	-	-
2	T2	7.2044	-	-	12	L3	14.703	-	-
3	B1	7.802	7.6	7.6	13	B2	16.539	15.2	15.2
4	T3	7.8723	-	-	14	T9	17.462	-	-
5	T4	10.313	9.8	9.8	15	T10	18.255	-	-
6	L1	10.337	-	-	16	T11	22.458	22.0	22.0
7	L2	10.675	-	-	17	B3	23.108	22.6	-
8	T5	11.197	-	-	18	B4	23.827	23.2	-
9	T6	12.969	12.2	12.2	19	T12	25.864	24.8	-
10	T7	13.747	13.2	13.2	20	T13	26.251	25.6	25.4

Table 7.1: Comparison of detected peaks from FRF with the eigenfrequencies found with DIANA

In order to reconstruct the modeshapes the imaginary part of the FRF is examined. Figure 7.16 shows the plot for Case 1, location 2 beam 1 (left) and beam 2 (right). The first bending mode is clearly visible in figure 7.16, at a frequency of 7.6Hz both plots show a peak meaning that at midspan both beams are moving in the same direction (in sync).

(a) Case 1: Imaginary part of FRF, beam 1

(b) Case 1: Imaginary part of FRF, beam 2
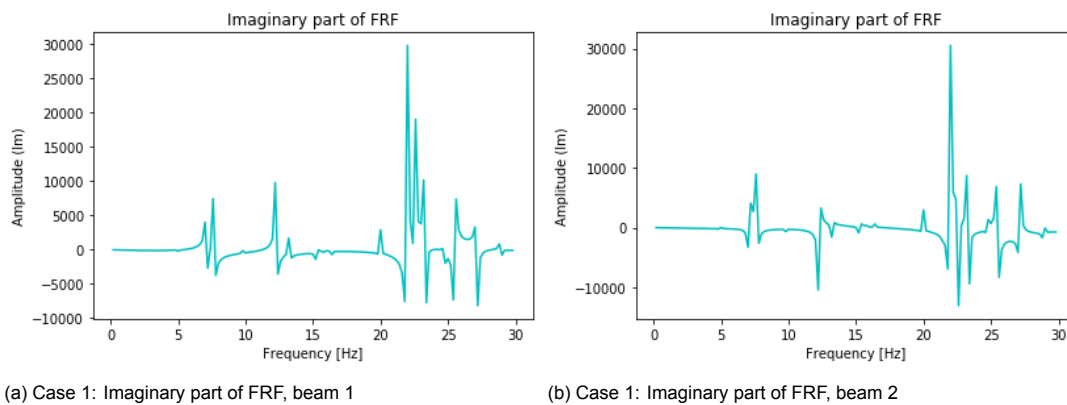
Figure 7.16: Case 1: Imaginary plot of complex FRF signal, to reconstruct modeshapes

Looking at the reconstructed animations of the modeshapes it can be concluded that modes 3, 13 and 17 are bending modes, both beams are moving in sync, all other modes are torsional modes. The contribution of the modeshapes has already been addressed in chapter 5. The local modes (L1-3) are not found with the test setup because these modes are mainly contributed by the steel links, from which the acceleration is not measured in this test setup.

7.3. Discussion

The FRF's presented in this chapter describe the acceleration response of the structure relative to the force excitation from the impact hammer. Two cases are proposed as test setup to identify the eigenfrequencies, damping ratios and modeshapes of the Glass Truss Bridge. Both cases detect a lot of the same eigenfrequencies. This is in line with expectations.

Damping of 0.4% is considered in both cases and is taken into account accordingly in the soil deck. Figure 7.10a shows the decrement in acceleration over time. To calculate the damping ratio the method of -3dB bandwidth is used. For different modes slightly different damping is observed. The first mode is a bending mode (7.6Hz) having large accelerations, in which case large mass-proportional damping forces can also develop [5]. The second mode is a torsional mode (12.2Hz), from the animation of the modeshapes retrieved from DIANA it is seen that this modeshape is driven more by the stiffness of the structure than the mass of the whole, resulting in a different effect of the considered Rayleigh damping.

Some research states that the half bandwidth method overestimates the damping [34] when used for higher frequencies, this should be taken into account in future work on the Glass Truss Bridge.

The modeshapes can be reconstructed with the measurements from the six proposed locations using the information provided in the FRF's. The FRF signal is a complex signal which can be described with a magnitude and a phase (figure 7.6a). It can also be described by means of a real and an imaginary part. When looking at the imaginary part of the FRF the modeshape can be reconstructed. The first bending mode is clearly visible in figure 7.16, at a frequency of 7.6Hz both plots show a peak meaning that at midspan both beams are moving in the same direction. Although the modeshapes can be estimated up to certain extend, it is better to place more accelerometers, if possible, in order to reconstruct the modeshapes with more accuracy. This will however result in a higher post processing time.

8
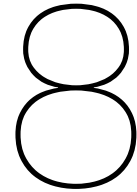
Conclusions and future recommendations

8.1. Conclusions

When structures come to vibrate in their natural frequencies this can have disastrous consequences such as complete collapse as happened to the Takoma Narrows bridge in 1940. To prevent this and be able to build safely it is important to know the dynamic response of a structure. For glass structures the limit values are not clearly defined. This thesis aims to predict the dynamic response of the TU Delft's Glass Truss bridge by answering the following research question:

"What is the structural static and dynamic response of the Glass Truss Bridge in its current design when it is subjected to static and dynamic loading for footbridges?".

The dynamic response of the Glass Truss Bridge was assessed by defining its modal parameters, i.e. mass, stiffness and energy dissipation. Therefore its eigenfrequencies, mode shapes and damping coefficients were determined using the finite element modelling technique. A sensitivity study is performed on the most uncertain parameters and a hammer test protocol is proposed in order to check the predicted dynamic characteristics.

Sensitivity Analysis

- From the sensitivity analysis it is concluded that the parameters having most influence on the eigenfrequencies of the bridge were the soil density and the diameter of the glass diagonals.

- The first eigenfrequency of the bridge was found to be around 5Hz, which is not in range of loading frequencies of pedestrians. Limit values of the accelerations were all met (accelerations were less than 700mm/s^2). It can thus be concluded that the motion magnitudes of the Glass Truss Bridge do not exceed the estimated serviceability limits, the dynamic response is safe and comfortable for pedestrians to cross the bridge.

- Modes T2 and B1 are mainly contributed by the soil deck (upper part of the bridge) whereas T1 and T3 are modes which movements are mainly contributed by the glass diagonals (lower part).

Hammer test

- The experimental test setup is depicted in figures 8.1. The optimal hitting location is at 1m from midspan and 3m from boundary. Next to that the locations where to place the accelerometers for the two cases are shown.
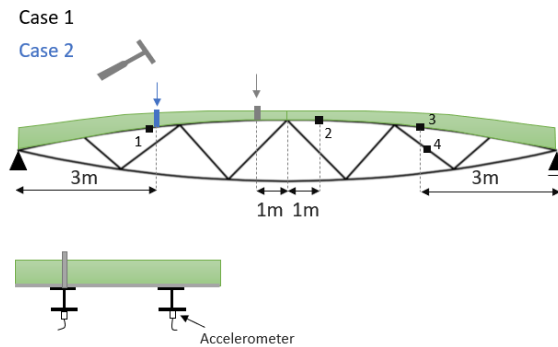
Figure 8.1: Hammer test setup: Case 1 and 2

- A minimum of six accelerometers is needed to be able to assess the dynamic characteristics of the Glass Truss Bridge, however to reconstruct the modeshapes with higher accuracy it is advised to place more accelerometers. This will however lead to a more time consuming post-processing of the obtained data.

- When performing the live hammer tests at least modes T1(4.6Hz), B1(7.8Hz), B2(16.5Hz) and T12(25.9Hz) need to be detected in order to be able to update the model with the outcomes of the hammer tests. Mode T1 can be tuned by updating the density of the soil, T12 can be tuned by updating the diameter of the glass. B1 and B2 are the first two bending modes and are tuned with both the glass diameter and the soil density, it should be checked if the parameters are updated in the predetermined range.

- Four bending modes and six torsional modes (B1, T4, T6, T7, B2, T11, B3, B4, T12 and T13) are expected to be found when performing the live hammer tests following the protocol provided in this report. Smaller peaks will not be visible because of the noise which will certainly be present in the signal.

Modal properties of the Glass Truss Bridge

- Ten of the twenty eigenfrequencies in a range of 0-30Hz were detected from the FRF's with the proposed test setup.

- For mode 3 (B1) with eigenfrequency 7,6 a damping of $\zeta = 0.01316$ is found. For mode 20 (T14), with an eigenfrequency of 26Hz, a damping of $\zeta = 0.0078$ is found. Both damping coefficients are found using the halfbandwidth method, however, this method is not applicable for very wide peaks.

- The modeshapes were reconstructed and visualized analysing the imaginary part of the complex valued FRF's. With six measurement locations only, the modeshapes are visible but rugged. It would thus be better to have at least two extra measurement points per beam.

After performing the hammer tests in real life on the Glass Truss Bridge, the FE model can be tuned and the modal properties (modal mass, stiffness and energy dissipation) can be determined. In this way a method of predicting the behavior of a glass structure is generated which can be used for future designs.

8.2. Future recommendations

Sensitivity Analysis

- To get a more accurate model of the bridge, more parameters should be analysed. One parameter with a high level of uncertainty which is expected to have a high influence on the dynamic behavior of the bridge is the rotational stiffness at the boundaries of the soil deck.

- The sensitivity analysis is only performed for vertical an torsional modes. The horizontal effects should also be investigated.

- The effective area of the glass diagonals is estimated based on the number of rods activated when loaded in compression. It should be noticed that this area might differ because minor load is applied when the bridge is forced dynamically. A design recommendation was already given by Verleg et al.: The material of the end-plate used must be soft enough to be able to equalize the ends of the rods. In this way no peak stresses occur in one of the rods leading to failure of one or more rods. It should be investigated if the total area of the glass rods can be considered when performing a modal analysis.

Hammer test

- First of all, when performing the hammer tests, it is recommended to measure the deflection of the bridge to a specific loadcase to be able to statically validate the FE model.

- The availability of the hammer and accelerometers from the University of Technology Delft should be checked. The kind of hammer used influences the range of frequencies excited. A hard tip has a short pulse and will excite a wide range of frequencies weather a soft tip has a relatively long pulse and will excite a narrow range. This influences also the minimal needed sampling rate, which was now set to 100Hz.

- A different manner to check the obtained results on its accuracy is through the Mode Indicator Parameter (MIP). At a resonance frequency all parts of the structure are moving sinusoidally at the same frequency, this is a so called normal mode. So if the MIP shows a value close to 1, this indicates a modeshape.

Modal properties of the glass truss bridge

- The boundary conditions are assumed to be simply supported with free rotation at both ends. This assumption is made based on an iterative study of the DIANA model of the Glass Truss Bridge together with the sensitivity analysis. To have a more realistic model, insight is needed in the boundary conditions of the bridge under consideration. Not only its stiffness but also the effect on the damping of certain modes should be investigated.

- Small changes of the rotational stiffness at the boundaries show no changes in eigenfrequencies. The threshold of the rotational stiffness for the dynamic case should be investigated.

- Other parameters like for example water content of the soil, connection properties of the nodes, structural damping and material damping might also be of influence but due to time limitations the focus was on the deck- and the glass-properties.

Loads

- The weight of the people standing on the bridge to perform the hammer excitation is not taken into account in this study, it is recommended to take this into account in future research. This might influence the predicted eigenfrequencies.

- Following the European guidelines an extra load representing 67 students (fully loaded) is taken into account for calculating the eigenfrequencies. The extra load influences the latter significantly, due to an increase in mass the eigenfrequencies found are lower. This should definitely be taken into account when performing the hammer tests.

- It would be interesting to look into the available methods of modelling pedestrian loads. Following European guidelines a total of 5 joggers is taken into account for the case of the Glass Truss Bridge. This is modelled like a point load of 6250N (5*1250N for joggers) acting in the middle of the bridge with a frequency of 3Hz. Modelling the joggers like this is an overestimation of the actual loading because the total load is centralized at one specific point.

Interesting topics for future research
1. Effect of different types of soil on the damping

From a dynamics point of view the soil has high influence on the damping of the structure. It basically acts as a mass-damper-system. One classical and world known example of a mass damper system is the the Taipei 101. The soil dissipates energy introduced by pedestrians walking over the bridge. Energy dissipation has been widely used as a key parameter to evaluate damage in elastic-plastic materials. It would be interesting to investigate the effect that different type of soil have on the damping of the structure.

2. Effect of plants on the stiffness of the soil-deck

Another interesting point for future investigation is the effect of the presence of plants on the stiffness of the structure. Soil does on itself have nearly any bending stiffness, from literature it is known that the roots of plants act as reinforcement. It is also known that a wide range of root types exist (see figure 8.2).
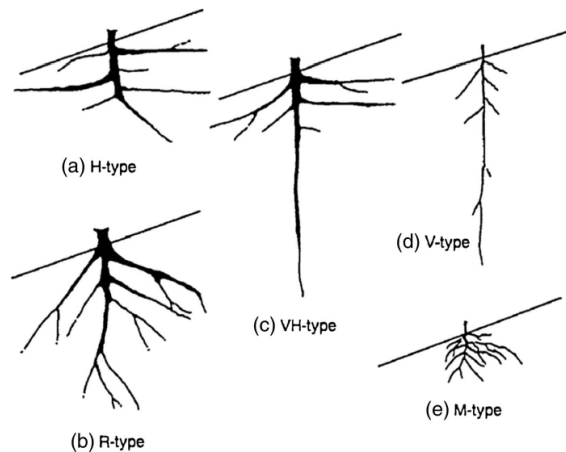
Figure 8.2: Different root patterns

A
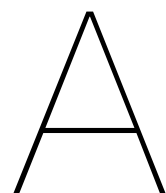
Technical drawings The Glass Truss Bridge
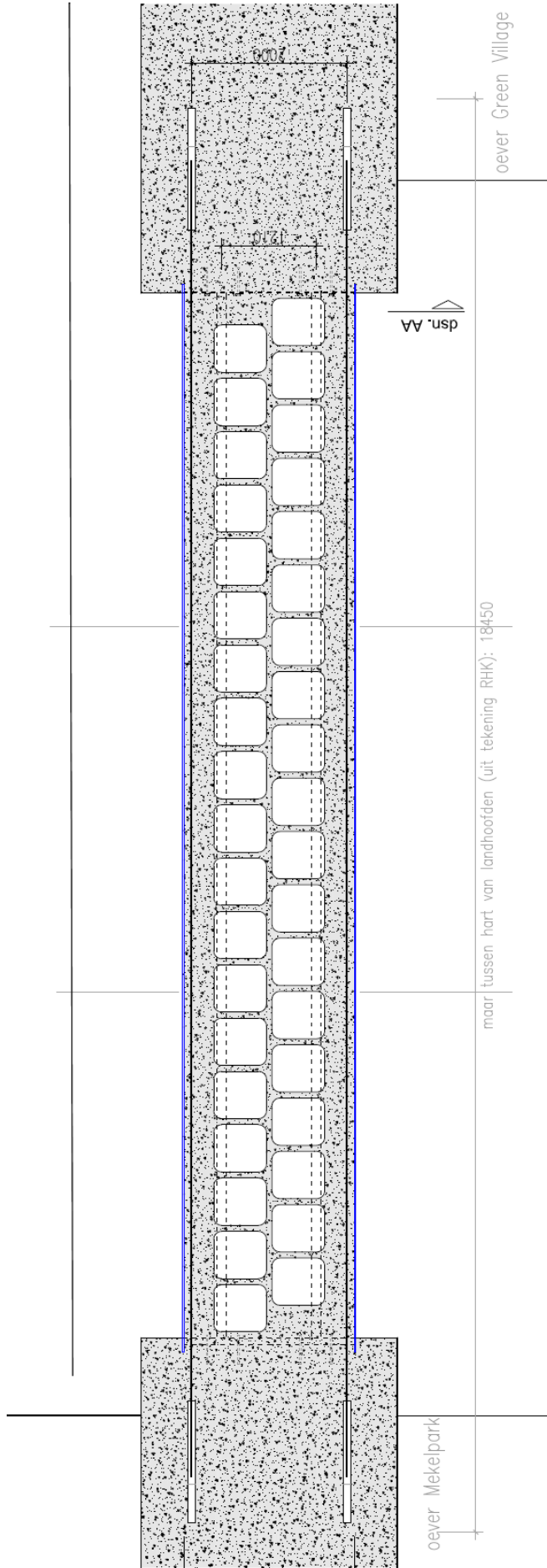
Figure A.1: Plan of Glass Truss Bridge, scale 1:50 from [26]

Figure A.2: Side view of Glass Truss Bridge, scale 1:50 retrieved from [26]
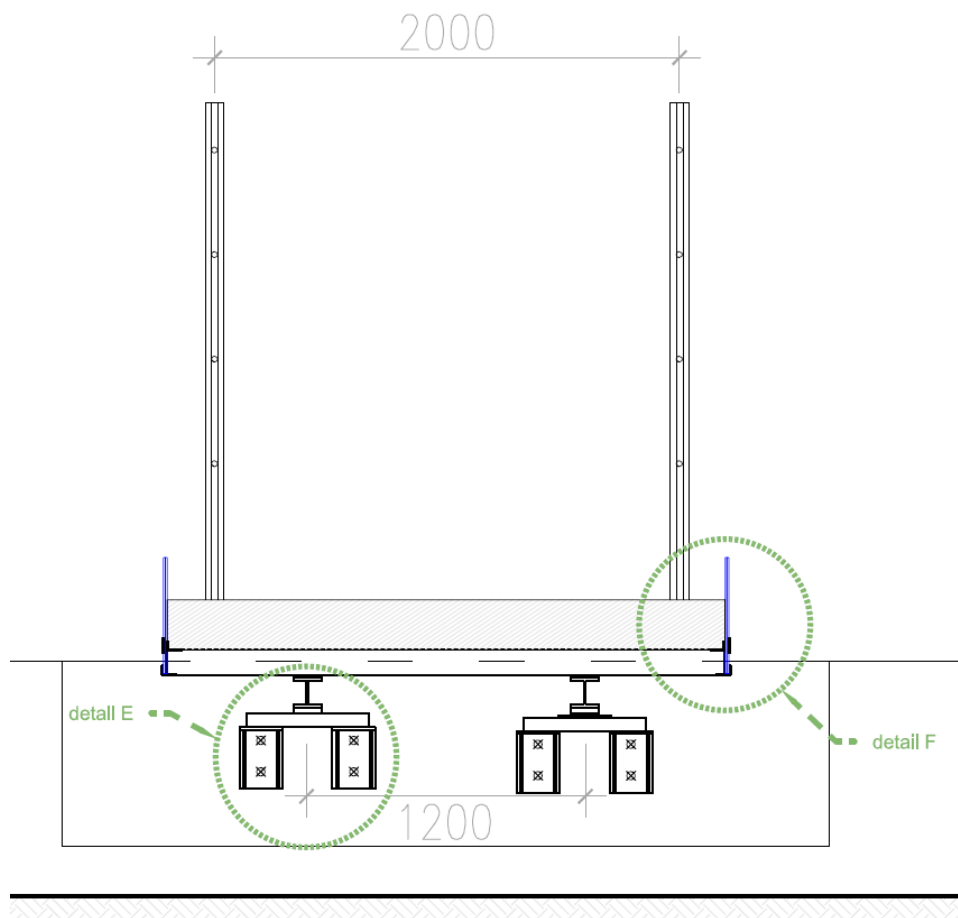
Figure A.3: Cross-section AA, scale 1:20 [26]

glazen balustrade fln.
4 platen van 10 mm
1 plaat van 8 mm
opbouw; 10 10 8 10 10
versterkt glas polygeslepen
met sentryglas gelamineerd.

463

rvs koker profiel 30 x 2 mm gebogen
en mee in gelamineerd

282

450

450

20 mm dlameter
staal kabel
voorgespannen

1305

550

bevestlglng van glazen fln
aan landhoofd mlddel stalen
hoek profielen

1084
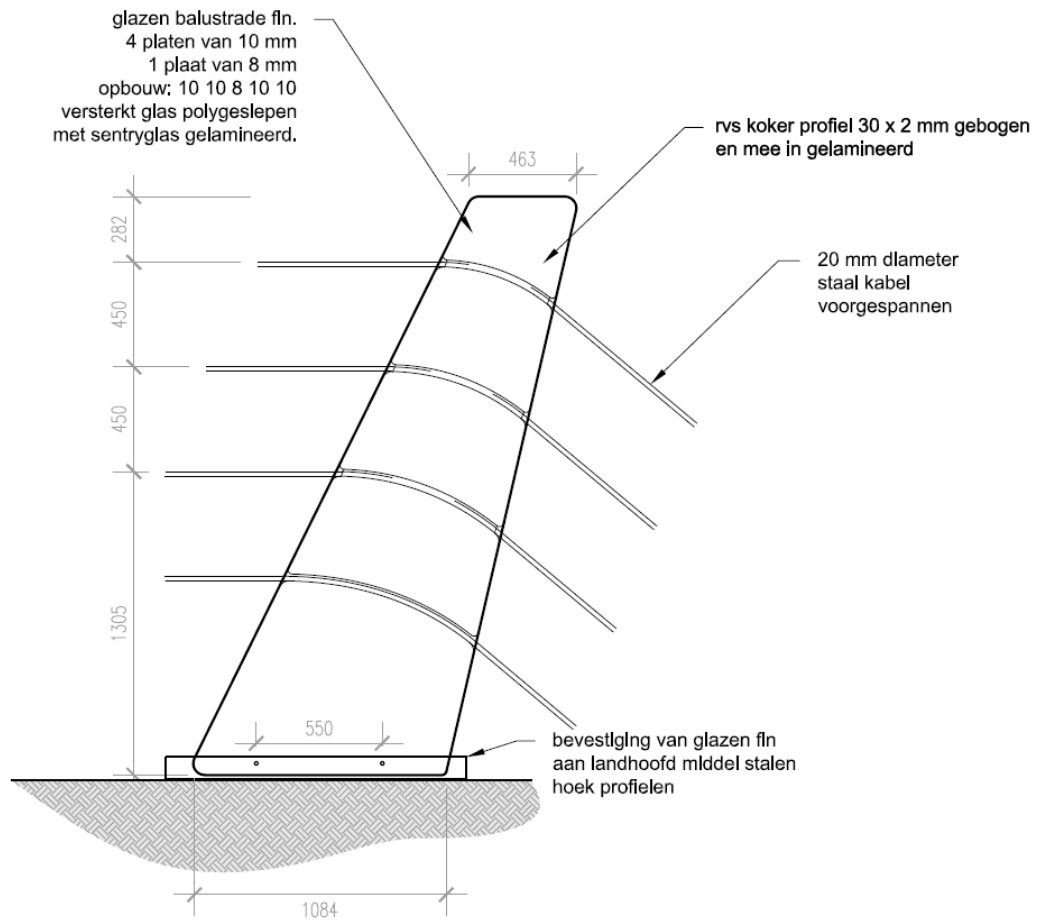
Figure A.4: Detail A, scale 1:20 [26]
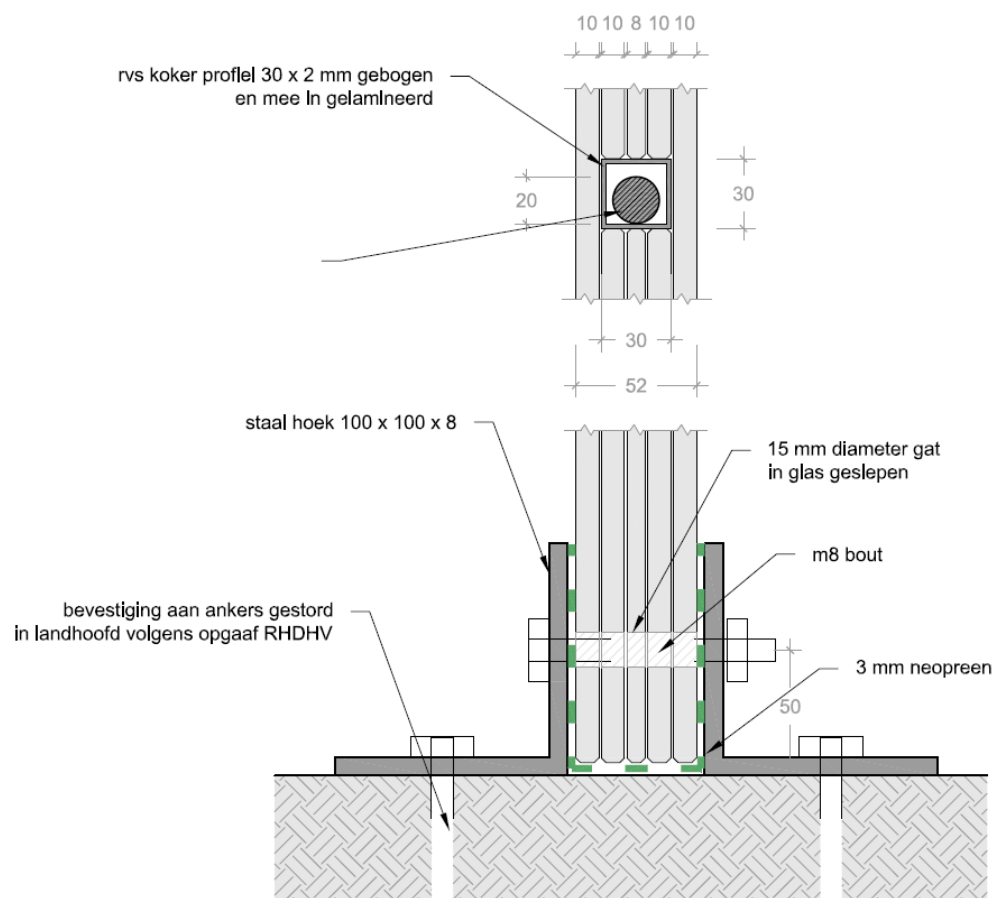
Figure A.5: Detail A, scale 1:2 [26]
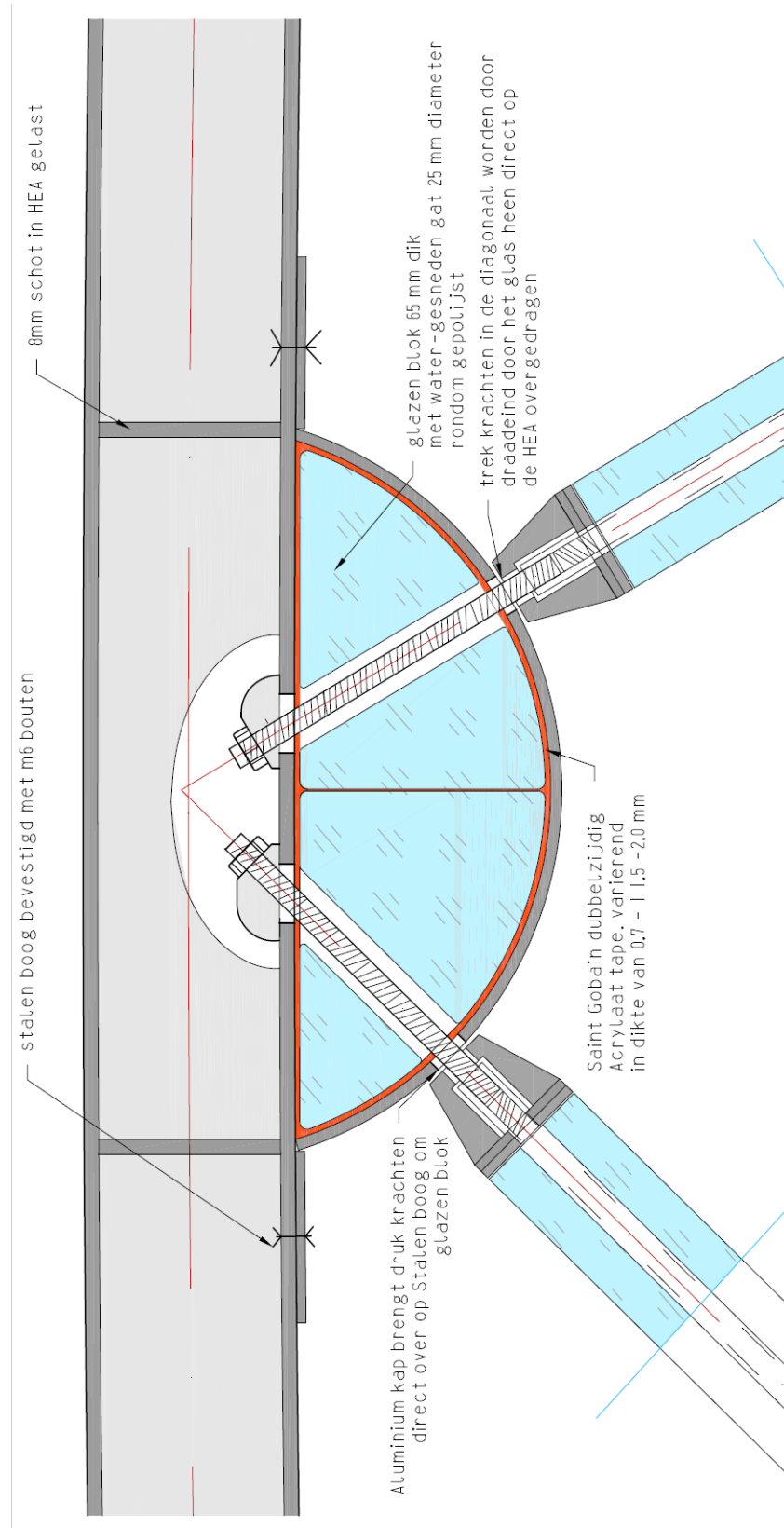
Figure A.6: Detail B, scale 1:2 [26]

bundel van 22 mm diameter glas staven
aan elkaar gelamineerd met DELO lijm

12 mm diam draadeind als trekstang

2 mm PVC between steel
tension rod and glass
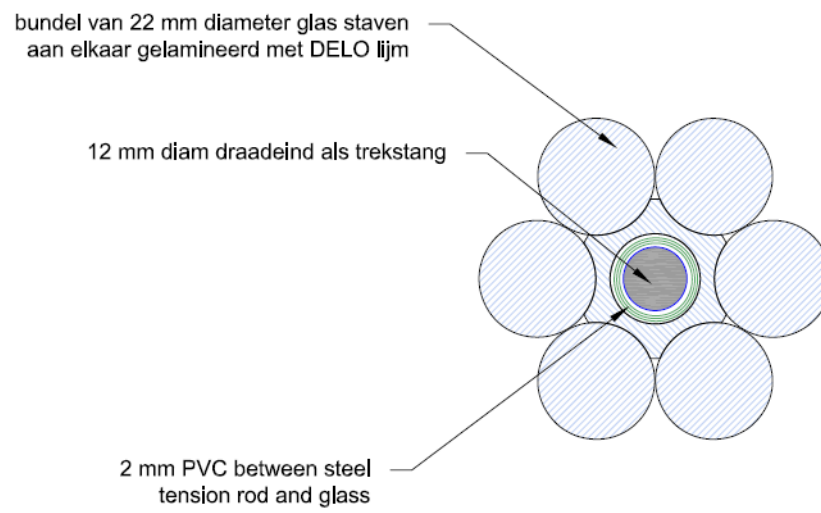
Figure A.7: Detail C, scale 1:1 from [26]

3 mm neopreen

betonnen landhoofd volgens
tekeningen RHDHV

ankers volgens
tekeningen RHDHV

soll

geprofileerde staalplaat 106R/7750 mm verzinkt

stalen kopplaat en schot
met las bevestigt

2 x 8 mm stalen schotten aan vakwerk
en vlakke 8 mm oplegplaat.gelast
geheel met bouten aan opleg steun

steel bar 60x60 mm

staal HE120A

stalen strip 120x30 mm
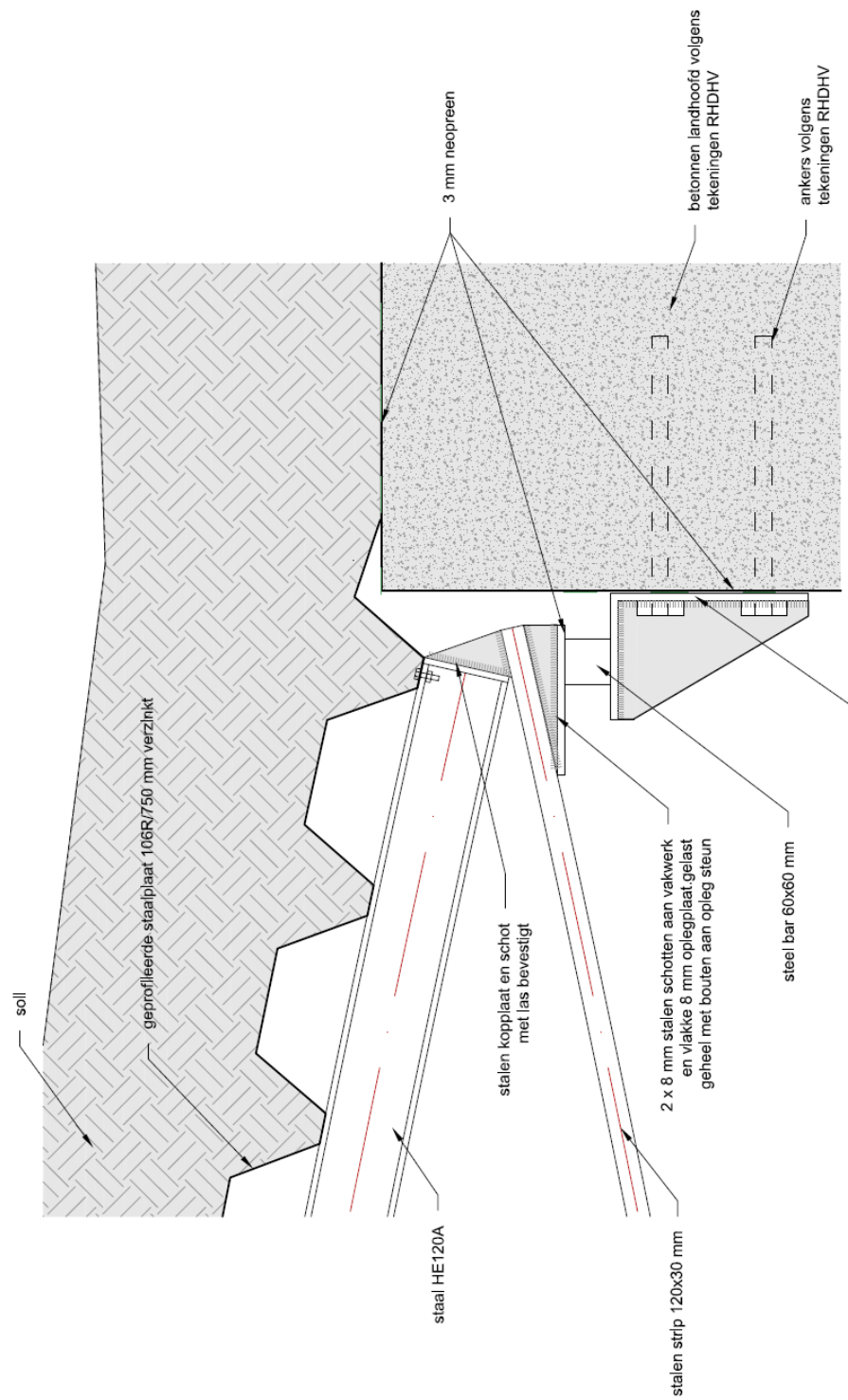
Figure A.8: Detail D: boundary condition, scale 1:5 [26]
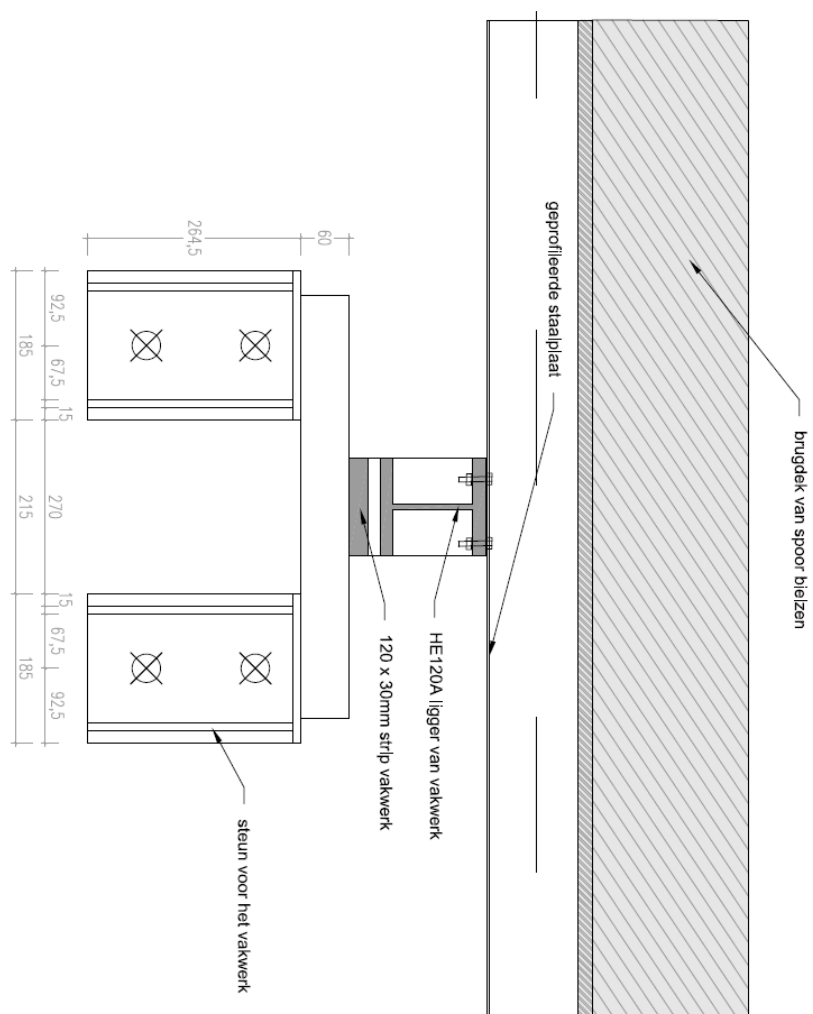
Figure A.9: Detail E, scale 1:5 [26]

corrugated steel sheeting 106x1,5 mm

L steel profile 60x40x5 mm

soil

worteldoek

glass retaining wall
laminated 6.6.2

M6 bolt
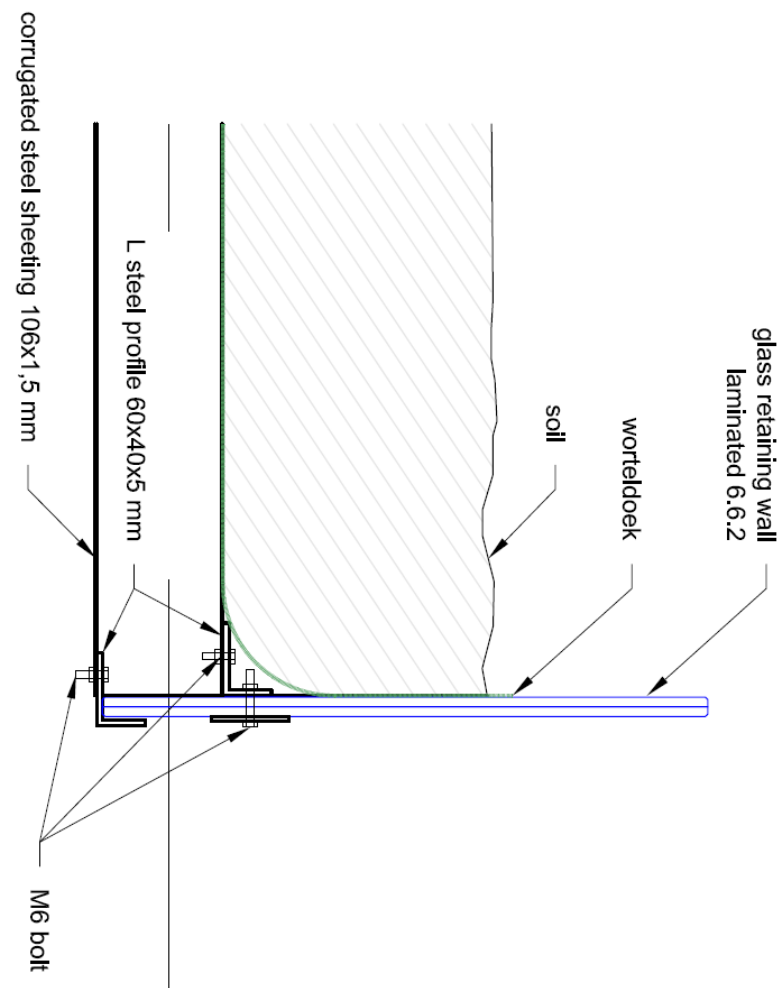
Figure A.10: Detail E, scale 1:5 [26]

B
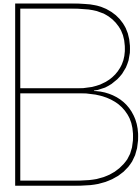
Modal analyses from literature

Modal analysis is the process of determining the dynamic properties of a system in forms of natural frequencies, damping factors and mode shapes. These parameters are then used to formulate a mathematical model for the dynamic behaviour. The mathematical model is referred to as the modal model of the system and the information for the modal properties are known as its modal data.

The dynamics of a structure can be described by frequency and position. This can be visualised through the analytical solution of partial differential equations of continuous systems. Modal analysis is based upon the fact that the vibration response of a linear time-invariant dynamic system is expressed as the linear combination of a set of simple harmonic motions called the natural modes of vibration. The use of a Fourier combination of sine and cosine waves to represent a complicated waveform is used. The natural modes of vibration are inherent to a dynamic system and are determined completely by its physical properties (mass, stiffness, damping) and their spatial distributions. Each mode is described in terms of its modal parameters: natural frequency, the modal damping factor and characteristic displacement pattern, or in other words, mode shape. The mode shape may be real or complex, each mode corresponds to a natural frequency. The degree of participation of each natural mode in the overall vibration is determined both by properties of the excitation source and by the mode shapes of the system [2]. To apply modal analysis methods, it is important that the assumption of a linear, time-invariant system is valid, this is why a Fourier transform is often applied to transform the time-dependent signal into a frequency dependent signal.

B.1. Fourier transform

The Fourier Transform is a mathematical algorithm that decomposes a signal into its constituent frequencies. Each signal can be described by a summation of sines and cosines.

The Fourier transform of a time-dependent signal is a complex-valued function of frequency. The amplitude of the function represents the amount of that frequency present in the original function. The Fourier transform is not limited to functions of time, but mostly a function of time is inserted as input. There is also an inverse Fourier Transform whose name gives already an explanation of the use.

An example of a Fourrier series is found in the paper **Human induced vibrations on foot-bridges, Pawel Hawryszków, 2014**. In this paper a methodology for footbridges classification with regard to their dynamic sensitivity is worked out. The correlation between the structure's properties and its dynamic response due to pedestrian traffic is formulated. It has been determined that there is a possibility to effectively prognosticate the pedestrian bridge dynamic sensitivity. Characteristics of human movement have been described, with special emphasis placed on the statistic distribution of the frequency of a human step. The formulas are as follows:

$$Mu''(t) + Cu'(t) + Ku(t) = F_p(t)$$

$$F_p(t) = \sum_{i=1}^{n} G_i \sin(2\pi i f_i t - \phi_i)$$

B.2. Types of modal analyses

Operational Modal Analysis vs Experimental Modal Analysis

A frequently used method for bridges and high rise buildings is Operational Modal Analysis (**OMA**), often called Ambient Response Analysis. With this method a modal analysis is carried out without knowing and/or controlling the input excitation. Operational Modal Analysis separates noise and inputs from the outputs and returns the unbiased modal information only.

A second well known method is Experimental Modal Analysis (*EMA*), the main difference is that with EMA the input is known. The excitation is normally produced by either an Impact Hammer or by one or more shakers. Both these types of devices can produce a force and at the same time measure it. The structure is mounted with one or more accelerometers at the positions where the response of the modes of interest is good. The impact hammer is used to impact the structure either at one location only or at all the positions where is needed. If a single accelerometer is used to measure the response the technique is normally called Single Reference technique, whereas in the case of several it is referred to as Multiple Reference technique.

Important in both OMA and EMA techniques are the locations where the accelerations should be recorded and the sampling rate at which the measures should be done. According to the Nyquist Theorem the sampling rate should be at least twice the highest frequency contained in the signal to avoid aliasing. Aliasing refers to the distortion that results when a signal reconstructed from samples is different from the original continuous signal. A good example is the wagon wheel effect, the effect that a moving wheel seems to stand still.

During a hammer test there are several sets of simultaneous measurements of the input forces and the output accelerations. These signals are transferred to the frequency domain by the Fast Fourier Transform (FFT) that produces an input force spectrum and an output acceleration spectrum. The trick now is to divide the output spectrum with the input spectrum to obtain the so-called Frequency Response Function (FRF). This function shows how the structure will respond to input at a certain frequency. It is a system function that is in principle very clean, since all input is divided out of the output. To keep the FRF clean it is important that the measurable force is the only excitation acting on the structure during the test. Any unmeasured input forces will cause a pollution of the FRF. The Coherence Function is normally used to evaluate the quality of the FRF.

Eigensystem Realization Algorithm

ERA is an input-output method. Using known values of the input f(t), and measuring the output of the system x(t) from m measurement locations, the Frequency Response Function (FRF) may be extracted with:

$$H_i(j\omega) = \frac{S_{xf}(j\omega)}{S_{ff}(j\omega)}, \quad i = 1 \ldots m$$

Figure B.1: Extracting the Frequency Response Function [23]

Then by applying the Inverse Fourier Transfom, the Impulse Response Functions (IRF) per measurement channel (usually this implied per degree of freedom) are obtained. The ERA method, as described previously, can then be implemented on the IRFs which essentially simulate the system's response to impulse.

Matrix Pencil (MP) Algorithm

The MP Algorithm uses noise-contaminated data to construct an eigenvalue problem of a non-square matrix from single channel measurement data. The solution of the eigenvalue problem gives

frequencies and damping ratios for each inherent vibration mode, which are not due to noise. To deal with noise contamination, a Singular Value Decomposition (SVD) is performed, which is a useful mathematical conversion to reveal the principal inherent system properties (eigenfrequencies, damping. [23]

Frequency Domain Decomposition

This is an output-only system identification technique. First an estimation is done for the power spectral density matrix at discrete frequencies. Then a singular value decomposition of the power spectral density is done. For an n degree of freedom system, the n dominating peaks are picked in the power spectral density. These peaks correspond to the mode shapes. Using the mode shapes, an input-output system realization can be written.[9]

Random Decrement Method

The basic idea of the method is to delete all parts of the signal that are not of interest for further analysis by averaging a large number of segments cut out from the signal at a certain trigger value. This method requires a white noise excitation. White noise is a random signal having equal intensity at different frequencies, giving it a constant power spectral density. It is not possible to apply a white noise excitation on the glass truss bridge, so this method is not further elaborated.

Windowing

Windowing consists of multiplying the time record by a finite-length window with an amplitude that varies smoothly and gradually toward zero at the edges. This makes the endpoints of the waveform meet, which results in a continuous waveform without sharp transitions. Two common time domain windows are Force and Exponential windows. The Force window is used to remove noise from the impulse (force) signal, the Exponential window is used to reduce leakage in the spectrum of the response.

$$C$$
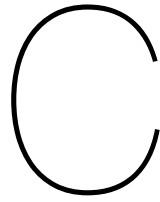
Damping

C.1. Continuous Damping

When a form of continuous damping, like viscous dashpots, is included in the finite element model then the direct solution method or the direct time integration procedure must be used. Discrete places of damping are obtained by specifying properties for spring elements.

C.2. Rayleigh Damping

Applying a non-modal solution technique, it is necessary to evaluate the damping matrix C explicitly and usually viscous damping effects can be included by assumption of Rayleigh damping which is of the form

$C = aM + bK$

where a and b are constants to be determined from given damping ratios.

C.3. Structural Damping

Another type of damping, frequently employed in dynamic analysis, is structural damping. This type of damping is proportional to displacement but in-phase to velocity of an harmonically oscillating system. In that way the equation of motion is expressed as

$M\ddot{u} + K(1 + i\gamma)u = f(t)$

where γ is the structural damping factor.

D
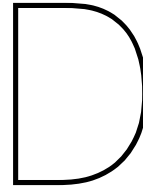
Glass as a structural material

In this chapter reference is made to different articles stated at the top of each paragraph.

D.1. Types of glass

Structural Glass reader CIE4285, 2019
  Structural use of glass, International Association for bridge and Structural Engineering, 2008
In this paper and reader the process of making glass and the different types as well as the properties are explained. A rough summary will be given here.

Throughout years different techniques have been developed to make glass. Also a lot of variations in recipes have been tested. The main compound is silica (SiO_2) which is the primary consistent of sand. Soda-lime-silica and borosilicate glasses remain as only options when considering glasses in construction. These types will be further analysed to know their differences. Next to that, fiber glass will be investigated, this is also highly used in construction, mainly as reinforcement of polymers.

D.1.1. Soda-lime-silica glass

This is the most common type of glass. It can be divided in flat glass used for windows, made by the float process, and container glass used for bottles, produced by blowing. Typically soda-lime-silica glass contains 69-74 % silica, 5-14 % lime, 10-16 % soda and other minor ingredients such as magnesia (MgO) and aluminia (Al_2O_3).

D.1.2. Borosilica glass

The main difference between Soda-lime-silica and Borosilica glass is that Borosilica glass contains a small amount of boron-oxide (B_2O_2) This glass is mainly used for laboratory glass and cooking utensils. Its resistance to thermal shock is much better compared to Soda-lime glass, which makes it more appealing for temperature-dependent functions.

D.1.3. Resistance to high temperatures

The resistance of glass to high temperatures is low and glass transmits heat rapidly. This differs per glass type. Glass also starts to soften and loses stiffness at temperatures above the glass transition temperature (500 degrees). The glass truss bridge is located above water, the risk of fire is thus considered to be low. Differences in temperature between the upper and lower parts of the bridge should be taken into account when changing the materialization of the bridge.

D.1.4. Glass fibers

Mechanical behavior of sintered submicron glass fiber mats, Seongpil et al, 2020
Glass fibers are produced using melt spinning techniques. The first step is melting the glass composition into a platinum crown with small holes. The molten glass will be extruded through these holes forming fibers with small diameters. Glass fibres come in several types. The most common ones are Alkali (A), Electrical (E), C-, R- and S-glass fibres. The single compound that is used the most in fibre

glass is silica. Silica takes 50 up to 70 percent of the weight to its count. The nowadays most common type of glass fiber is E-glass, this is alumino-borosilicate glass which provides good electrical, mechanical and chemical resistance. Another interesting type is S-glass, alumino-silicate glass with high MgO-content, resulting in a high tensile strength. [6] This information could be useful when redesigning the glass truss bridge in terms of materialization.

Glass fibers, also called fiberglass, is a lightweight, extremely strong, and robust material. It is widely used as reinforcement in concrete and polymers. Although strength properties are somewhat lower than carbon fiber and it is less stiff, the material is typically far less brittle, and the raw materials are much less expensive. Its bulk strength and weight properties are also very favorable when compared to metals, and it can be easily formed using molding processes. A picture of glass fibers is given in D.1.

Figure D.1: Glass fibers

In the paper stated at top of this section paper, glass fiber mats are tested in a longitudinal and transverse tensile test. The results show the differences in material properties between annealing temperatures as well as the stretching direction.
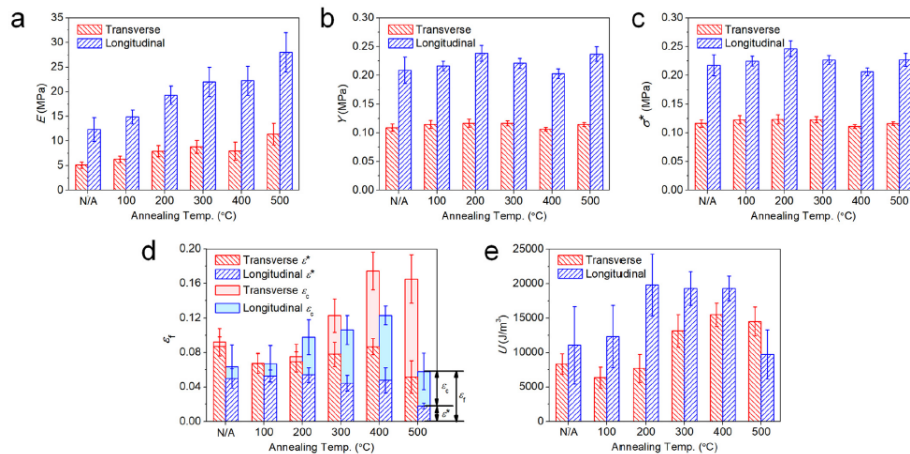
Figure D.2: Comparison longitudinal and transversal properties glass fiber mats

Interesting remarks are the formation of bridges or junctions between macroscopic glass fibers after sintering, which contributes to the tensile properties. The sintered junctions resist and delay fracture of the specimens beyond the maximum tensile strength.

The tensile stress is given by the following equation:

$$s\_xx = Y * tanh((E/Y) * e\_xx) \tag{D.1}$$

Where E is Young's modulus, Y is the yield stress, e_xx is the tensile strain, and x is the stretching direction.

D.2. Sustainability

Sustainability of glass in construction, Achintha, 2017

In this paper the potential applications of glass is discussed and a part of it is summarized in this section. Glass is a sustainable, fully recyclable material which provides great environmental benefits

such as contributing to mitigating climate change and saving natural resources. It is also highly appreciated in many applications for its inert nature and its contributions to safeguarding people's health and well being. Glass is a resource efficient material which is made of abundant natural raw material: sand and glass waste (cullets). Glass is a fully recyclable material that can be recycled in close loop over and over again.

The embodied energy/carbon of glass is the energy/carbon consumed by all the materials and the process associated with the construction of the structure. Similarly the embodied carbon of a structure is the total carbon associated with all materials and processes used over the total life cycle of the same [4]. A comparison between the embodied energy and carbon values of glass, steel and concrete can be seen in table D.1.

Material	Embodied energy (MJ/kg)	Embodied carbon (MJ/kg)
Reinforced concrete	1.39	0.057
Toughened glass	23.5	0.346
Steel(Bar and rod)	24.6	0.466

Table D.1: Comparison of embodied energy and carbon values of glass, concrete and steel [4]

A major contribution of the embodied energy/carbon is due to the high temperature production process. Although concrete has a lower impact per unit mass, its global impact is much greater due to the large volumes of concrete used in construction. In addition glass is more durable than steel and concrete due to its non-corrosive and inert nature.

D.3. Modelling glass in a finite element program
1. The structural behaviour of bundled glass columns, Verleg, 2019
The modelling of glass in a finite element program is not as easy as it is for other materials as steel or concrete. As mentioned in this paper, glass fails in a certain way due to cracks and/or flaws on the surface or bubbles within the glass. These geometrical imperfections are the reason why glass is very weak in tension. Different factors including flaw size, orientation and quantity influence the strength of glass. This can be easily compared to a single paper sheet with an arbitrary flaw in the middle, see figure D.3. When applying a tensile force in the direction of the flaw (sigma2), the material can resist a higher stress (in comparison with the other direction). When applying the stress perpendicular to the flaw (sigma1) the flaw will propagate easily with a relatively low stress.
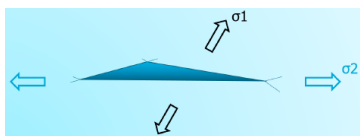
Figure D.3: Schematized figure of a microscopic flaw within the glass [31]

From literature it can be stated that glass fails due to tensile stresses exceeding the ultimate tensile strength where a critical flaw is present [31]. From here it can be stated that the variety of geometrical imperfections along a piece of glass causes a variety of tensile strengths. This phenomenon is used to model the glass using the finite element method. The glass is divided into a finite number of elements, which all have a certain ultimate tensile strength. Because it is not possible to predict the position and orientation of the flaws in a certain glass element different Weibull distributions are used to make a good estimation. More information about the Weibull distribution can be read in chapter 7 of [31].
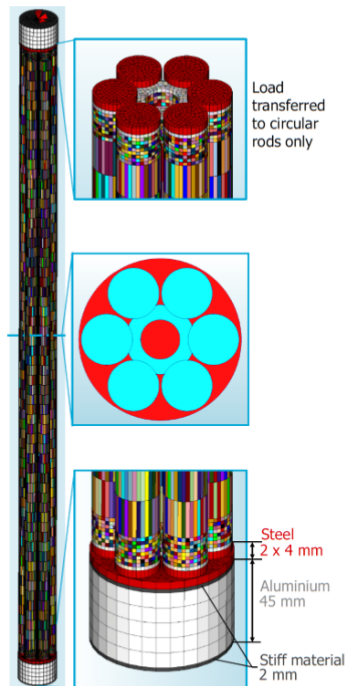
Figure D.4: FEM model of Glass Truss Bridge diagonal including boundary conditions [31]

In figure D.4 the finite element model of one column is shown, the boundary conditions are also pictured. The main conclusion is that the glass columns show stiffer behaviour in reality than the models do. The addition of the adhesive to the columns (which was not modelled) causes them to behave stiffer.

From this study mechanical properties of the glass diagonals including the buckling load and the probability of occurrence might be useful.

D.4. Comparison between Finite element programs

In the past decades different FEM programs have been developed. In this section a comparison is made between DIANA, SCIA and RFEM. These are the programs which are available from either the TU Delft or Witteveen& Bos. First an overview is made of the requirements which will most probably be needed to achieve the goal set in chapter 2 of this document. An overview of the findings are depicted in figure D.5. As can be seen, no big differences are found, prerequisites are mostly covered by all three programs.

Requests	SCIA	RFEM	DIANA
Possible to get a license			
Dynamic analysis possible			
Visualization eigenfrequencies			
Eigenmodes			
Easy to work with			
Good tutorials			
Possible to model glass			
Works with python			
Posibility of optimilization			
People who can help me with			

Figure D.5: Comparison between FEM programs

My conclusion is to perform the dynamic analysis of the Glass Truss Bridge in DIANA, its features are good and it will be interesting when modelling the soil, in that case 3D elements might be necessary.

D.5. Dynamics

The general approach for determining vibrations in the design stage of the footbridge is as follows:

- Build a numerical model or an equivalent SDOF-oscillator of the structure and select realistic damping characteristics.

- Choose a load model (single person, walking, running, dancing).

- Analyse the frequencies and the accelerations caused by the chosen load.

- Compare to the limit values.

As soon as a dynamic load is applied on a footbridge, the bridge can act as an oscillator. A dynamic load is a load that varies over time. Oscillators can have multiple degrees of freedom, here the single degree of freedom system will be discussed as an example. An oscillator with a single degree of freedom (SDOF) is shown in figure . In figure the dynamic force F(t) is applied on the oscillator.
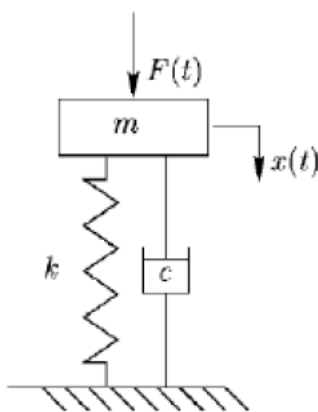
(a) The glass truss bridge as a Single Degree of Freedom system
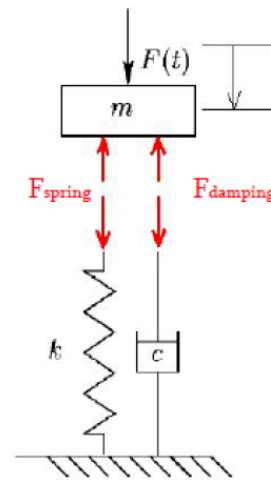
(b) SDOF oscilator in motion

From Newton's first law one can state that the sum of the forces should be equal to the mass times the acceleration:

$$\sum F = m * a \qquad \text{(D.2)}$$

The acceleration is the second derivative of the displacement.
From figure D.6b the following is true:

$$m\ddot{x}(t) + kx(t) + c\dot{x}(t) = F(t) \qquad \text{(D.3)}$$

where: m = Mass of the (moving) object c = Damping coefficient of the structure k = Stiffness coefficient x(t)= Displacement of the mass of the moving object F(t)= External excitation force

In the same way a multiple degrees of freedom system can be constructed and the response of the system to the dynamic load can be approached. The difficulty lays in determining the stiffness and damping parameters of the system because of its particular form, the materials used and the fact that damping depends on a lot of factors.

One method of determining these dynamic parameters is through on-site vibration testing. The already constructed Glass Truss bridge is a perfect opportunity to perform these tests. The resulting parameters can be used to built a numerical model of the bridge describing its response to dynamic loads.

E
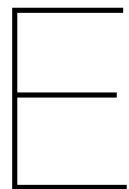
Regulations on footbridges

In 2012 the Eurocodes have been included in the Dutch building regulations. These are European standards providing technical rules for the structural design of construction works in the European Union. All members of the EU may also add so called National Annex including national parameters which differ per country. In Euro-code some guidelines are given for the design of footbridges. Because no regulations are given for designs with structural glass in the Eurocode, some recommendations of other codes (fib, Sétra and Hivoss) are given.

In figure E.1 the structure of the system of the different Euro-codes is shown. It can be seen that the guidelines for designing with structural glass are missing. There are however guidelines for the design of footbridges and pedestrian loads. The content of these documents will be shown here as the paper of K.Verleg has already selected the chapters needed for this study.
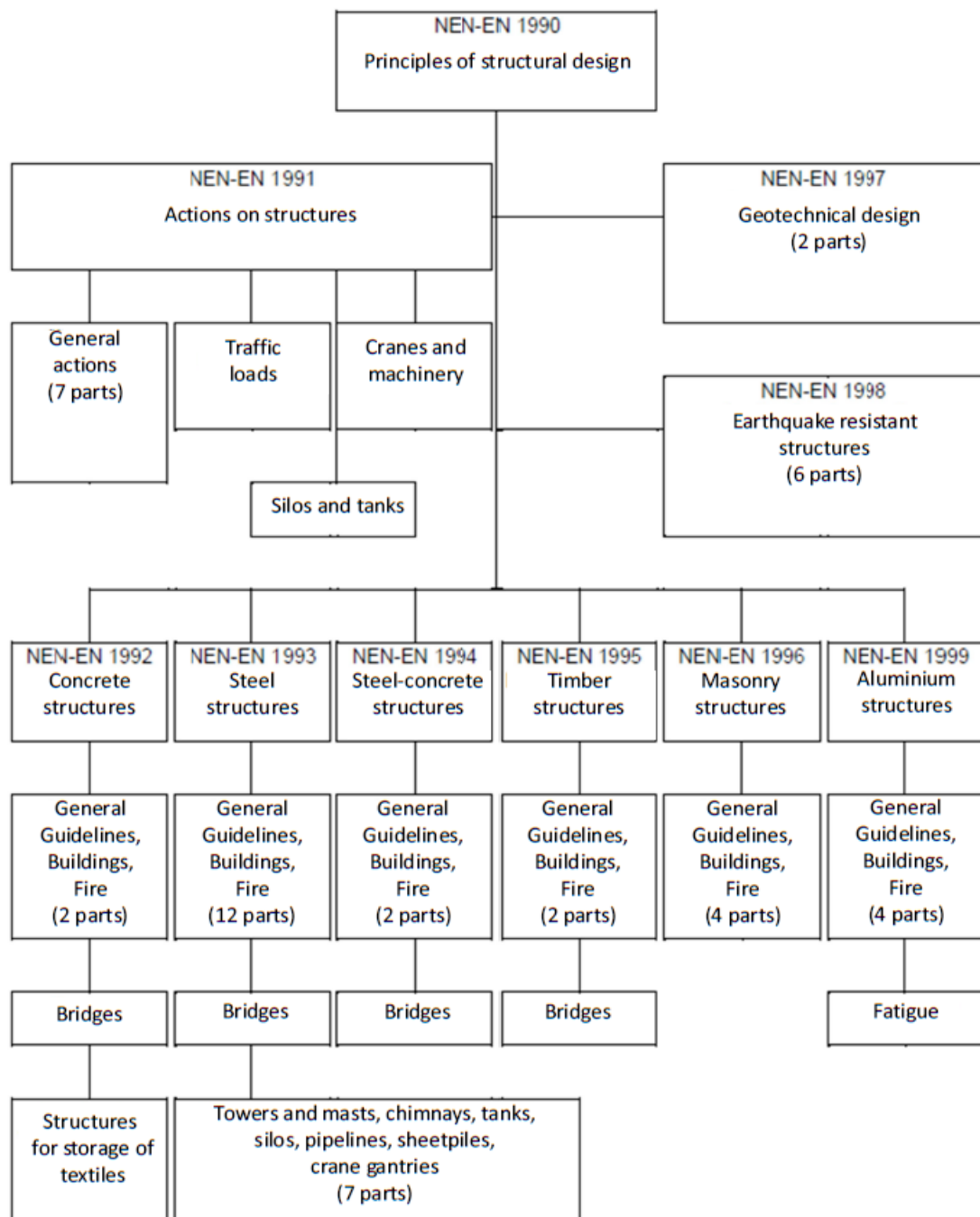
Figure E.1: structure of Eurocode systems on footbridges

E.0.1. Design load cases
EN 1990

1. The design situations have to be selected, these depend on the allowed amount of pedestrians on the footbridge during the design lifetime of the bridge.

2. A group of 8 to 15 walking people has to be taken into account in permanent design situations.

3. Different traffic scenarios have to be specified

E.0.2. Comfort criteria
EN 1990

1. The maximum allowed acceleration of a random part of the deck are defined:
   0.7 m/s^2 in case of vertical vibrations
   0.2 m/s^2 in case of horizontal vibrations
   0.4 m/s^2 in case of exceptional circumstances of a crowd

2. Verification of the requirements of the comfort criteria should be made if the natural frequency is smaller than:
   5Hz vertical
   2.5 Hz horizontal and torsional vibrations

Comfort class	Degree of comfort	Vertical a_{limit}	Lateral a_{limit}
CL 1	Maximum	< 0,50 m/s²	< 0,10 m/s²
CL 2	Medium	0,50 – 1,00 m/s²	0,10 – 0,30 m/s²
CL 3	Minimum	1,00 – 2,50 m/s²	0,30 – 0,80 m/s²
CL 4	Unacceptable discomfort	> 2,50 m/s²	> 0,80 m/s²

Figure E.2: Comfort classes

National Annex
In the NA point the following remark is made: The first two items correspond to the medium comfort class (CC2) in combination with traffic class 2 according to EUR23984.

E.0.3. Static models for vertical loading conditions
EN 1991

The following has to be taken into account:

1. Uniform distributed load q_fk = 5kN/m^2

2. Concentrated force Q_Fvd = 10kN at an area of 0.1x0.1m^2

3. Service vehicle

4. Extraordinary vehicle: a biaxial load settlement of 80kN and 40kN with wheelbase of 3m

National Annex

1. No adjustments

2. Q_Fvd = 7kN at an area of 0.1x0.1 m^2

3. Q_serv = 25kN as the characteristic value of the axle load, taking into account two axes with wheelbase 3m

4. In case no permanent obstacle is present preventing a vehicle drive on the bridge, an extraordinary vehicle has to be taken into account, dimensions same as EN

E.0.4. Static models for horizontal loads - characteristic values

EN 1991 [ch. 5.3] Only for footbridges a horizontal load Q_flk needs to be taken into account, which is applied along the axis of the bridge deck at the height of the wear layer.

   National Annex

   The characteristic values of the horizontal load needs to be equal to the largest of the following two values:

   • A load that corresponds with 10 percent of the total uniformly distributed load (5.3.2.1)

   • 30 percent of the total weight of the service vehicle, if such a vehicle is prescribed (5.3.2.3)

   The horizontal load needs to be applied in the longitudinal direction in the same time span as the matching vertical load, and never with the concentrated load. This force is in general enough to ensure the horizontal stability in the longitudinal direction of footbridges. It does not ensure the horizontal stability in the lateral direction, these need to be ensured by taking into account other loads or by taking appropriate measures in the design.

E.0.5. Dynamic models of pedestrian loads

EN1991 [ch.5.7]

   Three items are mentioned for the dynamic models of pedestrian loading:

1. The natural frequencies of the main structure need to be determined

2. Load exerted by pedestrians with a frequency equal to the natural frequencies of the bridge can cause resonance. For pedestrians the limit states are: in vertical direction 1 - 3 Hz in horizontal direction 0.5 - 1.5 Hz In case of joggers 3 Hz

3. Appropriate dynamic models and comfort criteria for pedestrian

   National Annex

1. No adjustments

2. No adjustments

3. Load models in appendix A of the National Annex have to be taken into account

4. In case of normal use traffic class 3 and loading by joggers has to be taken into account: for L ≤ 20 m, 5 joggers

5. In the project specifications different traffic classes with corresponding comfort criteria can be defined

6. It has to be proven that the bridge can not exceed the ultimate limit state by vibrations applied by vandalism. Unless specified otherwise in the project specifications, traffic class 5 according to annex NB.A needs to be applied. A damping with a lower limit of the damping measure equal to 50% of the nominal damping of the structure needs to be applied.

   NB A1: Harmonic load model A uniformly distributed harmonic load may be assumed that represents the equivalent pedestrian stream:

$$p(t) = P * cos(2pi * f^s * t) * n' * \zeta \qquad (E.1)$$

   where:

   $P*cos(2pi*f^s*t)$ is the harmonic load that is caused by a single pedestrian; P is the force applied by a single pedestrian with step frequency f^s, which can be divided in vertical, longitudinal and lateral direction; f^s is the step frequency, which is assumed to be equal to the considered natural frequency of the bridge; n' is the equivalent number of pedestrians at the loaded surface S zeta is the reduction coefficient accounting for the change of the step frequency actually being in the critical range of the natural frequencies.

   For the different directions, force P is divided into three components as can be seen in table E.1

Vertical	Longitudinal	Lateral
280 N	140 N	35 N

Table E.1: Components of force P caused by a single pedestrian

(a) Reduction coefficient 1a:Vertical and longitudinal

(b) 1b: Sideways
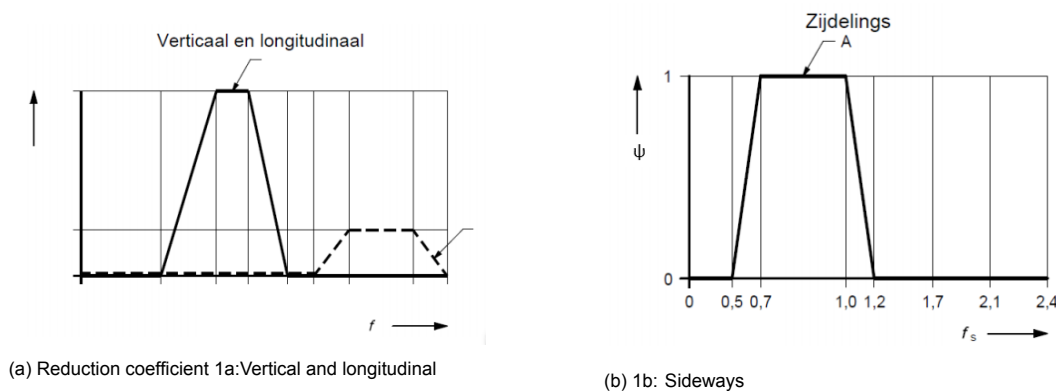
In figure E.4 the equivalent number of pedestrians per traffic class (TC) on loaded surface for load models TC1 to TC5 is shown.

Traffic class	People density d (1/m^2)	Equivalent number of pedestrians n' (1/m^2)
TC1		
TC2	$d < 1,0$	$n' = \dfrac{10,8\sqrt{\xi.n}}{S}$
TC3		
TC4	$d \geq 1,0$	$n' = \dfrac{1,85\sqrt{n}}{S}$
TC5		

Figure E.4: Table 5.6 of NA Equivalent number of pedestrians

where:
xi is the logarithmic decrease of the structural damping coming from table F.2 of NEN-ENb1991-1-4+A1+C1 (not given for steel-glass composite truss bridges);
n is the number of pedestrians on the loaded surface S
d is the number of persons per m2
S is the loaded surface in m2

The load model (in traffic class TC1) accounts for the unrestricted movement of pedestrians. This is why the synchronisation between the pedestrians is equal to that of a stream with low density. For high stream density (in traffic class TC4 and TC5) it will be harder to walk, therefore the synchronisation between pedestrians will increase. Walking becomes impossible for limit values of 1.5/m2 which cause dynamic effects to decrease significantly.

Load model for runners The load model is a single load p(t,v) that moves across the bridge with a velocity v of the runners. The single load can be calculated using:

$$p(t,v) = P * cos(2 * pi * f * t) * n' * \zeta \tag{E.2}$$

where:
P*cos(2pi*f*t) is the harmonic load that is caused by a single runner;
P is the force applied by a single runner with step frequency f
f is the considered natural frequency;
n' is the equivalent number of pedestrians at the loaded surface S
zeta is the reduction coefficient accounting for the change of the step frequency actually being in the critical range of the natural frequencies.

The maximum load P applied by an individual runner (only in vertical direction), the equivalent number of pedestrians and the reduction coefficient are defined in table and figure

Vertical	Longitudinal	Lateral
1250 N	-	-

Table E.2: Components of force P caused by a single runner

Figure E.5: Figure 5.7 of NA: Reduction factor of a single runner. A = first harmonic vibration.

Runners move with a velocity greater than 3 m/s across the bridge. It can be assumed that v= 0 where the load P(t,v=0) is located at the maximum translation amplitude of the vibration shape.

Extra information about dynamic analysis of bridges and strength verification can be found in Eurocode NEN-EN 1998-2 chapter 4. Design of structures for earthquake resistance - Part 2.

E.0.6. Summary of previous findings

Most codes specify the live load q as 5 kN/m2 which can be reduced when the span of the footbridge increases. This is comparable to the graph given in figure 5.2 given in the Dutch national annex of NEN-EN 1991. This load is a relatively high load, since it is the same live load that is used for the main traffic lane of a road bridge in many codes.

The Eurocode states (in 5.3.2.1) that the live load needs to be applied in such a way that the most unfavourable load case will come to be. In lateral direction this can be due to e.g. spectators that stand at the railing at only one side of the bridge. This will cause asymmetric loading in lateral direction.

Inspection, emergency and cleaning vehicles, in some codes, only have to be taken in to account if the bridge is designed for such a vehicle. In section 5.1 5.3.2.3 it is given that the Eurocode states that such a vehicle has to be taken into account when no permanent obstacle prevents such a vehicle from entering the bridge. The specifications of such loads differ per design code.

Vandalism is a serious problem regarding footbridges, due to the hands-on nature of these bridges. Accidental loads regarding traffic underneath the bridge are no threat in this graduation project since the Glass Truss Bridge spans over small water where no boat-traffic is present.

Wind loads are a problem for footbridges that are located in countries where wind gusts are present or for bridges with long spans, movable bridges or covered bridges. The Glass Truss Bridge does not fall in these categories so no further attention will be given to wind loads.

E.0.7. fib: Guidelines for the Design of Footbridges

fib (fédération internationale du béton) published the book 'Guidelines for the design of footbridges' in 2005 to produce guidelines for the design of footbridges which are internationally valid. In the book multiple references are made to at that time already existing guidelines, such as Danish, Japanese, British and French design codes. Although references to other published articles in which researches to pedestrian loads are elaborated are also present in the book. The purpose of the book is to assist the designers of footbridges with their decisions regarding the design of footbridges.

The interesting chapters of this book are:

• 4. Loads

Stage	Pedestrian Density [Pers/m²]	Characteristics
1	$0 < q < 0.3$	One can walk comfortably and freely
2	$0.3 \leq q < 0.6$	Freedom of movement is intermittently inhibited
3	$0.6 \leq q < 1.0$	Freedom of movement restricted
4	$q \geq 1.0$	Dense crowd, one can no longer freely choose pace

Figure E.6: Classification of pedestrian density according to Oeding

$$F_v = F_0 + F_{1,v}sin(2\pi f_s t) + F_{2,v}sin(4\pi f_s t - \phi_2) + F_{3,v}sin(6\pi f_s t - \phi_3)$$

Figure E.7

- 5. Dynamics

Pedestrian Traffic and Actions This section of the book of fib provides several formulas, graphs and values regarding pedestrian induced actions on the bridge. It shows relations between the pedestrian density and the velocity of the moving persons. When the crowd becomes more dense, they tend to walk slower. The density of the crowd also influences the ability of the individuals to move freely. When the crowd gets more dense, the individuals will move in a more synchronised way. Figure 5.8 shows this classification according to Oeding, 1961. Formulas to calculate synchronisation factors s for certain crowd densities are given in the book. These formulas are developed by Grundmann and Kramer and are based on probabilistic considerations and test results respectively.

Vibrating of a footbridge may cause the pedestrians on the bridge to counteract these vibrations by slight lateral movements. These pedestrians will adjust there pace in such a way that the step frequency will be close to the natural frequency of the bridge, which in turn can cause resonance. This is called the **lock-in effect**. This effect is dominating in the lateral movement in comparison with the vertical movement of the bridge. According to Baumann and Bachmann (1988) a limit displacement of the bridge of 2 mm in lateral direction and of 10-20 mm in vertical direction needs to be avoided. These were confirmed by analysing the Millennium Bridge, London. As stated before, the lateral displacements are governing for the lock-in effects. By investigating the behaviour of the Millennium Bridge, ARUP came up with an expression to determine the number of pedestrians needed for lateral instability and the necessary damping factor of the structure for prohibiting synchronisation. These formulas are given in the book of fib.

When a bridge is loaded by a dense human crowd, this may change the modal characteristics of the structure. This is due to an increase in mass and damping caused by their vertical movements. Horizontal movements may however experience negative damping in the case of a dense crowd moving across the bridge.

For modelling the behaviour of one or more pedestrians passing over the bridge the following formula produced by Bachman (1987) should be taken into account. The force components of both feet need to be added together to get the total load. This load can be divided into various sinusoidal loads which together form the an approximation of the real load by Fourier transformation.

where:
F_0 is the dead load $F_{i,v}$ is the participation of the ith harmonic to the resulting load f_s is the step frequency phi is the phase angle of the ith harmonic

Furthermore Bachmann gives recommended force factors which are $F_{1,v}/F_0 = 0.4$ and 0,5 for fs=2Hz and fs=2.4Hz respectively. $F_{2,v}/F_0 = F_3/F_0 = 0.1$.

Comfort criteria and limit values for frequencies and accelerations According to fib the comfort criteria in codes fall mainly in two categories:

- limit values for structural frequencies. Pedestrian induced dynamic loading falls within certain frequencies. If the natural frequencies of the structure fall outside these loading frequencies, generally no risk of resonance is present. For this reason frequency ranges are provided dor which no dynamic calculation is required.

- limit values for accelerations. If the natural frequencies of the structure fall within the range of pedestrian induced loading frequencies, a dynamic calculation is needed. The resulting accelerations are then limited to ensure pedestrian comfort.

The following tables summarize the limit values in international codes:

Code / Standard	Limit values	
	Vertical	Horizontal
American Guide Spec.	< 3 Hz	
Eurocode 2 (ENV 1992-2)	1.6 Hz - 2.4 Hz	0.8 Hz – 1.2 Hz
DIN-Fachbericht 102	1.6 Hz - 2.4 Hz, 3.5 Hz - 4.5 Hz	
Eurocode 5 (ENV 1995-2)	< 5 Hz	< 2.5 Hz
SBA (former East Germany)	1.0 Hz – 3 Hz	
SIA 260 (Switzerland)	1.6 Hz – 4.5 Hz	< 1.3 transverse < 2.5 longitudinal
BS 5400 (Great Britain)	< 5 Hz	
Austroads (Australia)	1.5 Hz– 3 Hz	
Japanese Footbridge Design Code (1979)	1.5 Hz– 2.3 Hz	

Figure E.8: Summary of critical frequencies from international codes

Vertical acceleration $a_{V,max}$ [m/s²]		
ISO 2631	$1.9 \cdot \sqrt{f_1}$	f_1 = fundamental natural frequency of the bridge
AISC Guide 11	0.5	
Eurocode 1	$Min \begin{cases} 0.50\sqrt{f_h} \\ 0.70 \end{cases}$	for f = 1 to 3 Hz for f = 3-5 Hz: check dependant on case from f = 5 Hz: no check necessary
DIN-Fachbericht 102	$0.5 \cdot \sqrt{f_1}$, vert.	for $f_1 \leq$ 5 Hz; f_1 = fundamental natural frequency of the unloaded bridge
VDI 2057	$0.6 \cdot \sqrt{f_1}$, vert. 0.214 , hor.	f_1 = fundamental natural frequency of the bridge
SBA	0.39	
BS 5400	$0.5 \cdot \sqrt{f_1}$	f_1 = fundamental natural frequency of the bridge
Ontario Bridge Code ONT83	$0.25 \cdot \sqrt{f_1^{0.78}}$	f_1 = fundamental natural frequency of the bridge
Eurocode 5 (ENV 1995-2)	0.7	
Bachmann [40]	$0.5 - 1.0$	
Japanese Footbridge Design Code (1979)	1.0	
Lateral acceleration $a_{L,max}$ [m/s²]		
Eurocode 1	$Min \begin{cases} 0.14\sqrt{f_h} \\ 0.15 \end{cases}$	for f = 0.5 to 1.5 Hz for f = 1.5-2.5 Hz: check dependant on case from f = 2.5 Hz: no check necessary
Eurocode 5 (ENV 1995-2)	0.2	for f < 2.5 Hz (for standing individuals)

Figure E.9: Summary of critical accelerations from international codes

For lateral vibrations the lock-in effects are governing.

F

Soil properties

In figure F.1 the distribution of soil in the Netherlands is depicted [20]. As can be seen when zooming into the west of the Netherlands, the area where Delft is the soil is classified as rather peat or clay. Combining this overview with the technical drawings given in appendix A it can be concluded that the soil is classified as peat. It's water content is relatively high because of the small water underneath the bridge, this leads to the assumption the soil consists of saturated peat.
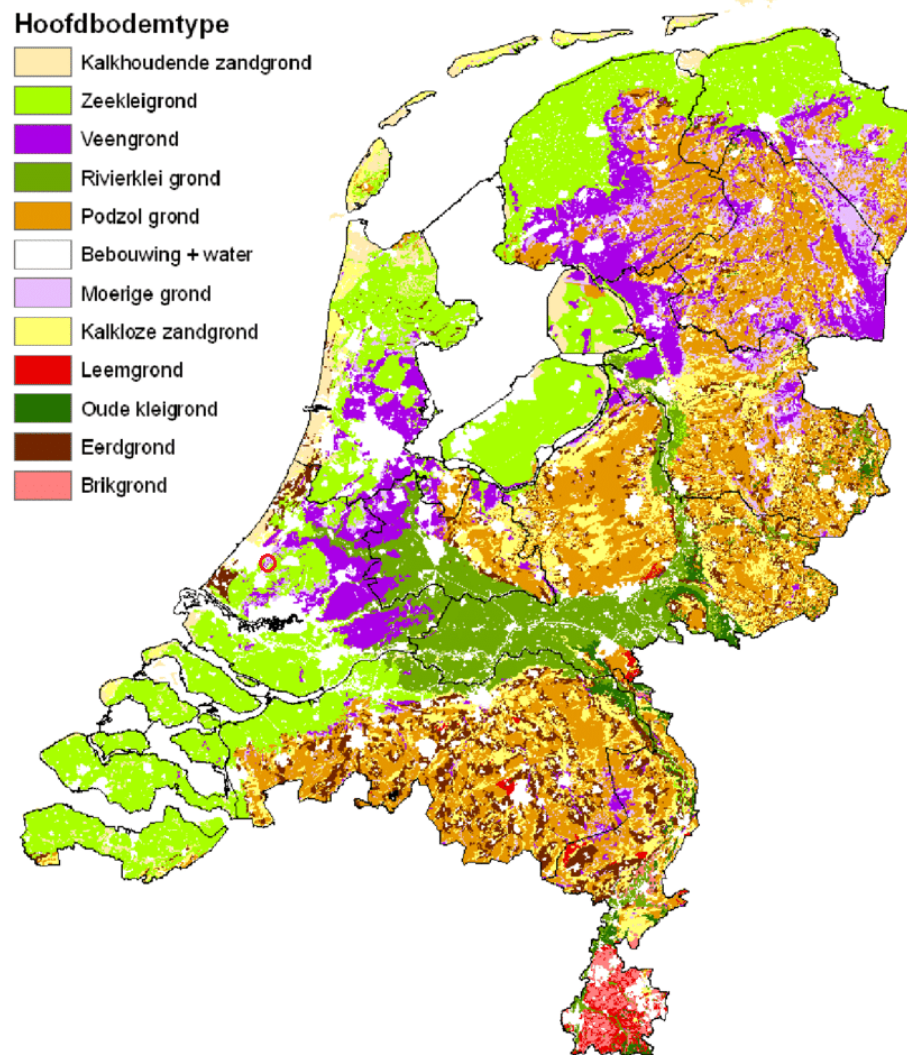
Figure F.1: Distribution of the main soil types in the Netherlands, Delft is indicated with a red dot [20]

Peat is an accumulation of partially decayed vegetation or organic matter. It is resulting from the decomposition of dead organic substances, i.e. remains of plants and animals. The parameters of these soils are different than that from mineral soils. The shear strengths of organic soils are usually lower than for other soils. Also the stiffness and density is significantly lower than for other soils. Another important parameter of peat is the elasticity modulus [21]. Three different organic soils are identified with also independent characteristics, for this soil fibric peat will be assumed as it can be assumed is has a botanical origin.

The following quantities F.1 are found for the mentioned parameters of saturated peat soils. In table the range for each parameter is indicated, values are retrieved from http://www.fao.org/3/x5872e/x5872e00.htm (Andriesse, 1988).

The specific density (particle density) indicates the true densities of the solid peat material. The measurements are done by a pycnometer which is depicted in figure F.2.
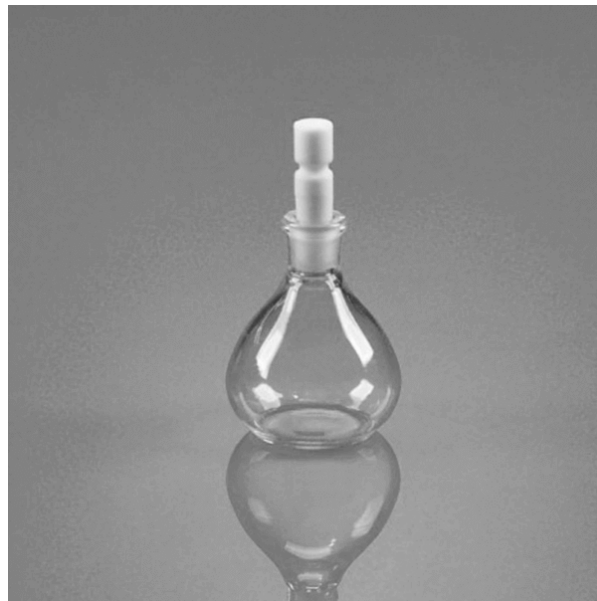
Figure F.2: Pycnometer (picture retrieved from: Science Equip)

Density	1.26	1.8	g/cm^3
Moisture holding capacity	289	1057	%
Elasticity modulus	320	400	kPa

Table F.1: Peat soil properties

In order to check weather these values are reliable, the soil density is measured in a similar place in Rotterdam, a grassy place near a small water. The ground is investigated and it is found that is consists of saturated fibrous peat (like was concluded before based on literature). With a circular mall four samples are taken from different places/depths of the ground, measurements are done as can be seen in the photos. It is decided to do the measurements in Rotterdam because Rotterdam and Delft have the same soil properties according to the map F.1.

(a) Measurement tools

(b) Samples of soil
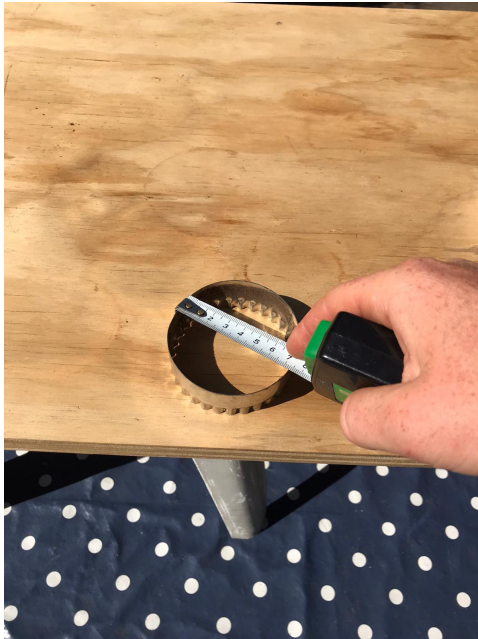
(c) Mall, diameter=75mm, height=25mm

(d) Mall filled with soil

(e) Calibration of measurement equipment: full sac of 100g

(f) Calibration of measurement equipment: empty sac weighting 8g

Figure F.3: Measurement of soil density, area Rotterdam

Samples are then taken from the deck of the bridge. It can be seen that these samples show very different properties. The soil is much more sandy and has some stones and shells in it. Also the soil is very dry although is has rained a lot past days.

(a) Soil on top of the bridge (picture taken on 4-6-2020) (b) Sample of soil

Figure F.4: Measurement of soil density, glass truss bridge Delft

Results of the measurements are stated in table F.2.

Sample	1	2	3
Weight [g]	172	167	176
Volume [mm3]	110447	-	-
Density [kg/m3]	1557	1512	1594

Table F.2: Density of soil layer on top of the Glass Truss Bridge

The average density of the soil from the bridge deck is thus 1554.3kg/m^3. Comparing this with the values found in literature (1260-1800kg/m^3) the measured values are matching.

G

Example of sensitivity analysis

G.1. FINITE ELEMENT MODEL UPDATING OF A LIVELY FOOTBRIDGE, Iban et. al. 2015

The following example from literature is given where a similar sensitivity study is done. Here a 40m long arched bridge is modelled in a Finite element software, static and modal response are numerically estimated. Then, experimental measurements using ambient vibration tests are performed. An outline of the sensitivity study will be given.

Figure G.1: Footbridge under study: Photograph and numerical FE model [16]
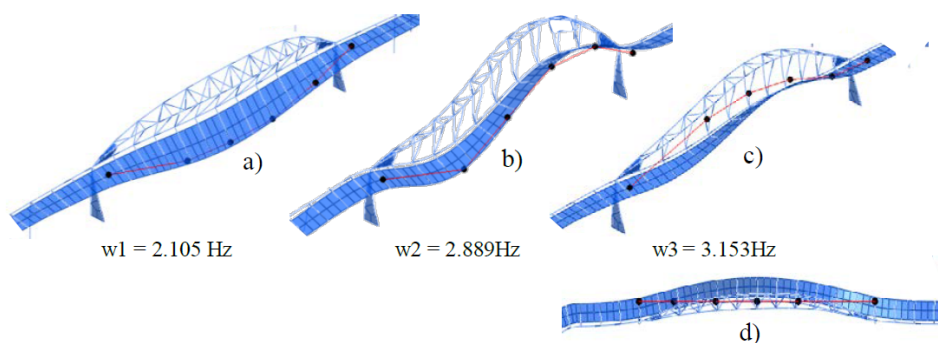
Figure G.2: First three natural modeshapes [16]

Three parameters are chosen, the first one was the flexibility of the joints, initially these were modelled as perfect hinges. After changing the flexibility of the joint it resulted in a bending lost of F=83% (considering a perfect rigid joint to have a value of 0% and a hinge one 100%). The second parameter which was adjusted was the Young's modulus of of the concrete deck. After several iterations a value of $0.9E10N/m^2$ was found to match the static deflection. This was a decrement of 70% from the

117

initial value of the Young's modulus) ($E\_c = 3E10N/m2$). It is mentioned that such a big reduction is not consistent in nominal conditions, but after knowing the on-site construction procedure carried through, pouring the concrete in more than one layer, the results obtained were assumed to make sense.

The next step was automatic updating of the mass distribution along the deck. This is done choosing an initial density of $rho = 2300kg/m^3$. After the automatic modal updating a mean value for rho is found to be 2168kg/m3. In stead of updating the Young's modulus and the density it would have been possible to adjust the deck thickness (giving similar results)

Figure G.3 shows the sensitivity of the selected parameters to the first, second and third modes.
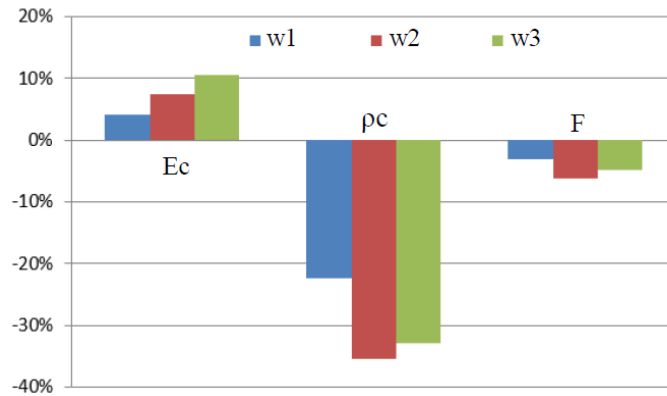
Figure G.3: Sensitivity of the selected parameters [16]

A main remark on this approach is that the parameter that is chosen to be tuned are not all representative. For example changing the Young's modulus of the concrete deck with 70% is not the best thing to do because in this way the model is tuned to the right mode shapes and frequencies by changing a known parameter (Young's Modulus of concrete) in stead of looking into the unknown parameters and changing those. In this way, several shapes and frequencies might match the real situation, but several other mode shapes might probably not. This way of updating will only be useful for this particular case and when looking at these particular modes.

H
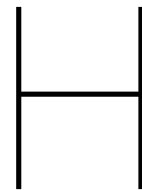
Results of sensitivity analysis of parameter changing on the natural frequency of the Glass Truss Bridge

The base values for the properties are shown in table H.1. In the figures below the eigenmodes are depicted for the change in parameter to its extreme case. The first figure shows a set of 20 eigenvalues for the neutral case, where the base values are inserted. After that, the Youngs' Modulus of the soil is varied, first $E_1 = 300 \text{N/mm}^2$ is inserted and the eigenvalues are calculated, then $E_2 = 400 \text{ N/mm}^2$, and so on.

Parameter	value	
E_{soil}	350	MPa
d_{glass}	47	mm
rho_{soil}	1.53E3	kg/m^3
k_r	2.0E7	Nmm/rad

Table H.1: Base values of the parameters used for the sensitivity analysis

H.1. Eigenmodes neutral case

(a) Mode T1 (4.46 Hz)

(b) Mode T2 (7.2044 Hz)

(c) Mode B1 (7.8018 Hz)

(d) Mode T3 (7.8723 Hz)

(e) Mode T4 (10.313 Hz)

(f) Mode L1 (10.337 Hz)

(g) Mode L2 (10.675 Hz)

(h) Mode T5 (11.197 Hz)

(i) Mode T6 (12.969 Hz)

(j) Mode T7 (13.747 Hz)

(k) Mode T8 (14.405 Hz)

(l) Mode L3 (14.703 Hz)

(m) Mode B2 (16.539 Hz)

(n) Mode T9 (17.462 Hz)

(o) Mode T10 (18.255 Hz)

(p) Mode T11 (22.458 Hz)

(q) Mode B3 (23.108 Hz)

(r) Mode B4 (23.827 Hz)

(s) Mode T12 (25.864 Hz)

(t) Mode T13 (26.250 Hz)
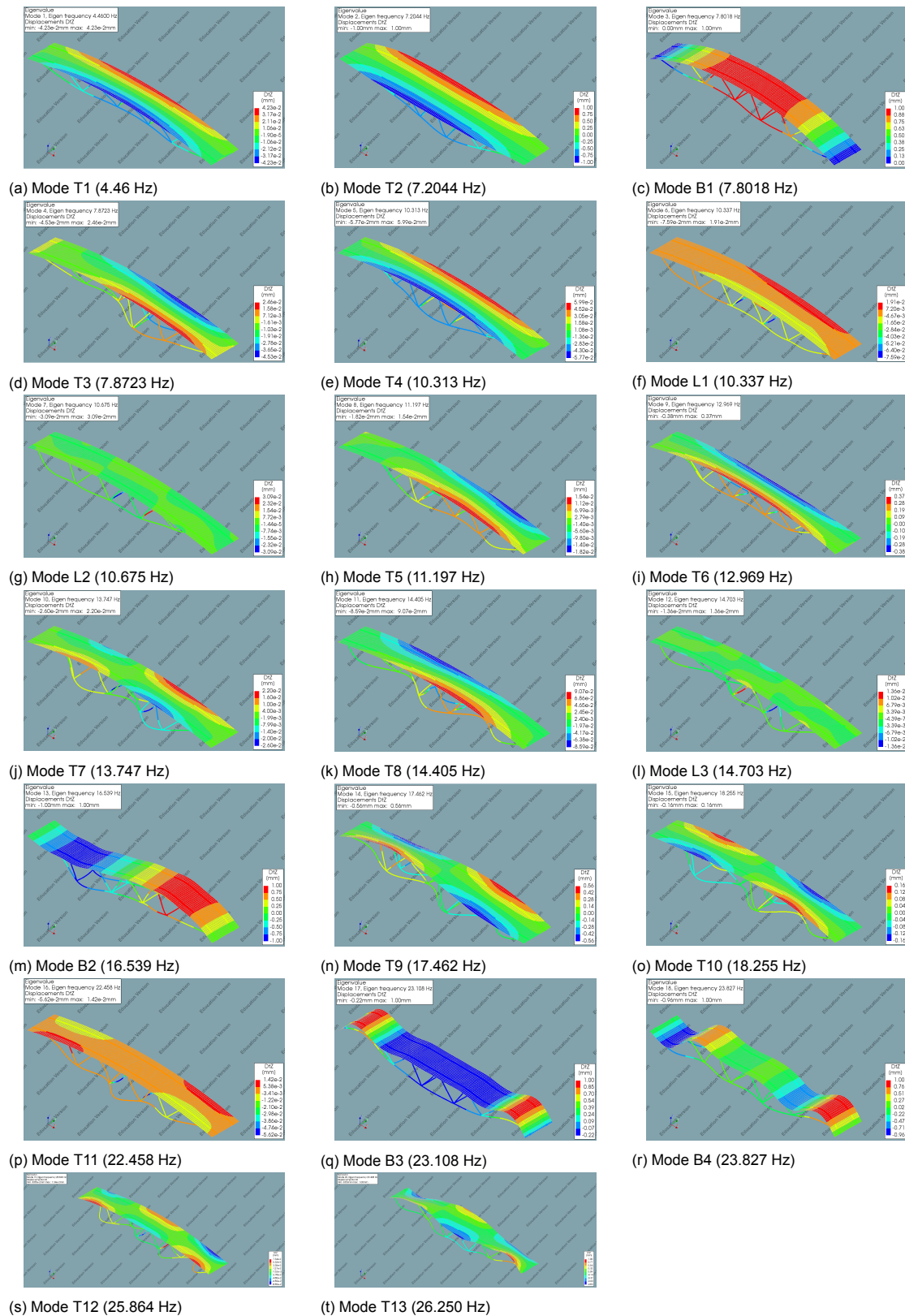
Figure H.1: Mode shapes of the preliminary FE model of the Glass Truss Bridge, considering the base values for the aforementioned parameters

H.2. Eigenmodes with E_{soil} = 300N/mm^2

(a) Mode T1 (4.46 Hz)

(b) Mode T2 (7.2044 Hz)

(c) Mode B1 (7.8018 Hz)

(d) Mode T3 (7.8723 Hz)

(e) Mode T4 (10.313 Hz)

(f) Mode L1 (10.337 Hz)

(g) Mode L2 (10.675 Hz)

(h) Mode T5 (11.197 Hz)

(i) Mode T6 (12.969 Hz)

(j) Mode T7 (13.747 Hz)

(k) Mode T8 (14.405 Hz)

(l) Mode L3 (14.703 Hz)

(m) Mode B2 (16.539 Hz)

(n) Mode T9 (17.462 Hz)

(o) Mode T10 (18.255 Hz)

(p) Mode T11 (22.458 Hz)

(q) Mode B3 (23.108 Hz)

(r) Mode B4 (23.827 Hz)

(s) Mode T12 (25.864 Hz)

(t) Mode T13 (26.250 Hz)
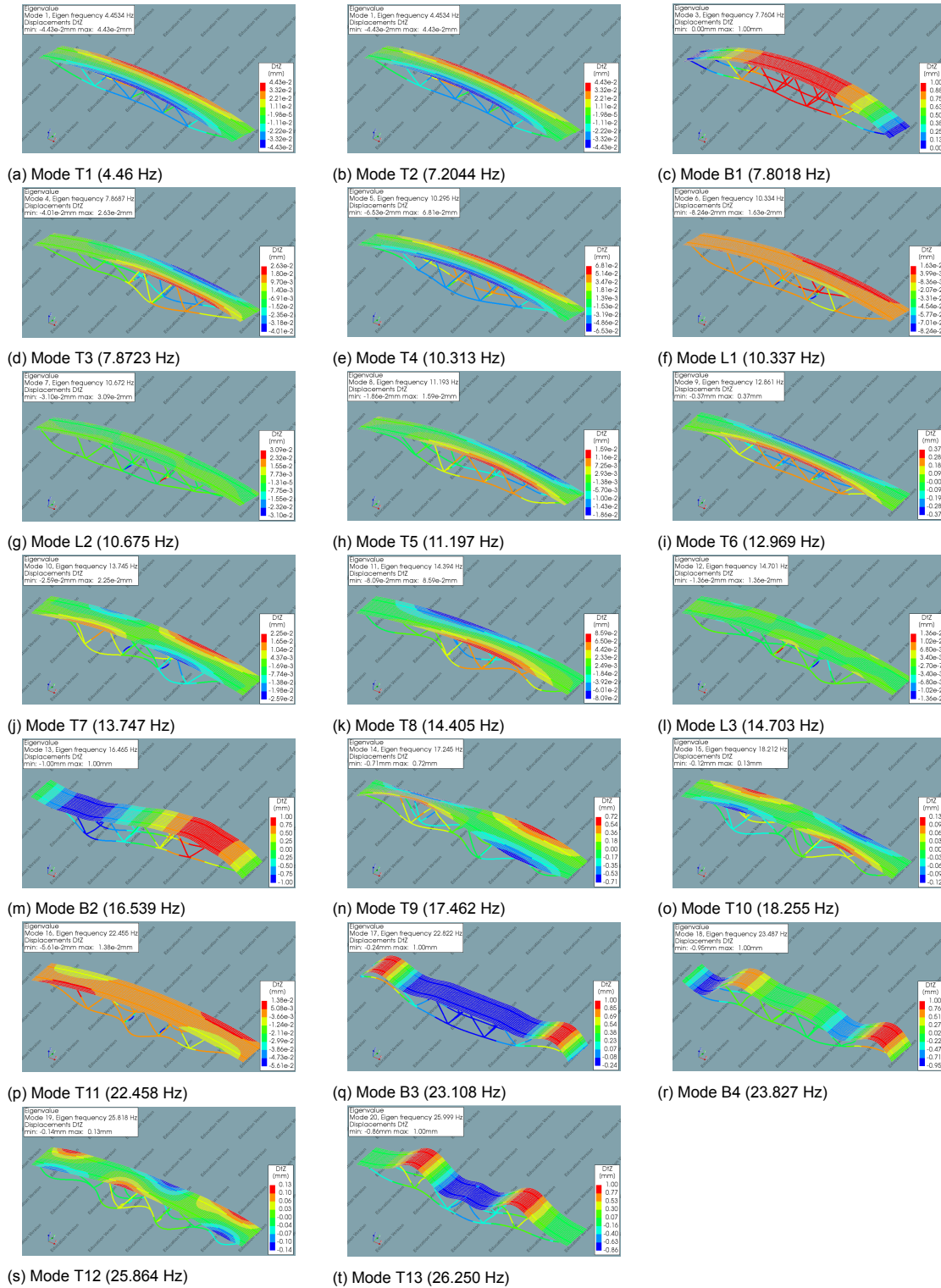
Figure H.2: Mode shapes considering E_1 = 300N/mm^2

H.3. Eigenmodes with E_{soil} = 400N/mm^2

(a) Mode T1 (4.46 Hz)

(b) Mode T2 (7.2044 Hz)

(c) Mode B1 (7.8018 Hz)

(d) Mode T3 (7.8723 Hz)

(e) Mode T4 (10.313 Hz)

(f) Mode L1 (10.337 Hz)

(g) Mode L2 (10.675 Hz)

(h) Mode T5 (11.197 Hz)

(i) Mode T6 (12.969 Hz)

(j) Mode T7 (13.747 Hz)

(k) Mode T8 (14.405 Hz)

(l) Mode L3 (14.703 Hz)

(m) Mode B2 (16.539 Hz)

(n) Mode T9 (17.462 Hz)

(o) Mode T10 (18.255 Hz)

(p) Mode T11 (22.458 Hz)

(q) Mode B3 (23.108 Hz)

(r) Mode B4 (23.827 Hz)

(s) Mode T12 (25.864 Hz)

(t) Mode T13 (26.250 Hz)
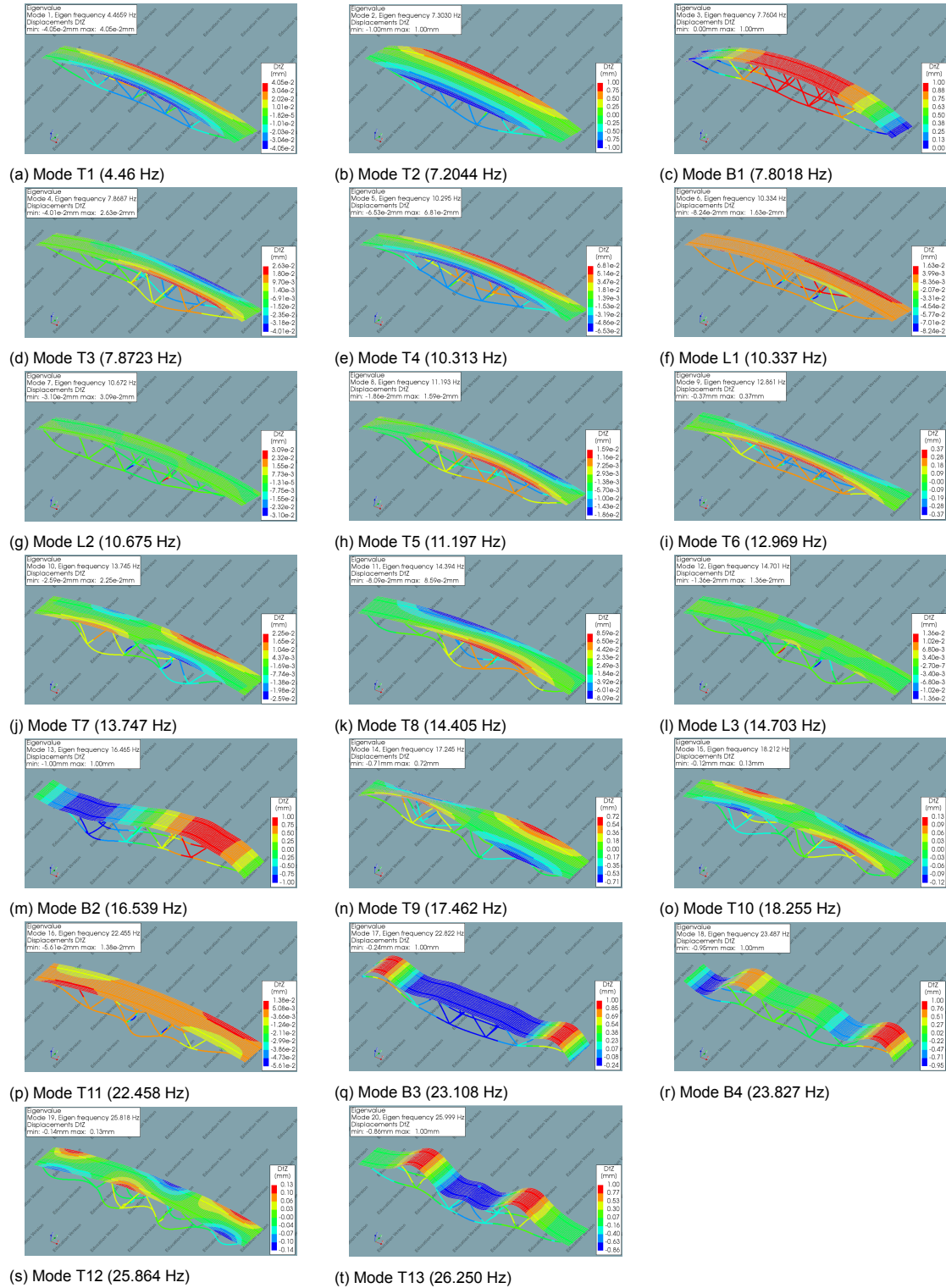
Figure H.3: Mode shapes considering E_1 = 300N/mm^2

H.4. Eigenmodes with d_{glass} = 44mm

(a) Mode T1 (4.0709 Hz)

(b) Mode T2 (7.1844 Hz)

(c) Mode T3 (7.5945 Hz)

(d) Mode B1 (7.8014 Hz)

(e) Mode T4 (10.250 Hz)

(f) Mode L1 (10.282 Hz)

(g) Mode L2 (10.656 Hz)

(h) Mode T5 (11.153 Hz)

(i) Mode T6 (12.941 Hz)

(j) Mode T7 (13.592 Hz)

(k) Mode T8 (14.250 Hz)

(l) Mode L3 (14.578 Hz)

(m) Mode B2 (16.154 Hz)

(n) Mode T9 (17.109 Hz)

(o) Mode T10 (18.120 Hz)

(p) Mode T11 (22.338 Hz)

(q) Mode B3 (22.931 Hz)

(r) Mode B4 (23.729 Hz)

(s) Mode T12 (25.744 Hz)

(t) Mode T13 (25.751 Hz)
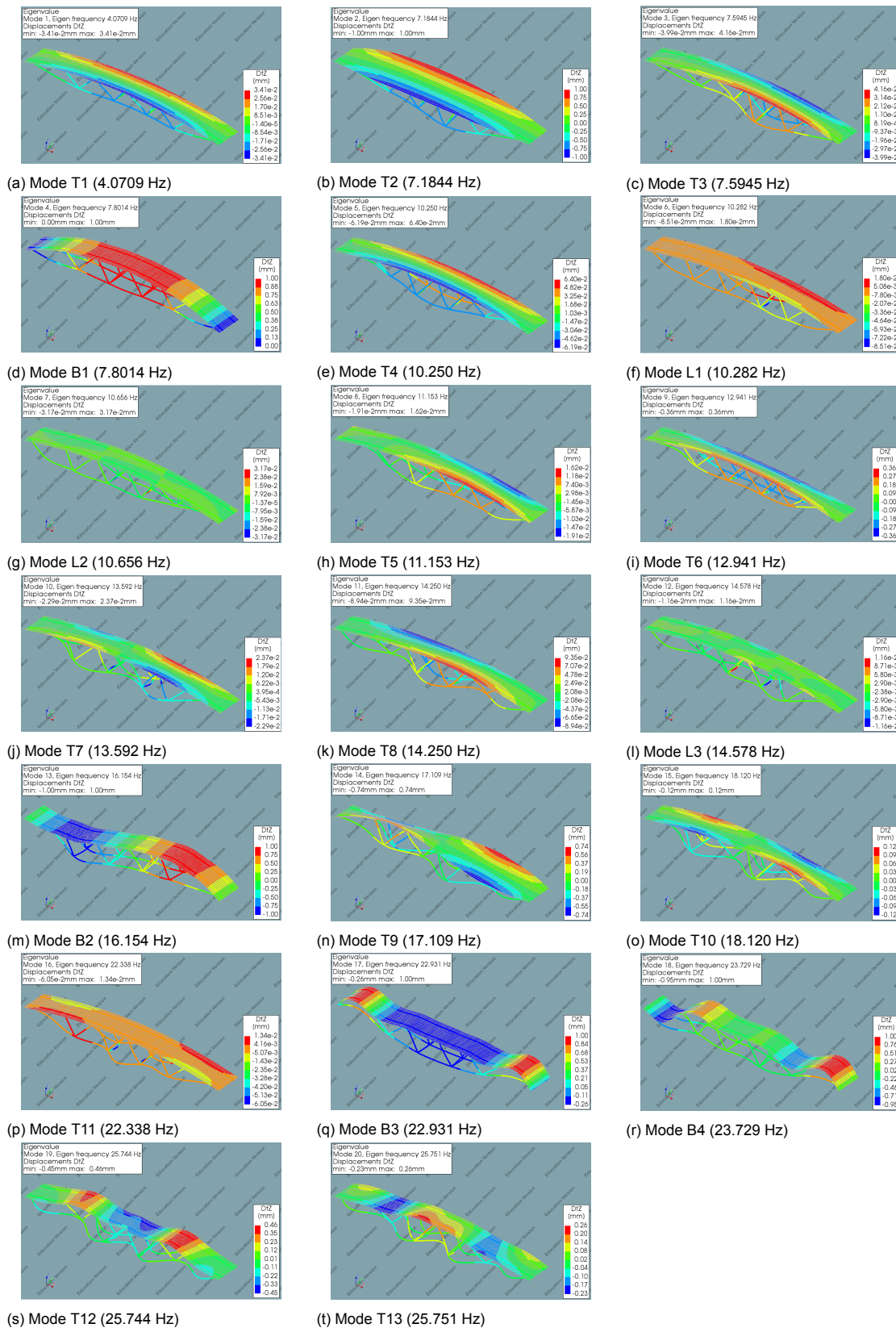
Figure H.4: Mode shapes of the FE model of the Glass Truss Bridge, d_1 = 44mm

H.5. Eigenmodes with d_{glass} = 47mm

(a) Mode T1 (4.0709 Hz)

(b) Mode T2 (7.1844 Hz)

(c) Mode T3 (7.5945 Hz)

(d) Mode B1 (7.8014 Hz)

(e) Mode T4 (10.250 Hz)

(f) Mode L1 (10.282 Hz)

(g) Mode L2 (10.656 Hz)

(h) Mode T5 (11.153 Hz)

(i) Mode T7 (13.592 Hz)

(j) Mode T8 (14.250 Hz)

(k) Mode L3 (14.578 Hz)

(l) Mode B2 (16.154 Hz)

(m) Mode T10 (18.120 Hz)

(n) Mode T11 (22.338 Hz)

(o) Mode B3 (22.931 Hz)

(p) Mode B4 (23.729 Hz)

(q) Mode T12 (25.744 Hz)

(r) Mode T13 (25.751 Hz)
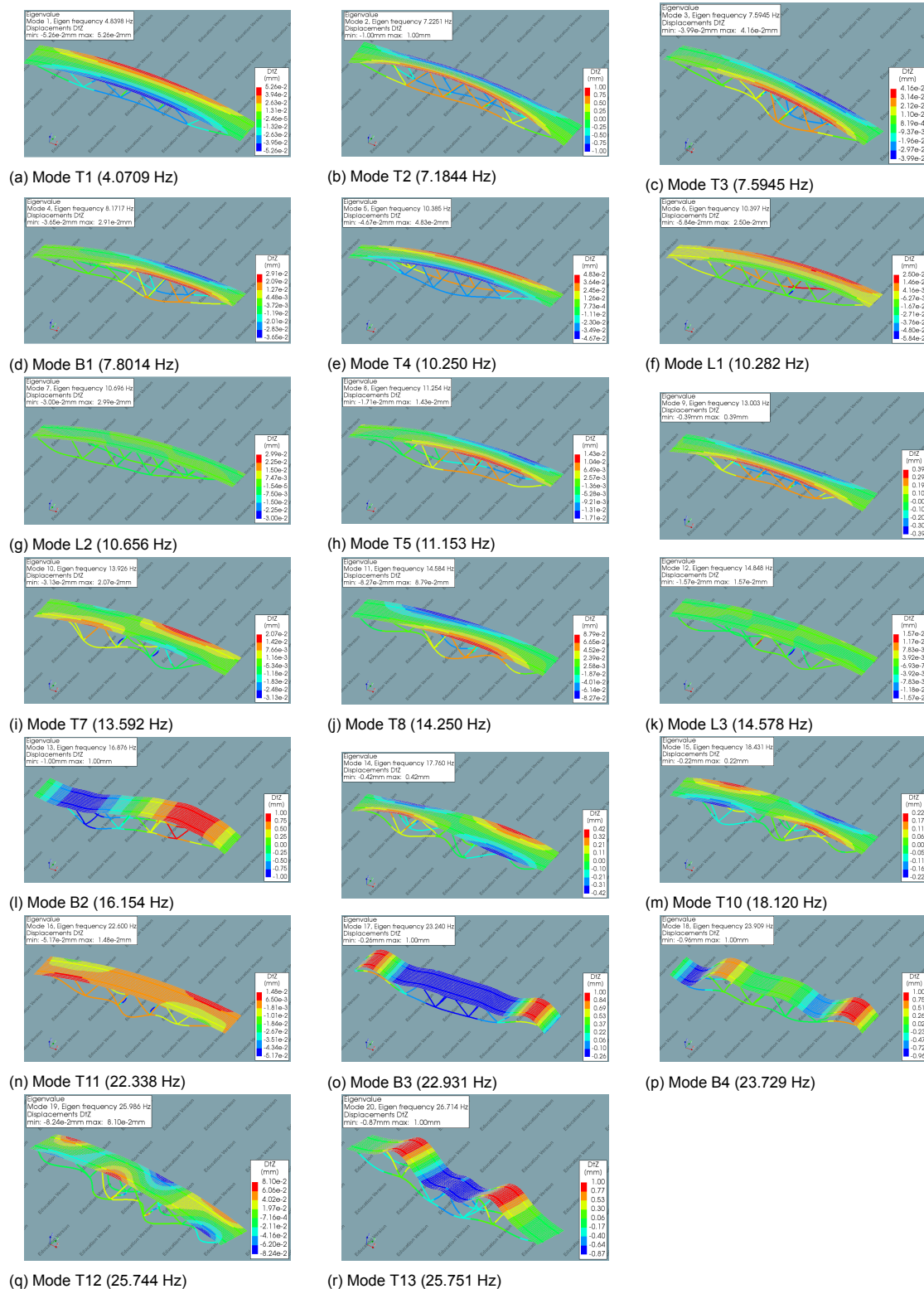
Figure H.5: Mode shapes of the FE model of the Glass Truss Bridge, d_2 = 50mm

H.6. Eigenmodes for simply supported case

The simply supported case shows exactly the same eigenmodes as the neutral case H.1.

H.7. Eigenmodes for fixed case (k$_2$)

(a) Mode T1 (4.4718 Hz)

(b) Mode T2 (7.5104 Hz)

(c) Mode T3 (7.8771 Hz)

(d) Mode B1 (7.9964 Hz)

(e) Mode T4 (10.333 Hz)

(f) Mode L1 (10.489 Hz)

(g) Mode L2 (10.675 Hz)

(h) Mode T5 (11.279 Hz)

(i) Mode T6 (13.175 Hz)

(j) Mode T7 (13.739 Hz)

(k) Mode T8 (14.474 Hz)

(l) Mode L3 (14.697 Hz)

(m) Mode B2 (16.939 Hz)

(n) Mode T9 (17.813 Hz)

(o) Mode T10 (18.321 Hz)

(p) Mode T11 (22.451 Hz)

(q) Mode T12 (25.931 Hz)

(r) Mode B3 (26.093 Hz)

(s) Mode B4 (27.244 Hz)

(t) Mode B5 (27.982 Hz)
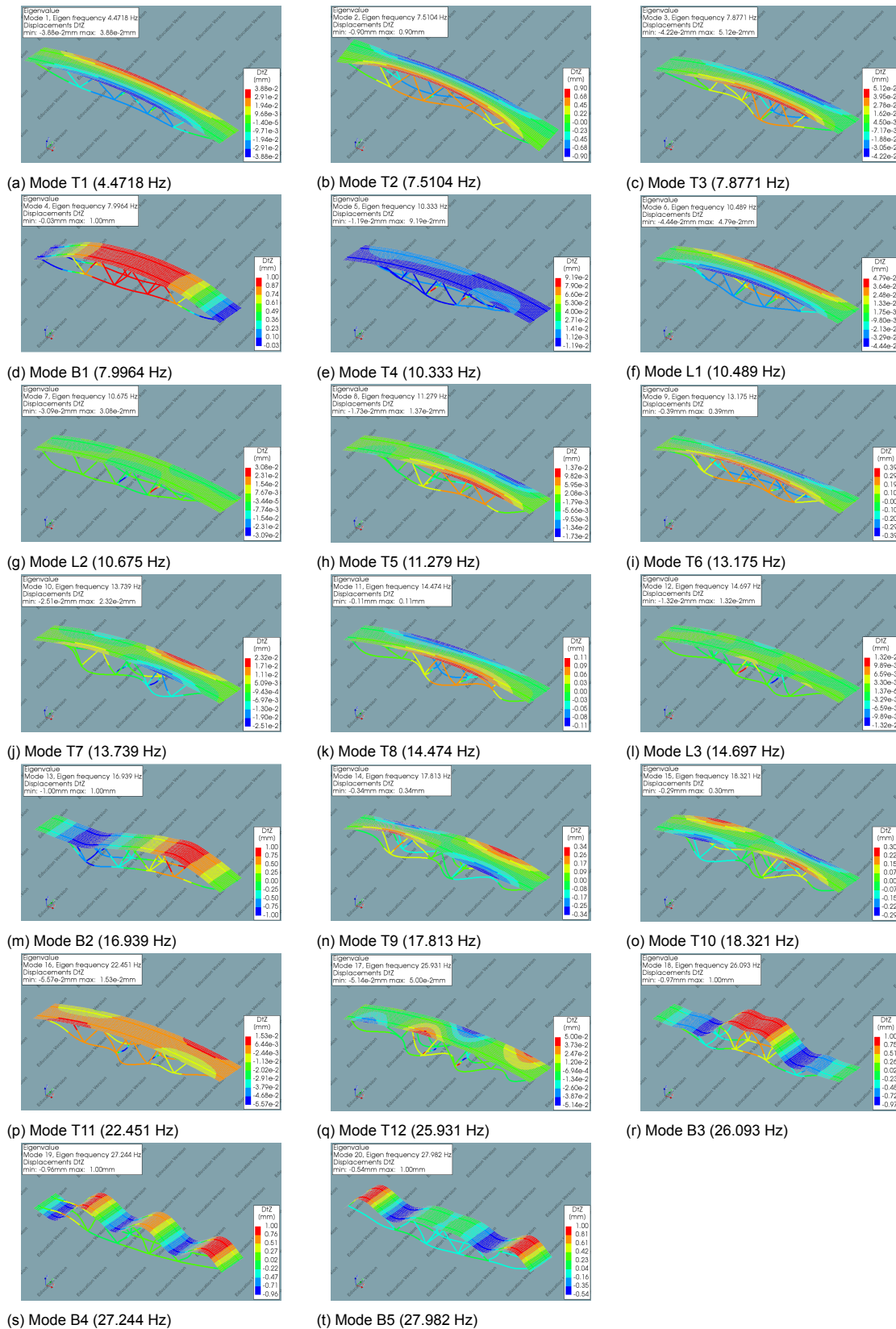
Figure H.6: Mode shapes of the FE model of the Glass Truss Bridge, k$_r$ = fixed

Derivation of the equation of motion

If the Glass Truss Bridge is simplified as a mass connected to a spring and a damping device the model depicted in figure I.1 can be considered. Two degrees of freedom are considered here: z and α.
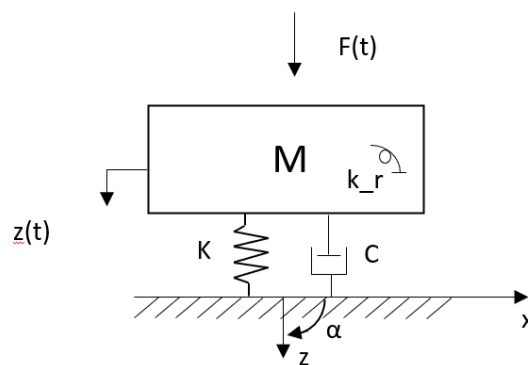
Figure I.1: Simplified model Glass Truss Bridge

When applying a displacement in the positive z-direction the following forces are generated due to the damping device and the spring (I.2. The same can be done for the second degree of freedom I.3.

Figure I.2: Displacement method: forces acting on the mass

Figure I.3: Displacement method: moments acting on the mass

Applying Newton's second law the governing Equations of motion are derived.

$$M * a = \sum F (Newton's second law) \tag{I.1}$$

$$M\ddot{z} = -Kz - C\dot{z} + F \tag{I.2}$$

$$M\ddot{\alpha} = -k_r \alpha \tag{I.3}$$

Python script for extracting modal parameters

```python
# -*- coding: utf-8 -*-
"""
Created on Wed Sep  2 11:29:45 2020

@author: VRIM7
"""

import numpy as np
import matplotlib.pyplot as plt
import scipy.fftpack
import pandas as pd
from scipy.signal import find_peaks, peak_prominences, peak_widths
from scipy import signal
from matplotlib.animation import FuncAnimation, PillowWriter


#FRF estimate
##H1=Y(f)/X(f)
##H2 = Sxy/Sxx
#When performing real tests noise will be inevitable, this is why a noisy signal
#is created (in order to show how to filter the signal)
#For the hammer test simulation noise is not taken into account,
#when preferred, uncommand the lines

##Data
data = pd.read_csv('D:/Users/vrim7/Documents/excel/FFT simply supported beam dtz7.csv',sep=';')

##Frequency and time variables
dt = 0.01                                              #(s)
t = np.arange(0,5,dt)
a = np.array(data['atz28'])                            #output data
in1 = np.array(data['in1'])                            #input force
a_pure = a
n = len(t)
freq = (1/(dt*n)) * np.arange(n)                       #x-axis of frequencies
L = np.arange(1,np.floor(n/2),dtype = 'int')           #only first half needed
L_eff = np.arange(1,150,dtype = 'int')




##Noise
#a_noisy = a_pure + 1*np.random.randn(len(t))

##Input and output plots
plt.plot(t, in1, color = 'c')
plt.xlim(t[0],t[-1])
plt.xlabel('time (s)')
plt.ylabel('Force (N)')
plt.title('Input signal')
plt.show()

##Timehistory of response
#plt.plot(t,a_noisy,color='k', LineWidth=1,label='Noisy')
plt.plot(t,a_pure,color='c',LineWidth=1)
plt.xlim(t[0],t[-1])
plt.legend()
plt.xlabel('time (s))')
plt.ylabel('Acceleration (mm/s^2)')
plt.title('Response from accelerometer')
plt.show()

##Fast Fourier Transforms
a_hat = np.fft.fft(a_noisy)                             #compute FFT of noisy signal to get data
                                                       #in frequency domain
a_hat_pure = np.fft.fft(a_pure)                        #compute FFT of pure signal
In_hat = np.fft.fft(in1)                               #FFT of input load

##Spectral Densities plot
Syy_a_pure = a_hat_pure * np.conj(a_hat_pure)          #Auto spectrum of output fhat*conjugate
Sxx = In_hat * np.conj(In_hat)                         #Auto Spectrum of input
Sxy_a_pure = a_hat_pure  * np.conj(In_hat)             #Cross spectrum of in- and output
Sxy_a_noisy = np.conj(In_hat) * a_hat
```
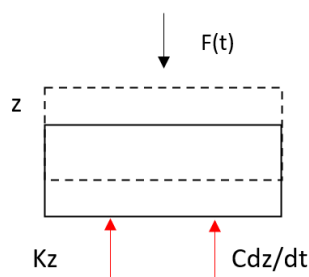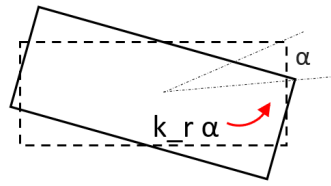
```python
plt.plot(freq[L],Sxy_a_pure[L],color='c',LineWidth=1)
plt.xlim(freq[L[0]],freq[L[-1]])
plt.legend()
plt.xlabel('frequency [Hz]')
plt.ylabel('Sxy(f) [dB]')
plt.title('Cross spectrum acceleration')
plt.show()

plt.plot(freq[L],Sxx[L],color='c',LineWidth=1,)
plt.xlim(freq[L[0]],freq[L[-1]])
plt.xlabel('frequency [Hz]')
plt.ylabel('Sxx(f) [dB]')
plt.title('Auto spectrum of input')
plt.show()

##Filter data (remove noise)
#indices = Sxy_a_noisy > 330                            #find all freq with large power
#Sxy_filt = Sxy_a_noisy * indices                       #zero out all others
#a_hat = indices * a_hat                                #zero out all small fourrier coeff in y
#a_filt = np.fft.ifft(a_hat)
#a_hat_filt = np.fft.fft(a_filt)
#Sxy_filt = np.conj(In_hat)*a_hat_filt

##Plot filtered cross spectrum
#plt.plot(freq[L],Sxy_filt[L],color='c',LineWidth=1,label='Filtered')
#plt.xlim(freq[L[0]],freq[L[-1]])
#plt.legend()
#plt.xlabel('frequency (Hz)')
#plt.ylabel('Power (dB)')
#plt.title('Cross spectrum filtered output')
#plt.show()

##Plot input power
plt.plot(freq[L],20*np.log10(np.abs(In_hat[L])), color ='c')
plt.xlabel('frequency [Hz]')
plt.ylabel('Modulus [dB]')
plt.title('DFT of input signal')
plt.show()



##FrequencyResponseFunction 1: H1 = Y/X
In_hat_R = In_hat.reshape([500,1])                     #reshape arrays
a_hat_pure_R = a_hat_pure.reshape([500,1])

H_a1 = a_hat_pure_R/In_hat_R                            #H1 = Output/Input

FRF_a1 = 20*np.log10(np.abs(np.sqrt(H_a1)))

plt.plot(freq[L_eff],FRF_a1[L_eff],color ='c')
plt.xlabel('Frequency [Hz]')
plt.ylabel('FRF Modulus [dB]')
plt.title('FRF H1 of signal (output over input)')
plt.show()

##FrequencyResponseFunction 2: H2 = Sxy/Sxx
Syy_a_pure_R = Syy_a_pure.reshape([500,1])             #reshape
Sxx_R = Sxx.reshape([500,1])
Sxy_a_pure_R = Sxy_a_pure.reshape([500,1])
Sxy_a_noisy_R = Sxy_a_noisy.reshape([500,1])
#Sxy_filt_R = Sxy_filt.reshape([500,1])

H_a2 = Sxy_a_pure_R/Sxx_R                               #complex values
y_FRF_p = 20*np.log10(np.abs(np.sqrt(H_a2)))           #real valued and in logscale

##Plot phase
angles = np.unwrap(np.angle(H_a2))

fig, axs = plt.subplots(2)
fig.subtitle('FRF and phase plot')
axs[0].plot(freq[L_eff],y_FRF_p[L_eff],color ='c')
plt.ylabel('FRF Modulus [dB]')
axs[1].plot(freq[L_eff], angles[L_eff],'g')
plt.ylabel('FRF phase [rad]')
plt.xlabel('Frequency [Hz]')
plt.show()
```

```python
#Coherence
coh = np.absolute(Sxy_a_pure_R)**2/Sxx_R.real/Syy_a_pure_R.real
plt.plot(freq[L_eff], coh[L_eff],color ='c')
plt.ylim([0.5,1.5])
plt.xlabel('Frequency [Hz]')
plt.ylabel('Coherence [-]')
plt.title('Coherence of input and output signal')
plt.show()

#With noise
#coh_n = np.absolute(Sxy_a_noisy_R)**2/Sxx_R.real/Syy_a_pure_R.real
#plt.plot(freq[L_eff], coh_n[L_eff],color ='c')
#plt.ylim([0.5,1.5])
#plt.xlabel('Normalized frequency')
#plt.ylabel('Coherence')
#plt.show()

#Find peak values
#Converted from https://gist.github.com/sixtenbe/1178136/6767a0b06ad67bca787c8d702fe4f873faf27e6c

def peakdetect(y_axis, delta, x = None):
    """
    Algorithm for detecting local maximas (and minimas) in a signal.
    Searched for values which are surrounded by lower values

    keyword arguments:
    y_axis -- A list containing the signal over which to find peaks
    delta -- (optional) this specifies a minimum difference between a peak and
        the following points, before a peak may be considered a peak.
    """
    maximas = []  #all x- and y-values for the maxima are stored here
    minimas = []  #all x- and y-values for the minima are stored here


    #x and y need to be a numpy array
    x_axis = np.asarray(freq[L_eff])
    y_axis = np.asarray(y_FRF_p[L_eff])
#delta is taken as 0.3, this is arbitrary, but delta must be positive and low
#enough to detect the peak
    delta = 0.3
    look4maxvalue = True

#maxima and minima candidates are temporarily stored in my, mx and mny, mnx resp
    my = -np.Inf
    mny = np.Inf
    mx = 0
    mnx = 0

#A for-loop is used to find the peaks (min and max)
    for i in range(len(y_axis)):
        value = y_axis[i]
        if value > my:        #if the value is higher than previous my, this becomes the new my
            my = value
            mx = x_axis[i]  #and its resp x-value
        if value < mny:        #same for the minima
            mny = value
            mnx = x_axis[i]
        #maxima and minima are searched alternately
        if look4maxvalue:
            if value < my-delta:
                maximas.append((mx,my))
                mny = value
                mnx = x_axis[i]
                look4maxvalue = False
        else:
            if value > mny + delta:
                minimas.append((mnx,mny))
                my = value
                mx = x_axis[i]
                look4maxvalue = True

    return np.array(maximas), np.array(minimas)
```

```python
d = np.asarray(y_FRF_p[L_eff])
x_ax = np.asarray(freq[L_eff])                    #cut off at 30Hz
maximas, minimas = peakdetect(data, 0.3)

plt.plot(x_ax, d ,color ='c')
plt.xlabel('Frequency [Hz]')
plt.ylabel('FRF Modulus [dB]')
plt.title('FRF H2 peaks (Sxy/Sxx)')
plt.scatter(maximas[:,0],maximas[:,1],color='red')
plt.show()

#Damping
#Calculate peakvalue with (H1/sqrt(2))
p1 = 33.7-3
p2 = 37.9-3

plt.plot(x_ax, d,color ='c')
plt.xlabel('Frequency [Hz]')
plt.ylabel('FRF Modulus [dB]')
plt.title('FRF H2 peaks (Sxy/Sxx)')
plt.axhline(y=p1, color='r', linestyle='--')
plt.axhline(y=p2, color= 'g',linestyle='--')
plt.scatter(maximas[:,0],maximas[:,1],color='red')
plt.show()
```

K
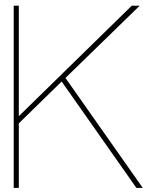
Protocol testing campaign

Hammer Test Protocol

A manual to test the Glass Truss Bridge dynamically
Necessities

- Multiple accelerometers, these devices must be able to measure frequencies higher than the frequencies of interest and the sampling rate should be double the maximum frequency according to the Nyquist theorem

- A PC or laptop with post-processing modal software (python)

- An Analogue to Digital Converter

- A micro SD memory card to store the recorded data

- A real time clock to synchronize between devices

- An impact hammer with enough weight to be able to reach numerous frequencies. The one available at TU Delft is a hammer weighing about 55N with a piezoelectric force sensor at its tip having a dynamic range of 22kN

Procedure

- Two holes should be made in the soil deck to ensure to hit the beam at the selected points (figure 6.2 and 6.3). The hitting location is at 1m from midspan and 3m from the boundary and on one beam only, both bending and torsional eigenfrequencies are being excited simultaneously. Double hits should be avoided, it might be helpful to practice with the hammer before doing the recordings.

- When a pre-trigger is used the eigenfrequencies are found more clearly but this is not of highest priority.

- The hammer impact should be in vertical direction (not with an angle).

- Install the accelerometers like shown in figure 6.3. It is important to install the accelerometers on both beams, otherwise it is not possible to distinguish between bending and torsional modes when postprocessing the data.

- For each input section a total of 5 to 10 time series should be recorded to be able to average the measured data.

- One test recording should be performed to know in what time frame the structural response to the hammer impulse vanishes, in other words, to know the time frame in which all vibrations die out. In that case no leakage is encountered and no windowing is needed. Windowing reduces the amplitude of the discontinuities at the boundaries of each finite sequence [14]. More information about windowing can be found in Appendix B.

- If the structure continues to vibrate for a long period of time, or is background noise is present, the force or exponential window can be used. This windowing function forces the response to be zero at the end of the time frame. This forces the signal to be periodic, but at the same time it overestimates the damping of the structure because some artificial damping is added to the signal in a shorter time.

- The recordings are in time domain, a Fourier Transform (FFT) is applied to get each signal in the frequency domain.

- The cross spectrum of the obtained spectral descriptions (input and output) is generated by multiplying the FFT of the output signal with the complex conjugate of the input signal. The autospectra (S_{xx} and S_{yy}) are generated in the same manner, now multiplying each spectrum with its complex conjugate. The set of power spectra should be averaged for the set of series collected at each location to have a more reliable result.

- FRF's can now be estimated with following formula:

$$H_{xy}(f) = S_{xy}(f)/S_{xx}(f)$$

- For each FRF its phase spectrum can be estimated and plotted. When the phase is showing a 90 degree angle, this means that a resonance peak is present.

- The coherence should also be checked, this is a measure of the correlation between input output. Generally values of γ^2 = 1 should be obtained for ω far from the eigenfrequencies of the structure. Close to resonance, the value for the coherence should be low, for large displacements and low values of damping, deviations in the coherence are detected. Data with a coherence less than 0.75 should not be used, the test should then be done again. The coherence can be checked with next formula.

$$\gamma^2(f) = |S_{xy}(f)|^2 / (S_{xx}(f) * S_{yy}(f)$$

- Modal parameters can now be extracted. To extract the modal parameters from the FRF's obtained after previous steps, different techniques are available. The one best suitable for an impact/hammer test is the Eigensystem Realization Algorithm (ERA) [1] Some advantages of ERA is that the computational procedure is numerically stable and data from more than one test can be used simultaneously to identify eigenvalues that are close to each other [17].

- The eigenfrequencies can also be determined by using the Peak Picking method. From the FRF's these peaks are clearly visible. The obtained maximum values should be checked by hand to see if the peak shows a real resonance peak.

- The damping parameters can be obtained making use of the half bandwidth method which is a classical method of deriving the damping of existing structures. The half power bandwidth is the width of the resonance peak where the response is half power down from the maximum value [34].

- The modal parameters can be compared to the ones obtained with DIANA, the FE model can be updated accordingly.

---

[1]ERA is a system identification technique mostly used in structural health monitoring to check weather a structure needs to be updated, reinforced or repaired. This technique can be implemented on free response data, which makes it suitable for a hammer test (after the impact load all vibrations are free vibrations).

Bibliography

[1]

[2] CT 4140 Dynamics of Structures. Exam: April 2006. 1(April):1–84, 2006.

[3] H E U R O P E a N N I O N. 1(2005), 2011.

[4] Mithila Achintha. Sustainability of glass in construction. (December 2016):0–22, 2017. doi: 10. 1016/B978-0-08-100370-1.00005-6.

[5] a Alipour and F Zareian. Rayleigh damping-14_14-0243. *14 th World Conference on Earthquake Engineering: Innovation Practice Safety*, 2008. URL http://www.iitk.ac.in/nicee/wcee/ article/14{_}14-0243.PDF.

[6] Seongpil An and Alexander L. Yarin. Mechanical behavior of sintered submicron glass fiber mats. *International Journal of Mechanical Sciences*, 170(August 2019), 2020. ISSN 00207403. doi: 10.1016/j.ijmecsci.2019.105354.

[7] Paul Archbold and Brian Mullarney. The relationship between pedestrian loading and dynamic response of an FRP composite footbridge. *Bridge Structures*, 13(4):147–157, 2017. ISSN 17448999. doi: 10.3233/BRS-180122.

[8] Chiara Bedon. Diagnostic analysis and dynamic identi fi cation of a glass suspension footbridge via on-site vibration experiments and FE numerical modelling. *Composite Structures*, 216(March): 366–378, 2019. ISSN 0263-8223. doi: 10.1016/j.compstruct.2019.03.005. URL https: //doi.org/10.1016/j.compstruct.2019.03.005.

[9] Rune Brincker, Lingmi Zhang, and Palle Andersen. Modal identification of output-only systems using frequency domain decomposition. *Smart Materials and Structures*, 10(3):441–445, 2001. ISSN 09641726. doi: 10.1088/0964-1726/10/3/303.

[10] Michéle Dal, Toé Casagrande, Matthew Richard, Nilo Cesar Consoli, Michele Casagrande, and Joseph F Labuz. Closure to " Behavior of a Fiber-Reinforced Bentonite at Large Shear Displacements " by Retaining Wall " by Joseph G . Bentler and. *Journal of Geotechnical and Geoenvironmental Engineering*, 1(October):1–7, 2007. doi: 10.1061/(ASCE)1090-0241(2007)133.

[11] C. Gentile and N. Gallino. Ambient vibration testing and structural evaluation of an historic suspension footbridge. *Advances in Engineering Software*, 39(4):356–366, 2008. ISSN 09659978. doi: 10.1016/j.advengsoft.2007.01.001.

[12] Mark F Green and Canada Kl. MODAL TEST METHODS FOR BRIIDGES : A REVIEW Queen ' s University. pages 552–558.

[13] Joseph K Hammond. *Fundamentals of signal theory*, volume 270. 1960. ISBN 9780470511886. doi: 10.1016/0016-0032(60)90684-0.

[14] Christophe Heinemeyer, Christiane Butz, Andreas Keil, Mike Schlaich, Arndt Goldack, S. TROMETOR, M. Lukic, Bruno Chabrolin, Arnaud Lemaire, Pierre-Olivier Martin, and Others. *Design of Leightweight footbridges for human induced vibrations*, volume 3. 2009. ISBN 9789279133879. doi: 10.2788/33846Luxembourg:.

[15] D. Honfi, A. Reith, L. G. Vigh, and Gy Stocker. Why glass structures fail? - Learning from failures of glass structures. *Challenging Glass 4 and COST Action TU0905 Final Conference - Proceedings of the Challenging Glass 4 and Cost Action TU0905 Final Conference*, pages 791–800, 2014. doi: 10.1201/b16499-109.

[16] N. Ibán, J. Castaño, J. Cara, J. Fernández, C. M. Pérez, I. Muñoz, and A. Lorenzana. Finite element model updating of a lively footbridge. *6th International Operational Modal Analysis Conference, IOMAC 2015*, (May), 2015.

[17] Jer Nan Juang and Richard S. Pappa. An eigensystem realization algorithm for modal parameter identification and model reduction. *Journal of Guidance, Control, and Dynamics*, 8(5):620–627, 1985. ISSN 07315090. doi: 10.2514/3.20031.

[18] John Macdonald. Lateral excitation of bridges by balancing pedestrians. *Proceedings of the Royal Society A: Mathematical, Physical and Engineering Sciences*, 465, 2009. doi: 10.1098/rspa. 2008.0367.

[19] R. Nijsse and M. Van Der Velden. CIE4285: Structural glass reader. (October), 2019.

[20] P. Oenema, O., Römkens. Quick Scan Soils in the Netherlands. 2004. doi: 1566-7197.

[21] Magdalena Olszewska. Determination of Peat Elasticity Modulus (Constrained Modulus) Based on Field Measurement Using Simplified Consolidation Model. *Civil and Environmental Engineering Reports*, 28(2):18–30, 2018. ISSN 2080-5187. doi: 10.2478/ceer-2018-0017.

[22] Inanç Onur M, Mustafa Tuncan, and Ahmet Tuncan. An Experimental Study for Determining the Shear Modulus of Toyoura Sand. *Second European Conference on Earthquake Engineering and Seismology*, pages 1–7, 2014.

[23] T H E Rose. Wcte 2016. *WCTE 2016 World Conference on Timber Engineering*, (August):5886–5893, 2016.

[24] Ayad-t Saeed, Zhong-gui Jiang, and Zhuan-yun Yang. Dynamic analysis of coupled wind-railway vehicle-bridge systems. *Advanced in Civil, Environmental, and Materials Research (ACEM 14)*, 1:24–28, 2014.

[25] Brian J Schwarz and Mark H Richardson. By. pages 1–12, 1999.

[26] Ate Snijder. GTB_tekeningen_boekje.pdf, 2017.

[27] Ate Snijder, Rob Nijsse, and Christian Louter. Building and testing lenticular truss bridge with glass-bundle diagonals and cast glass connections. *Challenging Glass 6: Conference on Architectural and Structural Applications of Glass, CGC 2018 - Proceedings*, (May), 2018. doi: 10.7480/cgc. 6.2185.

[28] J.M.J Spijkers, A.W.C.M. Vrouwenvelder, and E.C. Klaver. Structural Dynamics CT 4140. *Lecture notes*, (January):1–204, 2005.

[29] K. Van Nimmen, G. Lombaert, G. De Roeck, and P. Van den Broeck. Vibration serviceability of footbridges: Evaluation of the current codes of practice. *Engineering Structures*, 59:448–461, 2014. ISSN 01410296. doi: 10.1016/j.engstruct.2013.11.006. URL http://dx.doi.org/10.1016/j.engstruct.2013.11.006.

[30] F A Veer and J R Pastunink. Developing a Transparent Tubular Laminated Column. *Proceedings of GPD 1999 Conference*, (June):277–280, 1999.

[31] K Verleg, Finite Element Modelling, and Experimental Validation. The Structural Behaviour Bundled Glass Columns. *Thesis*, 2019.

[32] David Wennberg, Per Wennhage, and Sebastian Stichel. Orthotropic Models of Corrugated Sheets in Finite Element Analysis. *ISRN Mechanical Engineering*, 2011:1–9, 2011. ISSN 2090-5122. doi: 10.5402/2011/979532.

[33] Hello World. Inhomogeneous Cross Sections. (Example 1):7–10.

[34] Baisheng Wu. A correction of the half-power bandwidth method for estimating damping. *Archive of Applied Mechanics*, 85(2):315–320, 2015. ISSN 14320681. doi: 10.1007/s00419-014-0908-0.